2013

The HITRAN2012 molecular spectroscopic database

L. S. Rothman

I. E. Gordon

Y. Babikov

D. Chris Benner
William and Mary, dcbenn@wm.edu

V. Malathy Devi
William and Mary, mdvenk@wm.edu

Journal of Quantitative Spectroscopy & Radiative Transfer 130 (2013) 4–50

Contents lists available at ScienceDirect

Journal of Quantitative Spectroscopy & Radiative Transfer

journal homepage: www.elsevier.com/locate/jqsrt

The HITRAN2012 molecular spectroscopic database

L.S. Rothman [a,*], I.E. Gordon [a], Y. Babikov [b], A. Barbe [c], D. Chris Benner [d], P.F. Bernath [e], M. Birk [f], L. Bizzocchi [g], V. Boudon [h], L.R. Brown [i], A. Campargue [j], K. Chance [a], E.A. Cohen [i], L.H. Coudert [k], V.M. Devi [d], B.J. Drouin [i], A. Fayt [l], J.-M. Flaud [k], R.R. Gamache [m], J.J. Harrison [n], J.-M. Hartmann [k], C. Hill [o], J.T. Hodges [p], D. Jacquemart [q], A. Jolly [k], J. Lamouroux [k,m], R.J. Le Roy [r], G. Li [a], D.A. Long [p], O.M. Lyulin [b], C.J. Mackie [a,1], S.T. Massie [s], S. Mikhailenko [b], H.S.P. Müller [t], O.V. Naumenko [b], A.V. Nikitin [b], J. Orphal [u], V. Perevalov [b], A. Perrin [k], E.R. Polovtseva [b], C. Richard [a], M.A.H. Smith [v], E. Starikova [b], K. Sung [i], S. Tashkun [b], J. Tennyson [o], G.C. Toon [i], Vl.G. Tyuterev [c], G. Wagner [f]

[a] Harvard-Smithsonian Center for Astrophysics, Atomic and Molecular Physics Division, Cambridge, MA 02138, USA
[b] V.E. Zuev Institute of Atmospheric Optics SB RAS, Tomsk 634021, Russia
[c] Université de Reims-Champagne-Ardenne, Groupe de Spectrométrie Moléculaire et Atmosphérique, 51062 Reims, France
[d] The College of William and Mary, Department of Physics, Williamsburg, VA 23187, USA
[e] Old Dominion University, Department of Chemistry and Biochemistry, Norfolk, VA 23529, USA
[f] DLR, Remote Sensing Technology Institute, Wessling 82234, Germany
[g] CAAUL, Observatório Astronómico de Lisboa, Lisboa, Portugal
[h] Laboratoire Interdisciplinaire Carnot de Bourgogne, UMR 6303 CNRS-Université de Bourgogne, 21078 Dijon, France
[i] Jet Propulsion Laboratory, California Institute of Technology, Pasadena, CA 91109, USA
[j] Université Grenoble 1/CNRS, UMR5588 LIPhy, 38402 Grenoble, France
[k] CNRS et Universités Paris Est et Paris 7, Laboratoire Inter-Universitaire des Systèmes Atmosphériques, 94010 Créteil, France
[l] Université Catholique de Louvain, Lab. de Spectroscopie Moléculaire, 1348 Louvain-la-Neuve, Belgium
[m] University of Mass Lowell, Department of Environmental Earth and Atmospheric Sciences, Lowell, MA 01854, USA
[n] University of York, Department of Chemistry, York YO10 5DD, UK
[o] University College London, Department of Physics and Astronomy, London WC1E 6BT, UK
[p] National Institute of Standards and Technology, Gaithersburg, MD 20899, USA
[q] UPMC Univ. Paris 06, UMR 7075, Laboratoire de Dynamique, Interactions et Réactivité, 75252 Paris, France
[r] University of Waterloo, Department of Chemistry, Waterloo, Ont N2L 3G1, Canada
[s] National Center for Atmospheric Research, Boulder, CO 80307, USA
[t] Universität zu Köln, I. Physikalisches Institut, Cologne 50937, Germany
[u] Karlsruhe Institute of Technology, Institute for Meteorology and Climate Research, Eggenstein-Leopoldshafen 76344, Germany
[v] NASA Langley Research Center, Science Directorate, Hampton, VA 23681, USA

ARTICLE INFO

Article history:
Received 6 April 2013
Received in revised form
2 July 2013
Accepted 4 July 2013
Available online 12 July 2013

Keywords:
HITRAN
Spectroscopic database

ABSTRACT

This paper describes the status of the 2012 edition of the HITRAN molecular spectroscopic compilation. The new edition replaces the previous HITRAN edition of 2008 and its updates during the intervening years. The HITRAN molecular absorption compilation is comprised of six major components structured into folders that are freely accessible on the internet. These folders consist of the traditional line-by-line spectroscopic parameters required for high-resolution radiative-transfer codes, infrared absorption cross-sections for molecules not yet amenable to representation in a line-by-line form, ultraviolet spectroscopic parameters, aerosol indices of refraction, collision-induced absorption data,

* Corresponding author. Tel.: +1 617 495 7474; fax: +1 617 496 7519.
E-mail addresses: LSR_JQSRT@verizon.net, LRothman@cfa.harvard.edu (L.S. Rothman).
[1] *Current address*: University of Western Ontario, Department of Physics and Astronomy London, Ont., Canada N6A 3K7.

http://dx.doi.org/10.1016/j.jqsrt.2013.07.002

Molecular spectroscopy
Molecular absorption
Spectroscopic line parameters
Absorption cross-sections
Aerosols

and general tables such as partition sums that apply globally to the data. The new HITRAN is greatly extended in terms of accuracy, spectral coverage, additional absorption phenomena, and validity. Molecules and isotopologues have been added that address the issues of atmospheres beyond the Earth. Also discussed is a new initiative that casts HITRAN into a relational database format that offers many advantages over the long-standing sequential text-based structure that has existed since the initial release of HITRAN in the early 1970s.

1. Introduction

This article describes the data that have been added, modified, or enhanced in the HITRAN (**Hi**gh Resolution **Tran**smission) compilation since the previous update of 2008 [1] (hereafter called HITRAN2008 in the text). The HITRAN compilation is comprised of several components that have been arranged into folders that include (1) line-by-line spectroscopic parameters for high resolution molecular absorption and radiance calculations (from the microwave through visible region of the spectrum); (2) infrared absorption cross-sections (generally representing absorption by molecules that have very dense spectra or many low-lying vibrational modes); (3) ultraviolet datasets (both line-by-line and cross-section); (4) tables of aerosol refractive indices; (5) collision-induced absorption datasets; and (6) global data and software for filtering and managing the data. The updates to these six portions of HITRAN will be discussed in the following sections.

The data that enter HITRAN or replace previous entries go through a rigorous process. Fig. 1 is a schematic of the general process. The vertical box on the left (source box) is a representation of the many sources that come to the attention of the HITRAN committee. This committee is formed of an international group of spectroscopists with expertise that cover all the molecules and spectral regions encompassed by HITRAN. Sources selected (which can include measurements or calculations of line positions, intensities, line-shape parameters, etc.) are then cast into the format of the HITRAN line list, or cross-section sets if that is applicable. Basic rules are applied to the line list as shown in the legend, and errors and outliers are culled. If possible, the line list is then provided for comparison with independent observations, often long-path high-resolution atmospheric measurements. The results are then discussed with the committee at large. This whole process is intensive; there are quality measurements and calculations appearing in the literature and presented at meetings that may not get into the source box and may later appear as updates to HITRAN editions. Finally, users play an important role in the process. Inevitably errors can appear in the database, or important newer information does not get incorporated. Users often conduct new laboratory or field measurements that provide additional input to the scheme.

It is necessary to call attention to some caveats. The units used throughout HITRAN and this paper do not strictly adhere to the SI system for both historical and application-specific reasons. Thus cm (centimeter) is seen throughout, as is atm (atmosphere) for pressure. We also employ the symbol ν throughout for line position in cm^{-1}, thereby dropping the tilde ($\tilde{\nu}$) that is the official designation of wavenumber. We normally express the HITRAN unit for intensity as

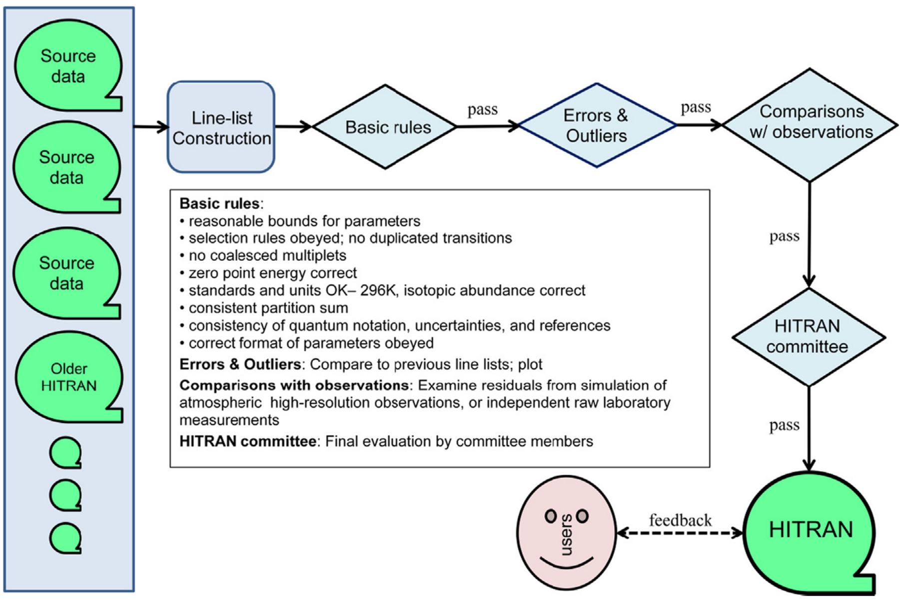

Fig. 1. Validation scheme for HITRAN line lists.

$cm^{-1}/(molecule\ cm^{-2})$ rather than simplifying to the equivalent cm/molecule. In this manner we emphasize the quantity as wavenumber per column density, which is consistent with the viewpoint of atmospheric radiative-transfer codes.

There are a number of transitions in the line-by-line portion of HITRAN that have not been fully assigned in terms of quantum identification. Their lower-state energy is not known, but these transitions have been carefully measured at room temperature (296 K is the standard HITRAN temperature) or, in the case of some methane lines, at different low temperatures. We have opted to retain many of these important lines in the database, using minus one (-1) as a flag to warn users; in some cases, a crude guess of the lower-state energy has been made for these unassigned lines.

The line positions in the microwave region can be measured with a great degree of precision. The previous HITRAN format for the transition wavenumber, while allowing for eleven significant digits, suggested a FORTRAN field of F12.6. This had the effect of placing only six places after the decimal, and thus valuable information in the microwave region was being lost. Considering that the flexible decimal point in the line positions can cause serious issues with existing computer codes, we have changed this format for only two molecules (HNO_3 and PH_3), but are planning to make the changes throughout the entire database in the future so researchers will have to start to prepare for this change now. For HNO_3 and PH_3, nine places after the decimal are given for line positions with $\nu \leq 1\ cm^{-1}$, eight for $1 < \nu \leq 10$, seven $10 < \nu \leq 100$, and six everywhere else.

2. Line-by-line parameters

It has been over four years since the release of HITRAN2008, and during this time frame many significant improvements have been accomplished and incorporated into this new edition of HITRAN. The suite of spectral line parameters which have been represented since 2004 [2] is displayed in Table 1. The improvements in the line-by-line parameters have been accomplished by vastly improved experimental techniques and analysis, as well as more sophisticated and robust theoretical treatments. In this section, we describe the changes, additions, and modifications of the molecules represented in the line-by-line portion of the HITRAN compilation in sub-sections ordered by the chronological HITRAN molecule number assignment; if no change was made, we still list the molecule in a sub-section. We emphasize that users of the molecular data should consult and reference the original sources of data. These sources are now easy to access (see Section 7).

Table 2 provides an overview of the high-resolution portion of the new edition of HITRAN. Columns 4 and 6 of Table 2 are presented to provide a rough comparison with the previous edition of HITRAN. Note that although for some of the molecules the amount of lines and the spectral ranges had not changed, some of the parameters may have changed (see sections below describing individual molecules). There are now 47 molecular species with 120 isotopologues overall (additional species are covered by cross-section data, see Section 3). The spectral coverage of the line-by-line portion ranges from the microwave region through the visible (UV transitions are discussed in Section 4).

2.1. H_2O (molecule 1)

The spectrum of water vapor has significant transitions throughout the complete spectral range of HITRAN. A detailed knowledge of the spectral line parameters of water vapor is paramount not only to remote sensing of planetary atmospheres, but also to disentangle their effect as interferents in the detection and characterization of

Table 1
Description of the quantities present in the 160-character records (transitions) of the line-by-line portion of the HITRAN database.

Parameter	Meaning	Field length	Type	Comments or units
M	Molecule number	2	Integer	HITRAN chronological assignment
I	Isotopologue number	1	Integer	Ordering by terrestrial abundance
ν	Vacuum wavenumber	12	Real[a]	cm^{-1}
S	Intensity	10	Real[a]	$cm^{-1}/(molecule\ cm^{-2})$ at standard 296 K
A	Einstein-A coefficient	10	Real	s^{-1}
γ_{air}	Air-broadened half width	5	Real	HWHM at 296 K (in $cm^{-1}\ atm^{-1}$)
γ_{self}	Self-broadened half width	5	Real	HWHM at 296 K (in $cm^{-1}\ atm^{-1}$)
E''	Lower-state energy	10	Real	cm^{-1}
n	Temperature-dependence coefficient	4	Real	Temperature-dependent exponent for γ_{air}
δ	Air pressure-induced line shift	8	Real	$cm^{-1}\ atm^{-1}$ at 296 K
V'	Upper-state "global" quanta	15	Character	See Table 3 in Ref. [2]
V''	Lower-state "global" quanta	15	Character	See Table 3 in Ref. [2]
Q'	Upper-state "local" quanta	15	Character	See Table 4 in Ref. [2]
Q''	Lower-state "local" quanta	15	Character	See Table 4 in Ref. [2]
Ierr	Uncertainty indices	6	Integer	Accuracy for 6 critical parameters (ν, S, γ_{air}, γ_{self}, n, δ), see Table 5 of Ref. [2]
Iref	Reference indices	12	Integer	References for 6 critical parameters (ν, S, γ_{air}, γ_{self}, n, δ)
*	Flag	1	Character	Pointer to program and data for the case of line mixing
g'	Statistical weight of upper state	7	Real	See details in Ref. [3]
g''	Statistical weight of lower state	7	Real	See details in Ref. [3]

[a] Double precision is recommended for these parameters in order to preserve significant digits and to accommodate some intensity values with very low exponents.

Table 2
Molecules and isotopologues represented in the line-by-line portion of HITRAN.

Molecule	Isotopologue[a]	HITRAN2012 spectral coverage (cm^{-1})	HITRAN2008 spectral coverage (cm^{-1})	HITRAN2012 number of transitions	HITRAN2008 number of transitions
(1) H_2O	161	0–25,711	0–25,233	142,045	37,432
	181	0–19,918	0–14,519	39,903	9753
	171	0–19,946	10–14,473	27,544	6992
	162	0–22,708	0–22,708	13,237	13,238
	182	0–3825	0–3825	1611	1611
	172	1234–1599	1234–1599	175	175
(2) CO_2	626	345–12,785	352–12,785	169,292	128,170
	636	406–12,463	438–12,463	70,611	49,777
	628	0–9558	0–11,423	116,482	79,958
	627	0–9600	0–8271	72,525	19,264
	638	489–6745	489–6745	26,737	26,737
	637	583–6769	583–6769	2953	2953
	828	491–8161	491–8161	7118	7118
	827	626–5047	626–5047	821	821
	727[b]	535–6933	[c]	5187	[c]
	838[b]	4599–4888	4599–4888	121	121
(3) O_3	666	0–6997	0–5787	261,886	249,456
	668	0–2768	0–2768	44,302	44,302
	686	1–2740	1–2740	18,887	18,887
	667	0–2122	0–2122	65,106	65,106
	676	0–2101	0–2101	31,935	31,935
(4) N_2O	446	0–7797	0–7797	33,074	33,074
	456	5–5086	5–5086	4222	4222
	546	4–4704	4–4704	4592	4592
	448	542–4672	542–4672	4250	4250
	447	550–4430	550–4430	1705	1705
(5) **CO**	26	3–8465	3–8465	1019	917
	36	3–6279	3–6279	797	780
	28	3–6267	3–6267	770	760
	27	3–6339	3–6339	728	728
	38	3–6124	3–6124	712	712
	37	1807–6197	1807–6197	580	580
(6) CH_4	211	0–11,502	0–9200	336,830	212,061
	311	0–11,319	0–6070	72,420	28,793
	212	7–6511	7–6511	54,550	45,024
	312	959–1695	959–1695	4213	4213
(7) O_2	66	0–15,928	0–15,928	1787	1431
	68	1–15,853	1–15,852	875	671
	67	0–14,538	0–14,537	11,313	4326
(8) **NO**	46	0–9274	0–9274	103,701	103,701
	56	1609–2061	1609–2061	699	699
	48	1602–2039	1602–2039	679	679
(9) SO_2	626	0–4093	0–4093	72,460	57,963
	646	0–2501	2463–2497	22,661	287
(10) NO_2	646	0–3075	0–3075	104,223	104,223
(11) NH_3	4111	0–7000	0–5295	45,302	27,994
	5111	0–5180	0–5180	1090	1090
(12) HNO_3	146	0–1770	0–1770	903,854	487,254
	156	0–923	[c]	58,108	[c]
(13) **OH**	61	0–19,268	0–19,268	30,772	30 769
	81	0–329	0–329	295	295
	62	0–332	0–332	912	912
(14) **HF**	19	24–46,985	41–11,536	10,073	107
	29	13–47,365	[c]	24,303	[c]
(15) **HCl**	15	8–34,250	20–13,459	11,879	324
	17	8–34,240	20–10,995	11,907	289
	25	5–33,284	[c]	29,994	[c]
	27	5–33,258	[c]	29,911	[c]
(16) **HBr**	19	13–16,034	16–9759	3039	651
	11	13–16,032	16–9758	3031	642

Table 2 (*continued*)

Molecule	Isotopologue[a]	HITRAN2012 spectral coverage (cm^{-1})	HITRAN2008 spectral coverage (cm^{-1})	HITRAN2012 number of transitions	HITRAN2008 number of transitions
	29	7–8781	[c]	1455	[c]
	21	7–8778	[c]	1455	[c]
(17) **HI**	17	10–13,908	12–8488	3161	806
	27	5–7625	[c]	1590	[c]
(18) **ClO**	56	0–1208	0–1208	5721	5721
	76	0–1200	0–1200	5780	5780
(19) **OCS**	622	0–4200	0–4200	15,618	15,618
	624	0–4166	0–4166	6087	6087
	632	0–4056	0–4056	3129	3123
	623	0–4164	0–4164	2886	2788
	822	0–4046	0–4046	1641	1626
(20) **H_2CO**	126	0–3100	0–3100	40,670	36,120
	136	0–117	0–73	2309	563
	128	0–101	0–48	1622	367
(21) **HOCl**	165	1–3800	1–3800	8877	8877
	176	1–3800	1–3800	7399	7399
(22) **N_2**	44	11–9355	1992–2626	1107	120
	45	11–2578	[c]	161	[c]
(23) **HCN**	124	0–3424	0–3424	2955	2955
	134	2–3405	2–3405	652	652
	125	2–3420	2–3420	646	646
(24) **CH_3Cl**	215	0–3198	0–3173	107,642	100,279
	217	0–3198	0–3162	104,854	95,892
(25) **H_2O_2**	1661	0–1731	0–1731	126,983	126,983
(26) **C_2H_2**	1221	604–9890	604–9890	12,613	11,055
	1231	613–6589	613–6589	285	285
	1222	1–789	[c]	7512	[c]
(27) **C_2H_6**	1221	706–3001	706–3001	43,592	28,439
	1231	725–919	[c]	6037	[c]
(28) **PH_3**	1111	0–3602	770–3602	22,189	20,099
(29) **COF_2**	269	696–2002	725–2002	168,793	70,601
	369	686–815	[c]	15,311	[c]
(30) **SF_6**	29	580–996	580–996	2,889,065	2,889,065
(31) **H_2S**	121	2–11,330	2–4257	36,561	12,330
	141	5–11,227	5–4172	11,352	4894
	131	5–11,072	5–4099	6322	3564
(32) **HCOOH**	126	10–1890	10–1890	62,684	62,684
(33) **HO_2**	166	0–3676	0–3676	38,804	38,804
(34) **O**	6	68–159	68–159	2	2
(35) **$ClONO_2$**	5646	763–798	763–798	21,988	21,988
	7646	765–791	765–791	10,211	10,211
(36) **NO^+**	46	1634–2531	1634–2531	1206	1206
(37) **HOBr**	169	0–316	0–316	2177	2177
	161	0–316	0–316	2181	2181
(38) **C_2H_4**	221	701–3243	701–3243	18,097	18,097
	231	2947–3181	2947–3181	281	281
(39) **CH_3OH**	2161	0–1408	0–1408	19,897	19,897
(40) **CH_3Br**	219	794–1706	794–1706	18,692	18,692
	211	796–1697	796–1697	18,219	18,219
(41) **CH_3CN**	2124	890–946	890–946	3572	3572
(42) **CF_4**	29	594–1313	594–1313	60,033	60,033
(43) **C_4H_2**	2211	0–758	[c]	124,126	[c]
(44) **HC_3N**	1224	0–760	[c]	180,332	[c]

Table 2 (*continued*)

Molecule	Isotopologue[a]	HITRAN2012 spectral coverage (cm^{-1})	HITRAN2008 spectral coverage (cm^{-1})	HITRAN2012 number of transitions	HITRAN2008 number of transitions
(45) **H_2**	11	15–36,024	[c]	4017	[c]
	12	3–36,406	[c]	5129	[c]
(46) **CS**	22	1–2586	[c]	1088	[c]
	24	1–1359	[c]	396	[c]
	32	1–1331	[c]	396	[c]
	23	1–156	[c]	198	[c]
(47) **SO_3**	26	0–2825	[c]	10,881	[c]

[a] Abbreviated code for isotopologues.
[b] Isotopologue 727 ($^{17}O^{12}C^{17}O$) introduced into HITRAN for the first time in this edition. Isotopologue 838, which existed in the database before but is of lesser terrestrial abundance, has been reassigned as the 10th isotopologue and has the number zero in the corresponding ASCII format transition field.
[c] Not included in HITRAN2008.

other species. The techniques of experiment and of theory have steadily advanced, and new results often disagree with HITRAN2008 values as well as among themselves. We have conducted a thorough investigation regarding which parameters need to be updated or included in the database. Below we describe deficiencies identified in the HITRAN2008 water-vapor line list and the improvements made to the line list in the HITRAN2012 compilation.

2.1.1. *Deficiencies in the HITRAN2008 H_2O line list*

Several deficiencies related to the water-vapor line list were identified and addressed:

(1) Due to the difficulties associated with measurements of water-vapor line intensities, some values given in HITRAN were reported to have problems. For instance, intensities in the 8000–9000 cm^{-1} spectral region were reported to have been systematically in error (10–15%) by authors of more recent experiments [4], theoretical calculations [5], and atmospheric retrievals [6,7]. Less dramatic, but still noticeable (5–10%) inconsistencies were identified below 8000 cm^{-1} (see, for instance, Refs. [8–10]) where a majority of intensities down to 1750 cm^{-1} (for stronger lines) originated from the unpublished SISAM database of Toth [11]. It is worth pointing out that the SISAM database tabulates intensities obtained both experimentally and using a semi-empirical model. However, only the calculated ones were adopted into the HITRAN database, and it was later determined that the experimental values were often superior to the calculated ones. In fact, the water vapor line list used by the TCCON (Total Carbon Column Observing Network) community [12] employs the measured values by Toth when the retrievals using HITRAN were not satisfactory.

(2) Air-broadened half widths in HITRAN2008 employed a rather sophisticated scheme, explained in Ref. [13], that determines and eliminates the experimental outliers and then either uses the experimental values or their averages if they exist, theoretical values calculated using the complex Robert–Bonamy (CRB) method (see for instance Refs. [14,15]), or if no experimental or theoretical value exists, semi-empirical values from Ref. [16]. There is room for improvement of these values. For instance, it was found that the CRB calculations should have included a larger number of correlation functions, higher-order cut-offs for convergence, and exact trajectories [17]. Failure to do so resulted in underestimation of the widths of some of the lines.

(3) The temperature dependence exponent, n, in HITRAN2008 originated from CRB calculations [14,15] and suffered from the same problems as CRB air-broadened half-widths, as identified by Ma et al. [17]. This problem was also confirmed experimentally by Birk and Wagner [18].

(4) To save disk storage and also due to limited knowledge of reliable spectral line parameters for weak transitions, the previous versions of HITRAN employed a nonlinear (with wavenumber of the transition) intensity cutoff designed to provide transitions that would contribute to absorption over very long paths at telluric temperatures. However, the current cutoff criterion was found to be overly restrictive for remote-sensing applications [6]. Since disk storages have significantly increased in their capacity in recent years and due to the development of new sensitive experimental techniques (e.g. cavity ring-down spectroscopy) on par with advances in theoretical calculations, it was decided that the cutoff criterion established in the first HITRAN edition needed to be relaxed.

2.1.2. *Construction of $H_2{}^{16}O$ line list*

Fig. 2 represents a flow diagram of the construction of the $H_2{}^{16}O$ line list (only for line positions and intensities) for this edition of HITRAN, while a detailed description is given below.

(1) The asymptote of the previous formula for the intensity cutoff has been changed to $S_{crit}=10^{-29}$ cm^{-1}/(molecule cm^{-2}) (from the previous value of 3×10^{-27} cm^{-1}/(molecule cm^{-2})). The formula for the cutoff is

$$S_{cut}(T)=\frac{S_{crit}\nu}{\nu_{crit}}\tanh\left(\frac{c_2\nu}{2T}\right)\quad 0<\nu\le 2000\ cm^{-1}, \tag{1a}$$

$$S_{cut}(T)=S_{crit}\quad \nu>2000\ cm^{-1}, \tag{1b}$$

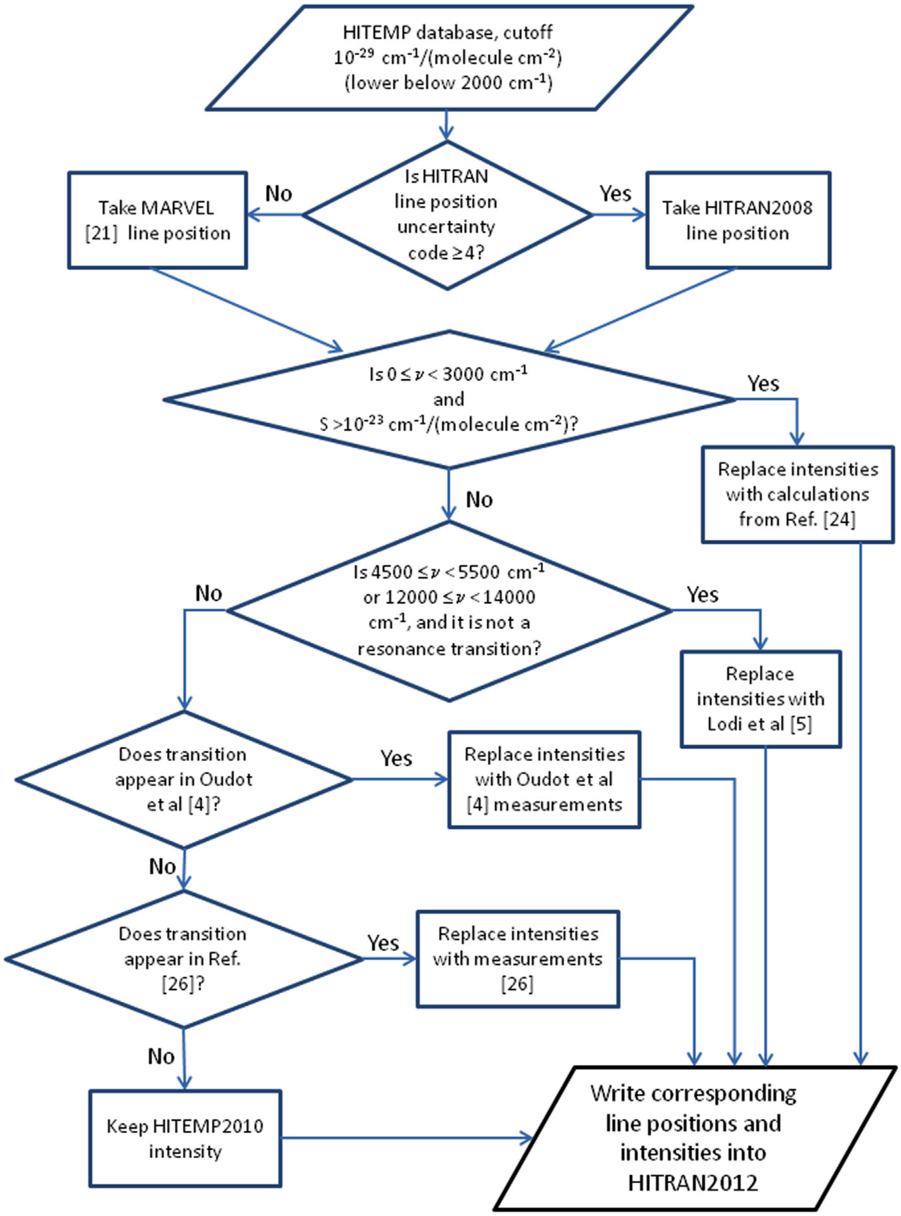

Fig. 2. Flow diagram for the construction of line positions and intensities for the $H_2{}^{16}O$ line list.

where c_2 is the second radiation constant and $T=296$ K. Lines with intensities greater than S_{crit} above $\nu_{crit}=2000\,cm^{-1}$, as well as weaker lines below 2000 cm^{-1}, are now able to enter the database. We applied this cutoff to the water-vapor lines in HITEMP2010 [19], which has intensities originating from the BT2 ab initio line list [20] with corresponding HITRAN2008 transitions, as well as empirically-derived transition wavenumbers replacing ab initio values whenever possible. In other words, instead of starting with a HITRAN2008 dataset, we started to work from the reduced HITEMP database which is essentially the HITRAN2008 database supplemented with weaker lines. Whenever a rotational quantum number could not be determined unambiguously, the index of symmetry (1, 2, 3, and 4 as defined in Ref. [20]) accompanied with a negative sign was used. Note that 1 and 2 indicate para states, whereas 3 and 4 indicate ortho states. For the case of unassigned vibrational quanta, a "-2" label has been adopted.

Owing to this approach, the database not only became more complete but also does not have any lines for which the lower-state energy is not provided (contrary to HITRAN2008 which contained over 800 such lines).

(2) The line positions in HITEMP are either from (a) HITRAN, or (b) a rather outdated collection of empirically-derived transition wavenumbers, or (c) an ab initio origin with uncertainty occasionally reaching 0.3 cm^{-1}. For HITRAN2012, some of these line positions were improved using the following procedure.

A very extensive international effort was recently carried out to derive empirical energy levels of water vapor from the available measured line positions [21] using a procedure known as MARVEL [22,23] which involves inverting a cleansed and weighted set of transitions. This database of energy levels is then used to generate a dataset of all allowed transitions between these levels. Here "allowed" refers to transitions with $\Delta J=0, \pm 1$, and ortho–ortho and para–para transitions. These transition wavenumbers replaced the HITEMP values, unless these values originated from HITRAN and have uncertainty indices larger than 4 (i.e. good to 0.001 to 0.0001 cm^{-1}). It is important to note that previous versions of HITRAN had erroneously assigned an uncertainty code "3" to *all* of the line positions originating from SISAM [11]. We have reassigned uncertainty codes for the line positions from the SISAM database in HITRAN before introducing MARVEL values using the abovementioned criteria.

(3) In HITRAN2008, experimental intensities from the work of Coudert et al. [8] were employed wherever available and the quality of these intensities has proved to be superior to HITRAN2004 data from SISAM [11] available in this region. We now employ calculated intensities from the work of Martin et al. [24] that now extend to higher wavenumber. Considering that only strong lines in the 0–3000 cm^{-1} region from that work were evaluated, we adopted intensities stronger than 10^{-23} cm^{-1}/(molecule cm^{-2}) from that work in the 800–3000 cm^{-1} region, and intensities stronger than 10^{-26} cm^{-1}/(molecule cm^{-2}) below 800 cm^{-1}.

(4) Newer ab initio intensities from the work of Lodi et al. [5] were incorporated in the 4500–5500 cm^{-1} and 12,000–14,000 cm^{-1} regions. These are the only regions from this work that were thoroughly evaluated and these theoretical intensities are superior not only in comparison with BT2 ab initio values but also with the available experimental data (for most of the transitions). The ab initio intensities improve on previous studies by (a) using high-quality ab initio calculations specifically designed to converge the dipole moment and (b) using sensitivity analysis to identify those transitions involved in intensity borrowing via resonances, for which the computed results are not reliable [19]. Fig. 3 clearly demonstrates that there is substantially better consistency among the bands in Lodi et al. than the BT2 work. Intensities shown in the figure span the 4700–5000 cm^{-1} region. In particular, one can see that in the BT2 work, line intensities calculated for the $3\nu_2$ band were consistently poor, while the $\nu_1+\nu_2$ and $\nu_2+\nu_3$ bands agreed very well with experimental data. We also evaluated the 4500–5000 cm^{-1} region using retrievals from the solar pointing FTS at Park Falls, Wisconsin, and found the Lodi et al. data superior to other publicly available datasets [25]. A separate publication describing this work is planned. Note that in the 12,000–14,000 cm^{-1} region, a rather large number of resonance lines occur for which reliable theoretical predictions are not yet available; for those lines the previous HITRAN entries have been retained.

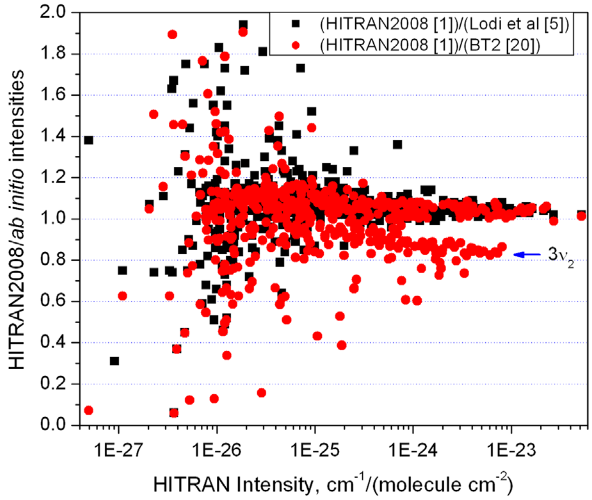

Fig. 3. Comparison of HITRAN2008 with the values of BT2 [20] (red circles) and with the values of Lodi et al. [5] (black squares) in the 4700–5000 cm^{-1} region.

(5) Intensities from the work of Oudot et al. [4] were adopted in the 8000–9000 cm^{-1} spectral region wherever available. Also, intensities from unpublished, high-accuracy work by Wagner and Birk [26] in the 1-μm region were taken wherever available. The quality of the intensity data was confirmed by intercomparison with cavity ring-down results [27]. Agreement in intensities with [27] was better than 1%. For the vibrational band (201←000), agreement with Lodi and Tennyson [5] is better than 1%.

2.1.3. Construction of $H_2{}^{18}O$ and $H_2{}^{17}O$ line lists

Line positions and intensities were taken from the line lists of Lodi and Tennyson [28] for the entire HITRAN2012 line list of the $H_2{}^{18}O$ and $H_2{}^{17}O$ isotopologues. In Ref. [28], line positions and intensities were calculated using the potential energy surface of Shirin et al. [29] and the dipole moment function of Lodi et al. [5]. Line intensities in the case of the ν_2 band of $H_2{}^{18}O$ were compared to experimental data which are an unpublished part of the line intensities [8] and line broadening [18] work of Birk and Wagner. Agreement better than 1% was found. The line positions were supplemented with transition wavenumbers derived from the corresponding MARVEL dataset [30].

For HITRAN2012, line positions from the SISAM database [11] with uncertainties better than 0.001 cm^{-1} were substituted in place of those from the Lodi and Tennyson list [28]. Finally, we made full quantum assignments for just under a hundred unassigned lines from the Lodi and Tennyson list [28].

2.1.4. HDO line list corrections

An error was discovered in the transcription of the intensities of HDO line parameters above 11,500 cm^{-1}. They were a factor of 10 too large in the 2008 release of HITRAN, and have now been corrected.

2.1.5. Line-shape parameters for $H_2{}^{16}O$, $H_2{}^{18}O$ and $H_2{}^{17}O$

The air-broadened half widths for the first three isotopologues of water molecules continue to be derived using the procedure described by Gordon et al. [13], with some experimental outliers identified and removed. Some of the outliers were identified in the work of Ma et al. [31]. It is worth noting that recent measurements by Birk and Wagner [18] in the ν_2 band region were given priority and were written into the database directly. These data were checked using the partner transition scheme [32] which indicates transitions with the upper and lower rotational quantum numbers reversed should have half widths that agree to within several percent in the ν_2 band region. This fact was confirmed for most of the two hundred pairs of transitions in the data indicating the high quality of the data. In fact the data are so good it is possible to see partner scheme differences between ν_2 and $2\nu_2-\nu_2$ transitions.

In the work of Birk and Wagner, a large effort was undertaken to deliver data with consolidated error bars. Agreement of measured and modeled data of the nadir-sounding satellite instrument IASI was significantly improved with the new pressure broadening data [33].

A new procedure has been developed for the temperature dependences of air-broadened half widths. For all the transitions in different bands that had the same rotational quantum assignments with those measured in Birk and Wagner [18], these measurements were used. Next, the temperature-dependence exponents of the air-broadened half widths from new CRB calculations using a 20 4 4 potential expansion, "exact" trajectories and full velocity integral for rotational band transitions, were added to the database. While the CRB potential is not fully optimized, the values for these temperature-dependence exponents are better than those obtained from *J*-averaged values. Lastly, for those transitions for which no data are available from the above procedures, experimental values from Ref. [18] averaged as a function of *J* were employed.

2.1.6. Future work

Further evaluation of the ab initio intensities from Lodi et al. [5] is ongoing, and in the future they may be recommended to be the main source of intensities throughout the entire database for the principal isotopologue of water vapor, with the exception of the resonant lines. So far, differences up to 8% between experimental data and ab initio work for entire vibrational bands are known [26].

As mentioned above, it was found that the quality of the CRB calculations of line-shape parameters should improve significantly, especially for narrower lines, if one uses a larger number of correlation functions, higher-order cut-offs for convergence, and exact trajectories [17]. The quality of calculations can also be improved by using the better-determined intermolecular potential constants and wavefunctions from ab initio calculations to replace the currently implemented Hamiltonian approach. This work is currently underway. Some of the semi-empirical values of Jacquemart et al. [16] employed part of the outdated CRB and experimental values in their derivation and therefore will also need to be reevaluated. We will also monitor the availability of parameters for alternative line-shape representations.

A line list similar to that of Lodi and Tennyson for $H_2{}^{18}O$ and $H_2{}^{17}O$ [28] is being constructed for HDO using the VTT ab initio dataset [34] supplemented with line positions derived from the corresponding MARVEL levels [35]. Although in this edition some of the HDO line shifts were introduced from the work of Jenouvrier et al. [10], most of the line shifts are still missing above 2000 cm^{-1} for this isotopologue and more experiments and calculations are needed, while some of the existing line shifts, including those from Ref. [36], need to be assessed.

2.2. CO_2 (molecule 2)

High-quality reference spectroscopic data for the carbon dioxide molecule remains one of the top priorities for the HITRAN database, due in part to its importance for the environmental satellite missions, including OCO-2 [37] and GOSAT [38] and its importance to the studies of the atmospheres of Mars and Venus [39].

HITRAN2008 featured an extensive update in the operational region of the OCO-2 satellite (4300–7000 cm^{-1}). Spectral parameters for the strong and medium-strength lines were taken from Toth et al. [40], while spectral parameters for weak lines were adapted from the Carbon Dioxide Spectroscopic Databank CDSD-296 [41] or experimental values from more sensitive CRDS experiments (see Fig. 4 in the HITRAN2008 paper). For the lines outside that range, only a few bands were updated with more recent results, while the CDSD values were used to fill in the majority of the missing lines to accommodate a low intensity cut-off of 4×10^{-30} cm^{-1}/(molecule cm^{-2}).

For the first four most abundant isotopologues in HITRAN2012, we replaced all parameters taken from the previous version of CDSD with its newer edition. We also used new CDSD values to replace a majority of the line parameters throughout the CO_2 dataset unless these lines originated from very accurate experiments (including those from Ref. [40]). It is therefore important to give some background on the new version of the CDSD databank.

In 2003 the first version of the Carbon Dioxide Spectroscopic Databank, CDSD-296, aimed at atmospheric applications, was created [42]. CDSD-296 line positions and energy-level wavenumbers were calculated values based on the effective Hamiltonian and the effective dipole moment models. Later, in 2008, this version was updated and expanded [41]. The expanded CDSD-296 included 419,610 transitions of the seven most abundant CO_2 isotopologues covering the 5.9 to 12,784.1 cm^{-1} spectral range. A large portion of CDSD-296 data was included into HITRAN2008.

Since that time a large number of experimental studies of CO_2 line positions and intensities have been performed. In particular, a considerable amount of new experimental information on rare isotopologues has become available [43–46].

Measured line positions and intensities previously collected [41] from the literature were augmented with measurements from recent papers (including those from

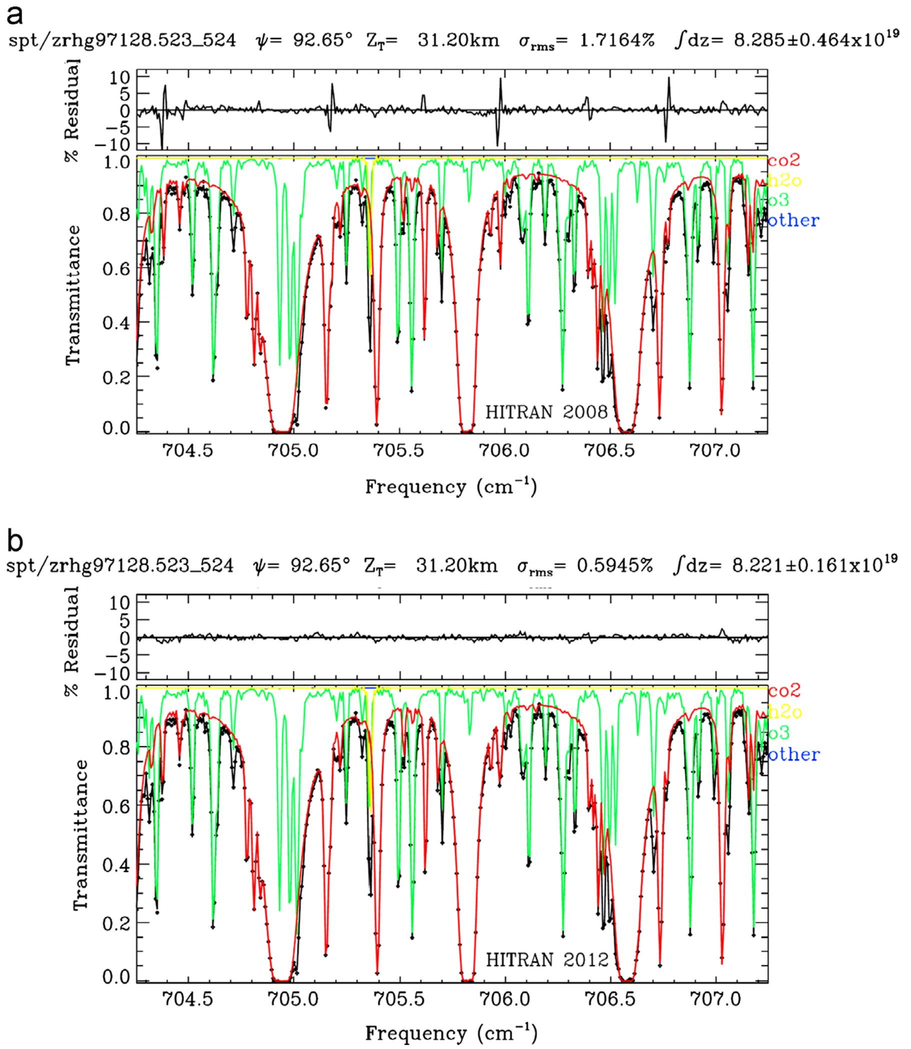

Fig. 4. MkIV balloon spectrum showing the residuals when using (a) HITRAN2008 and (b) HITRAN2012.

[43–60]). In total more than 140,000 measured line positions and nearly 44,000 measured line intensities belonging to the 12 isotopologues $^{12}C^{16}O_2$, $^{13}C^{16}O_2$, $^{16}O^{12}C^{18}O$, $^{16}O^{12}C^{17}O$, $^{16}O^{13}C^{18}O$, $^{16}O^{13}C^{17}O$, $^{12}C^{18}O_2$, $^{17}O^{12}C^{18}O$,$^{12}C^{17}O_2$, $^{13}C^{18}O_2$, $^{17}O^{13}C^{18}O$, $^{13}C^{17}O_2$ were used to form the line position and intensity data files. The data files of the measured positions were critically evaluated and the sets of experimental energy levels for each isotopologue were obtained. Details of this approach as applied to the CO molecule are given in Ref. [61]. The data files of the measured line intensities were also critically evaluated and cleansed of bad measurements. The resulting data files were used as input data to fit parameters of the effective Hamiltonians and effective dipole moment operators. Then the fitted models were used to calculate all possible transitions whose intensities are greater than 10^{-30} cm^{-1}/(molecule cm^{-2}) at 296 K (excluding those belonging to a number of bands of the asymmetric species with an even value of $\Delta\nu_3+\Delta\nu_2$ for which no line-intensity measurements have yet been performed). Finally, calculated transition frequencies were systematically substituted (where possible) by differences of the upper and lower experimental energy levels. The final line list covers the 3.68–12,784 cm^{-1} spectral range. So far only data for the four most abundant isotopologues ($^{12}C^{16}O_2$, $^{13}C^{16}O_2$, $^{16}O^{12}C^{18}O$, $^{16}O^{12}C^{17}O$) were validated. We therefore adapted only data corresponding to these isotopologues from this new version of CDSD into HITRAN2012. We also added a new isotopologue, $^{12}C^{17}O_2$, based on the CDSD database. With that we note that $^{12}C^{17}O_2$ is more abundant than $^{13}C^{18}O_2$ that was included into HITRAN2008 as isotopologue number "9". We therefore renumbered $^{13}C^{18}O_2$ to be isotopologue number "10", while $^{12}C^{17}O_2$ had become isotopologue number "9" in HITRAN2012. As one of the highlights of the HITRAN2012 data for carbon dioxide, we would like to stress the increase in the amount (72,525 lines as opposed to 19,264 in HITRAN2008) and the quality of spectral lines and their parameters for $^{16}O^{12}C^{17}O$. This became possible through new experimental data which previously were very sparse for this isotopologue. Fig. 4 shows the MkIV balloon spectra in the 706 cm^{-1} region fitted using HITRAN2008 and HITRAN2012. The residuals (RMS) change from 1.72% (using

HITRAN2008) to 0.59% (using HITRAN2012). This is due to substantial improvement in the line positions for this isotopologue.

The line-shape parameters now originate from the recent theoretical and semi-empirical calculations [62–65], which are in excellent agreement with high-quality experimental data. However, wherever these high-quality experimental data were available, they were substituted in place of the corresponding calculated ones.

The resultant dataset will then be used to update the line-mixing algorithm developed by Lamouroux et al. [66]. The new line-mixing algorithm will become available in one of the imminent updates to HITRAN2012.

2.3. O_3 (molecule 3)

Ozone is one of the most important molecules for atmospheric and environmental applications of spectroscopic data. Apart from the well-known issues concerning the control of the ozone pollution in the troposphere and the ozone layer in the upper-atmosphere, a detection of ozone in the atmospheres of exosolar planets might be an indicator of the presence of oxygen. In this HITRAN edition, a major improvement has been made concerning ozone bands corresponding to highly excited vibration states which are required for validation of the molecular potential energy surfaces (PES) [67,68] and for a correct account of non-local thermodynamic equilibrium effects [69] in the modeling of emission and absorption properties of the middle and upper atmosphere.

The information concerning the changes in HITRAN parameters is summarized in Tables 3 and 4. In total, seven updated bands between 3297.46 and 5526.30 cm^{-1} (Table 3) and 28 new bands between 3492.69 and 6996.68 cm^{-1} (Table 4) were added to the line-by-line ozone list using a two-step procedure. First, the parameters of spectroscopic models, line positions, intensities, and lower-state energy levels resulting from analyses of experimental spectra [70–78] have been introduced to the S&MPO (Spectroscopy and Molecular Properties of Ozone) information system [79] which offers various tools for spectra simulations and their comparison with experimental records. After the validation via S&MPO, the line-list in the HITRAN format has been generated with an appropriate cut-off. An overview of the resulting line list is presented in Fig. 5.

The data for updated bands (Table 3), as well as for newly provided bands up to 5800 cm^{-1} (Table 4), are based on analyses of FTS spectra [70–73] recorded by the Groupe de Spectrométrie Moléculaire et Atmosphérique (GSMA) laboratory of Reims University with improved signal-to-noise ratio. Spectral parameters of two bands, $\nu_1+2\nu_2+\nu_3$ and $2\nu_2+2\nu_3$ from Ref. [70], were replaced by new data of Ref. [71] completed by the previously unobserved band $2\nu_1+2\nu_2$. The analysis of this [(022), (121), (220)] triad has been improved due to better characterization of resonance coupling parameters (using the PES of Ref. [68]) which was not well defined in the previous studies. The drastically increased number of assigned transitions has allowed a significant improvement in line intensities of $2\nu_2+2\nu_3$ and of the Q-branch of $\nu_1+2\nu_2+\nu_3$ as well as for transitions corresponding to large values of rotational quantum numbers. An example of the improvement of the spectra modeling is given in Fig. 6.

The line positions of all four hot bands in Table 3 and of the $3\nu_1+2\nu_2-\nu_1$ band (Table 4) have been calculated by using effective Hamiltonian parameters of Ref. [72]. Line strengths of these five bands were improved from a fit of the corresponding dipole transition moment parameters to experimental intensities [71], whereas they were extrapolated from cold bands in previous studies.

The new dataset covers the spectral range up to 6996.68 cm^{-1} (Table 4). All data above 5800 cm^{-1} are based on analyses of very sensitive data obtained using cavity ring down spectroscopy (CRDS) [74–78] recorded in the Laboratoire Interdisciplinaire de Physique (LIPhy) of Grenoble University providing information on weak bands which were missing in previous HITRAN editions. For this dataset, we have slightly extended the format of vibration quantum numbers because the normal mode assignment for the corresponding excited vibrations is ambiguous for some states (a local mode assignment not being universally applicable as well). Following the original works [74–78], the vibrational assignment has been provided by the decomposition of the effective wavefunctions in the normal mode basis set as computed from the PES of Ref. [67] using the MOL_CT program suite [80]. As a result, the same normal mode basis function could give major contributions to two different vibration states. This occurs when the normal modes are strongly mixed due to anharmonic resonance interactions. In these cases, an additional (lower case) ranking index was thus added

Table 3
Updated bands for $^{16}O_3$.

Band	Number of lines	Spectral range (cm^{-1})	S_ν	References for ν, S
022–000	1336	3297.46–3478.53	9.936	[71,71]
121–000	1611	3383.04–3483.38	62.720	[71,71]
113–100	658	3490.53–3565.76	4.038	[72,71]
014–001	1136	3520.70–3605.15	12.251	[72,71]
014–100	13	3533.85–3562.08	0.029	[72,71]
113–001	12	3543.34–3604.91	0.036	[72,71]
213–000[a]	954	5447.73–5526.30	9.627	[71,71]

Note: S_v is the sum of line intensities in units of 10^{-23} cm^{-1}/(molecule cm^{-2}) at 296 K for the corresponding bands included in the line list, ν is the line position, and S is the line intensity.

[a] This band was labeled as 015–000 in the previous version of HITRAN.

Table 4
Newly included $^{16}O_3$ bands.

Band	Number of lines	Spectral range (cm^{-1})	S_v	References for ν, S
320–100	20	3492.69–3562.58	0.058	[72,71]
220–000	553	3500.08–3635.88	2.629	[71,71]
114–000	538	5443.69–5574.11	2.206	[71,71]
080–000	7	5474.65–5524.06	0.018	[71,71]
321–000	123	5532.36–5569.38	0.521	[71,71]
105_1–000	730	5708.95–5790.90	4.943	[73,73]
421–010	303	5815.58–5873.74	0.036	[74,74]
133–000	702	5852.44–5931.22	0.472	[75,75]
411–000	444	5895.17–5956.76	0.138	[75,75]
233_1–010	528	5941.73–6021.44	0.079	[76,76]
034–000	264	5956.88–6078.00	0.085	[77,77]
105_2–000	678	5983.44–6071.43	0.210	[77,77]
124_1–000	999	6019.98–6201.30	0.294	[77,77]
223_1–000	954	6031.75–6130.78	1.179	[77,77]
510–000	39	6067.96–6136.40	0.013	[77,77]
331–000	168	6163.49–6207.75	0.014	[77,77]
025–000	1003	6225.12–6311.46	0.770	[78,78]
124_2–000	78	6246.40–6363.42	0.034	[78,78]
430–000	111	6284.63–6395.38	0.031	[78,78]
501–000	749	6301.80–6365.48	0.637	[78,78]
223_2–000	777	6318.03–6393.74	0.679	[78,78]
421–000	409	6503.67–6574.40	0.087	[74,74]
205_1–000	570	6525.82–6593.61	0.197	[74,74]
233_1–000	754	6641.08–6722.18	0.158	[76,76]
242–000	457	6665.49–6822.32	0.029	[76,76]
520–000	33	6677.10–6771.82	0.002	[76,76]
511–000	317	6945.09–6989.76	0.024	[74,74]
233_2–000	417	6950.18–6996.68	0.045	[74,74]

Note: S_v is the sum of line intensities in units of 10^{-23} cm^{-1}/(molecule cm^{-2}) at 296 K for the corresponding bands included in the line lists, ν is the line position, and S is the line intensity.

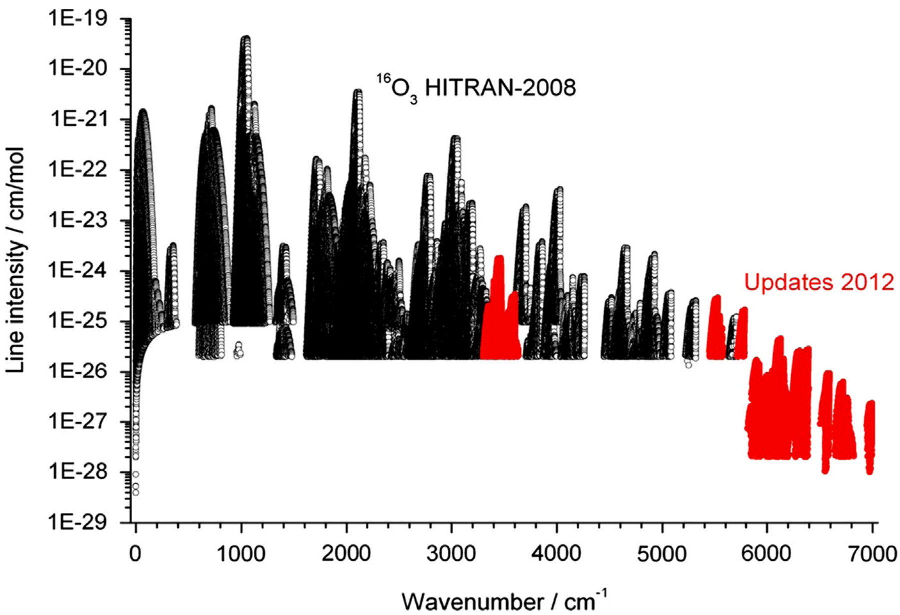

Fig. 5. Schematic overview of the ozone $^{16}O_3$ transitions in the HITRAN2012 edition. Each of the 261,886 lines corresponds to a circle or a triangle on the log intensity scale. New data added since the 2008 edition are marked with red full circles. (To understand the use of color in this figure, please see the web version of this paper.)

according to increasing vibration energy. Because of these considerations, the vibration labels for some states have been changed with respect to previous intuitive assignments: the band in the range 5625.97–5704.62 cm^{-1} previously labeled as (213)–(000) is now reassigned as (015)–(000).

The line lists were generated by the teams of GSMA (Reims) and of the Laboratory of Theoretical Spectroscopy

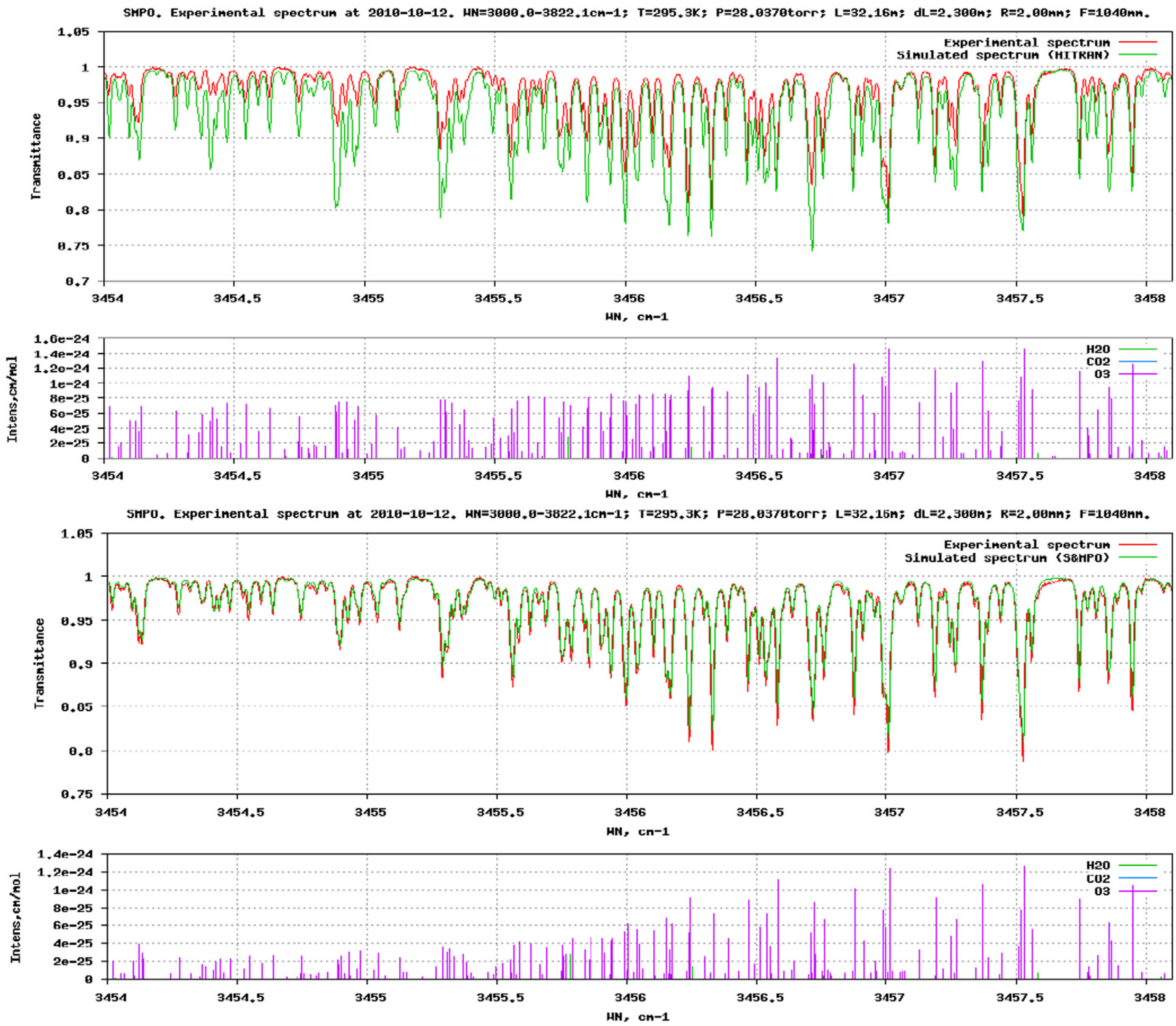

Fig. 6. Example of an improvement of the Q branch for the $\nu_1+2\nu_2+\nu_3$ ozone band. The top panel is a comparison of the observed spectrum (in red) with calculations using HITRAN2008 data (in green); the bottom panel is a calculation with new data from S&MPO (including a few impurity lines marked in blue in the stick diagram).

of the V.E. Zuev Institute of Atmospheric Optics (Tomsk) following the corresponding analyses of experimental spectra [70–78]. In the high wavenumber range above 5000 cm^{-1}, the line position fits using effective models gave a satisfactory agreement (rms$\sim$0.003–0.015 cm^{-1}) but did not reach the experimental accuracy ($\sim$0.001–0.003 cm^{-1}). This concerns particularly the CRDS range. In these cases, the empirical corrections on line positions were applied as follows: the corresponding line list contained all allowed transitions computed as differences among energy levels derived from experimental spectra measured in Grenoble. All line intensities were computed from effective dipole transition parameters. The intensity cutoff was fixed to 10^{-26} and 2×10^{-28} cm^{-1}/(molecule cm^{-2}) below and above 5800 cm^{-1}, respectively.

Altogether for this edition, 5720 ozone lines were updated (Table 3) and 12,725 lines of new bands (Table 4) were added for the $^{16}O_3$ list. The lesser ozone isotopologue line lists were not changed. The current state-of-art of the ozone high-resolution studies is described in the review paper of this Special Issue [81].

2.4. N_2O (molecule 4)

Unchanged.

2.5. CO (molecule 5)

The line parameters including line intensities, self- and air-broadening parameters, temperature dependence and air-induced line shifts, of the first overtone band of the three most abundant CO isotopologues $^{12}C^{16}O$, $^{13}C^{16}O$, $^{12}C^{18}O$, have been updated, based on the experimental works of [82], and of [83]. The fitting of the experimental data in these works has employed the speed-dependent Voigt profile and took into account line-mixing using the

Table 5
The format used for the additional spectroscopic parameters for CO and its isotopologues.

Parameter	Speed dependence	Air line-mixing	Rozenkranz air line-mixing	Temperature dependence of line shift	Self line-mixing	Rozenkranz self line-mixing
Field length	7	8	8	9	8	8
Data type	Real	Real	Real	Real	Real	Real

Note: For the line-mixing pair $P(J)\sim P(J+1)$ or $R(J)\sim R(J+1)$, the corresponding line-mixing parameters are listed with the $P(J)$ or $R(J)$ line.

Table 6
Overview of growth of the methane line list during the past 30 years of HITRAN editions.

HITRAN Year	Number of lines	Minimum IR intensity[a]	ν_{max} (cm^{-1})	Number of isotopologues[b]
2012	468,013	1×10^{-29}	11,500	4
2008	290,091	1×10^{-29}	9200	4
2004	251,440	1×10^{-29}	9200	3
2001	211,465	8×10^{-29}	6185	3
1996	48,032	1×10^{-24}	6185	3
1992	47,415	4×10^{-24}	6107	3
1986	17,774	4×10^{-24}	6107	3
1982	11,803	3×10^{-24}	4667	3

[a] The minimum intensity for the far-IR is several orders of magnitude weaker than the value selected for the IR. Units of cm^{-1}/(molecule cm^{-2}).
[b] The four isotopologues are $^{12}CH_4$, $^{13}CH_4$, $^{12}CH_3D$, and $^{13}CH_3D$ (the last one added in 2008).

off-diagonal relaxation matrix formalism [84]. Based on these works, for $^{12}C^{16}O$, the speed dependence of the broadening, self and air off-diagonal line-mixing, as well as Rosenkranz [85] self and air line-mixing parameters, and the temperature dependence of line shift were introduced in a separate file that lists HITRAN molecule and isotopologue numbers, quantum numbers and the new parameters in the order shown in Table 5.

For the bands where no measurements of air-induced line shifts are available, the values were derived indirectly from the highly-accurate measurements of the line shifts of the 2–0 band, using the approach based on the theory of Ref. [86].

The line list of the 0–0 bands of the three most abundant CO isotopologues $^{12}C^{16}O$, $^{13}C^{16}O$, $^{12}C^{18}O$, and the 1–1 band of $^{12}C^{16}O$, have been updated and extended to higher-J lines, based on the Cologne Database for Molecular Spectroscopy (CDMS) [87]. The 2–2 and 3–3 bands of $^{12}C^{16}O$ have been added to the HITRAN line list for the first time from CDMS. The data is largerly based on the fit of the data from experiments described in Refs. [88,89].

2.6. CH_4 (molecule 6)

An unprecedented update in terms of extent and quality of methane molecular line parameters was implemented for the HITRAN compilation by including new global analyses and measurements for $^{12}CH_4$, $^{13}CH_4$ and $^{12}CH_3D$. Details of the update can be found in Brown et al. [90]; here we summarize the major changes since the last edition of HITRAN [1].

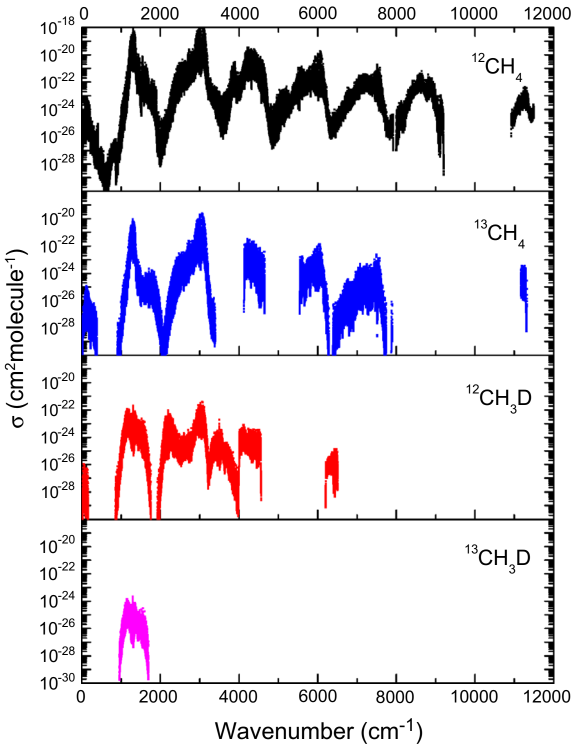

Fig. 7. Log plot of the cross-sections generated from the line list for the four isotopologues of methane from 0 to 12,000 cm^{-1} (generated at 0.05 cm^{-1} resolution, one atmosphere, and 296 K).

High-resolution spectroscopy of methane and the generation of accurate line lists, especially as one moves up the polyad ladder to shorter and shorter wavelength (necessary for many applications) is extremely challenging. Fortunately, the experimental techniques and the theoretical modeling continue to make great strides. Each new edition of the HITRAN database has witnessed major improvements for methane; Table 6 provides an overview of the evolution. The latest methane line list is a significant expansion of information (and in the near-infrared, of quality).

A rough graphical overview of the spectral coverage now available for the four isotopologues of methane is shown in Fig. 7. To visualize the spectral lines in the line list, the plot is of absorption cross-sections generated at 0.05 cm^{-1} resolution, assuming one atmosphere and 296 K. Of course the effects of the line-shape parameters and the density of lines cannot be fully appreciated in this figure.

For the new compilation, more than 70% of HITRAN2008 methane transitions have been replaced. Just over 84,000 existing lines were retained: CH_4 in two regions (4800–5550 cm^{-1} and 8000–9200 cm^{-1}), some hot bands of $^{12}CH_4$ (1887–3370 cm^{-1}), the dyad of $^{13}CH_4$ (6–8 μm), $^{12}CH_3D$ (7–4076 cm^{-1}), and the ν_6 band of $^{13}CH_3D$ near 8.7 μm. With a minimum intensity (at 296 K) set to 10^{-37} cm^{-1}/(molecule cm^{-2}) for the far-IR and 10^{-29} cm^{-1}/(molecule cm^{-2}) for the mid- and near-IR, the new database more than doubled the number of lines in the 2008 compilation. Part of the size increase occurred because the minimum intensity criterion for $^{12}CH_4$ and $^{13}CH_4$ transitions above 600 cm^{-1} was lowered by two orders of magnitude. In addition, global analyses for $^{12}CH_4$ [91] and $^{13}CH_4$ [92,93] obtained a better characterization of the dyad, pentad and octad polyads up through 2.2 μm. As a result, many weaker high-*J* and hot band transitions, important for outer planet and exoplanet atmospheres, could be compiled, including for the first time the Octad–Pentad difference bands whose transitions fall between 5 and 9 μm. Accuracies of some calculated positions were further improved by forming "empirical upper-state levels" based on secure quantum assignments and re-computing the line positions; entries changed in this manner are flagged by the position accuracy code set to be greater than 1. For the first time, the database (in the 2.2–4.0 μm region) added one $^{12}CH_4$ hot band $2\nu_3$–ν_4 [94], the three strongest bands of the $^{13}CH_4$ octad (ν_1+ν_4, ν_3+ν_4, ν_2+ν_3) [93] and eleven bands of $^{12}CH_3D$ [95].

For the most part, the predicted infrared transitions arising from the ground state are expected to be very similar to prior calculated values. However, in HITRAN2008, the far-IR intensities of the ground state to ground state lines had been scaled by 1.15 based on new measurements of cold methane manifolds [96]. Later, Boudon et al. [97] reported new line-by-line intensities that were on average higher than the original intensities by about 1%. The newer far-IR results were applied for HITRAN2012.

Above 5550 cm^{-1}, the new database was formed using observed line positions and intensities, some with empirical lower-state energies determined from cold spectra. Some 20,000 entries from the prior laboratory measurements [98] were replaced with 68,000 new values reported from extensive new FTIR analysis (5550–5852 cm^{-1}) [38] combined with differential absorption spectroscopy (DAS) and cavity ring down spectroscopy (CRDS) from 5852 to 7912 cm^{-1}. The latter study by Campargue et al. [99] relied on analysis of intensities measured at cold and room temperatures to provide empirical lower-state energies for many observed $^{12}CH_4$, $^{13}CH_4$ and $^{12}CH_3D$ features.

While no methane parameters between 8000 and 9200 cm^{-1} were altered, over 11,000 measured positions, intensities, and empirical lower-state energies from cold CH_4 spectra were added for the first time between 10,923 and 11,502 cm^{-1} [100]. However, the region near 10,100 cm^{-1} is still not included in the compilation.

There were some special modifications to the database that should be noted. To enable the use of methane line positions as frequency calibration standards, a few hundred high-accuracy (10^{-6}–10^{-5} cm^{-1}) values replaced predicted lines for selected transitions of ν_3 near 3000 cm^{-1} [101] and $2\nu_3$ near 6000 cm^{-1} [102]. We also revised the Einstein-A coefficients for both deuterated isotopologues.

Available Voigt pressure broadening measurements from HITRAN2008 were transferred into the new compilation, but most of the lines were given crudely-estimated half widths, as described in Brown et al. [90]. For stronger far-IR transitions, new measured nitrogen and self broadening half widths [103] were adopted.

Much of the extensive updates occurred because experimental and theoretical research were undertaken specifically to support the analyses of Saturn and Titan by the Cassini mission [104]. However, there is still much work to be done to have the comprehensive database required for remote sensing of all atmospheres (Earth, planets, exoplanets, moons, etc.).

Our knowledge of pressure broadening of methane by air, N_2, H_2, and He is incomplete, particularly for the near-infrared. Basic coefficients of Lorentz broadening (widths, shifts, temperature dependence) all vary as a function of the transition quantum numbers, and values obtained for the fundamentals are not easily applicable to the very complicated polyads having dozens of underlying vibrational states. Good theoretical models, confirmed by measurements, must be implemented in order to have accurate values, not the rough estimates used here for 99% of the present database. However, for applications that require the highest accuracies for intensities and broadening, Voigt line shapes are inadequate. Studies of line mixing, speed dependence and narrowing are required to provide the basic parameters for future methane compilations in the most utilized spectral regions.

Theoretical analyses of measured positions and intensities are required to identify the quantum numbers and produce models that predict all transitions that are likely to be required by applications, not just the ones seen in laboratory spectra. The extensive new cold and room temperature measurements between 5850 and 7900 cm^{-1} may successfully be reproduced in this decade using current Hamiltonian methods, but adequately characterizing the methane spectra at even shorter wavelengths still seems intractable. As discussed in Ref. [90], ab initio methods are being investigated to interpret near-infrared methane spectra. Forming a complete database requires predictions of both positions and intensities, and as usual, the accuracies of individual line intensities in the present effort will vary greatly. Intensity measurements are needed to confirm and improve the quality of predicted weak lines, particularly for the new hot-band transitions to support studies of exoplanet atmospheres.

2.7. O_2 (molecule 7)

In HITRAN, molecular oxygen is represented in HITRAN by both magnetic dipole and electric quadrupole transitions. Although these types of transitions are intrinsically weaker than electric dipole transitions, the large abundance of oxygen in the terrestrial atmosphere produces noticeable absorption. Another aspect of oxygen in HITRAN is that the transitions also involve several different electronic states. Owing to its uniformly-mixed constituent profile, it is often used as a benchmark in satellite retrieval algorithms. It is thus critical to provide highly accurate spectroscopic constants for oxygen. In the past, classic laboratory measurements were lacking in accuracy, coverage of higher rotational levels, and isotopologues. Recent experiments have made significant progress, and we have made use of these for improvements in HITRAN, as discussed below.

2.7.1. Microwave region

A detailed description of the update in the microwave region is described in Mackie et al. [105]. Here a brief summary is given.

The line positions for the $X\,^3\Sigma_g^-\ (v=0)-X\,^3\Sigma_g^-(v=0)$ and $X\,^3\Sigma_g^-(v=1)-X\,^3\Sigma_g^-(v=1)$ bands for $^{16}O_2$ and the $X\,^3\Sigma_g^-(v=0)-X\,^3\Sigma_g^-(v=0)$ band for $^{16}O^{18}O$ and $^{16}O^{17}O$ were recalculated using spectroscopic constants derived by Leshchishina et al. [106,107]. HITRAN line-shape parameters for the microwave bands of oxygen were previously estimated from the data from electronic bands and in particular did not distinguish between $\Delta N=0$ and $\Delta N=2$ transitions. Here we applied a semi-empirical model for calculating air-broadened half width values. This was derived based on N_2-broadening measurements of Tretyakov et al. [108] and Golubiatnikov and Krupnov [109] and self-broadening measurements in Refs. [108–111]. The self-broadened values are now based on Refs. [108–111].

Transitions with $N'=1$ were given a temperature-dependence of 0.97, transitions with $N'=2$ were given a temperature-dependence of 0.86, and transitions with $N'\geq 3$ were given a temperature-dependence of 0.72 based on measurements by Drouin [112].

Finally, the quantum assignments were corrected for some of the lines in the MW region.

This update of line parameters in the MW region is a substantial improvement, especially for the line-broadening parameters.

2.7.2. $a^1\Delta_g$–$X^3\Sigma_g^-$ transitions (around 1.27 μm)

In 2009 an update to the HITRAN2008 oxygen file was issued featuring substantial improvements based on the work of Newman et al. [113] and Washenfelder et al. [114].

For the 2012 release, further improvements for this band were made. A detailed description of the update for the $a^1\Delta_g-X^3\Sigma_g^-$ transitions is also described in Mackie et al. [105] with a brief summary given here.

Recent CRDS measurements of line positions and intensities in this band [106,107,115,116] for all stable isotopologues of molecular oxygen allowed a significant advance in extent and quality of the spectroscopic parameters in HITRAN.

The isotopologue line positions of $^{16}O_2$, $^{16}O^{18}O$, and $^{16}O^{17}O$ for the $a^1\Delta_g\ (v=0,\ 1)\ X^3\Sigma_g^-\ (v=0,\ 1)$ transitions were calculated using spectroscopic constants taken from two papers by Leshchishina et al. [106,107]. Note that $^{16}O^{17}O$ lines are made available for this band for the first time. Gordon et al. [115] have shown that in atmospheric retrievals one needs to account not only for magnetic dipole transitions traditionally provided in HITRAN for that band, but also for electric quadrupole transitions. The quadrupole transitions were therefore included into HITRAN2012 with the intensities calculated using a model described by Mishra et al. [117] with the input parameters based on experimental intensities reported in Gordon et al. At the present time, the intensities for magnetic dipole transitions have been retained from Newman et al. [113] and correlation between the electric quadrupole and magnetic dipole transitions that obey the same selection rules have not been removed. This will be addressed in the future with intensities of magnetic dipole transitions being recalculated using intensities from the work of Leshchishina et al. as input parameters.

The intensities in the $a^1\Delta_g\ (v=0)-X^3\Sigma_g^-\ (v=1)$ band were recalculated using input parameters from new experiments of Kassi and Campargue [118].

A new set of air- and self-broadening parameters and air-broadening temperature dependence was derived based on experimental data reported by Newman et al. [113].

2.7.3. A-band region near 762 nm

The line list for the O_2 *A*-band, $b\,^1\Sigma_g^+\leftarrow X^3\Sigma_g^-$ (0,0) magnetic dipole transitions near 762 nm (13,120 cm^{-1}) for the $^{16}O_2$, $^{16}O^{18}O$, and $^{16}O^{17}O$ isotopologues has been updated due to recent frequency-stabilized cavity ring-down spectroscopy (FS-CRDS) measurements [119–125]. Detailed discussions on the construction of this line list can be found in Refs. [124] and [125] for $^{16}O_2$ and the less abundant isotopologues, respectively.

These spectra were all fit with Galatry line profiles [126] which account for Doppler and pressure broadening as well as Dicke narrowing. The use of Galatry line profiles for the *A*-band is of critical importance in many applications and has been discussed extensively in the literature [119,124,127,128]. Dicke narrowing parameters for each of the included isotopologues can be found in the last two columns of the auxiliary A-band input file supplied as part of the HITRAN2012 update. These last two columns are the air- and self-broadened collisional (Dicke) narrowing parameters (in $cm^{-1}\,atm^{-1}$ at 296 K), respectively. These parameters were taken from Refs. [124] and [125] for $^{16}O_2$ and the lesser isotopologues, respectively.

As these measurements were performed at low pressures (generally below 20 kPa), line mixing and collision-induced absorption (CIA) were unobservable and not included in the spectral fitting. These effects have, however, been shown to be important at atmospheric pressures (and above) [129–131]. We note that CIA has been added to HITRAN for the A-band [132] as measured with Fourier-transform spectroscopy measurements [129,130] (see Section 6). Line-mixing parameters can be calculated for a range of temperatures using the code of Tran et al. [130] with the auxiliary A-band input file provided as part of this update.

For the $^{16}O_2$ A-band magnetic dipole transitions, the most significant updates were to the line positions, line intensities, self-broadening parameters, and lower-state energies. The intensities found in the present database are based upon FS-CRDS measurements and differ from those found in the HITRAN2008 database by $>1\%$ at high J. These measurements include a Herman–Wallis-like interaction and removed a calculation error in the HITRAN2008 A-band intensities. The self-broadening parameters were updated due to FS-CRDS measurements of high J (up to $J=50$) transitions [123]. The included parameters differ from those in HITRAN2008 by more than 10% for high-J transitions but are very similar at low J. Finally, the line positions and lower-state energies have been improved based upon a global fit of FS-CRDS measurements [121] and a large ensemble of ground-state measurements (see Ref. [133] for more details on this fit). At high J, differences exceeding 0.008 cm^{-1} for the line positions and lower-state energies are seen between the present database and HITRAN2008.

Similarly, for the $^{16}O^{18}O$ and $^{16}O^{17}O$ A-band magnetic dipole transitions, the line positions, line intensities, and lower-state energies were improved. In comparing to HITRAN2008, the largest differences are seen for the line intensities which differ by $\sim 3\%$ for $^{16}O^{18}O$ transitions and up to 10% for $^{16}O^{17}O$ transitions. In addition, the line positions and lower-state energies are now based on a global fit of FS-CRDS measurements [122,125] and an ensemble of ground-state measurements (see Ref. [125] for more details on this fit). Large differences are seen for the line positions found in the two databases of up to 0.001 cm^{-1} for $^{16}O^{18}O$ and 0.04 cm^{-1} for $^{16}O^{17}O$.

The line list for hot band transitions of $b^1\Sigma_g^+ \leftarrow X^3\Sigma_g^-(1,1)$ was also updated based upon the recent reevaluation of spectroscopic constants in the $b^1\Sigma_g^+$, $v=1$ state by Gordon et al. [134]. The new line positions are significantly improved over those found in the HITRAN2008 database.

Finally, A-band electric quadrupole transitions have been added to the database. The electric quadrupole line list is taken from Miller and Wunch [135] and is based upon recent FS-CRDS measurements [133]. These very weak transitions ($S=1\times10^{-28}$ to 3×10^{-31} cm^{-1}/(molecule cm^{-2})) have been observed in atmospheric spectra [135,136] and failure to include them in atmospheric retrievals can limit the resulting measurement precision.

2.7.4. B- and γ-bands

An extensive update of the so-called B- and γ-bands ($b^1\Sigma_g^+ \leftarrow X^3\Sigma_g^-(1,0)$ and $b\,^1\Sigma_g^+ \leftarrow X^3\Sigma_g^-(2,0)$) of oxygen around 0.69 and 0.63 μm respectively is described in the work of Gordon et al. [134]. These bands (in particular the B-band) are now being considered for future satellite missions. In this light, it is important to make sure that the reference spectroscopic parameters are accurate enough to provide means of deducing important physical characteristics from the atmospheric spectra. It was found that the HITRAN2008 parameters could not produce satisfactory fits of the observed high-quality spectra. In order to improve the database, we have collected the best available measured line positions that involve the $b^1\Sigma_g^+$ ($v=1$ and $v=2$) states for the three most abundant isotopologues of oxygen and performed a combined fit to obtain a consistent set of spectroscopic constants. These constants were then used to calculate the line positions. A careful review of the available intensity and line-shape measurements was also carried out, and new parameters were derived based on that review. In particular, line-shift parameters, that were not previously available, were introduced. The new data have been tested in application to high-resolution atmospheric spectra measured with the Fourier transform spectrometers at Park Falls, Wisconsin (B-band) and Kitt Peak, Arizona (γ-band) and have yielded substantial improvement [134]. No experimental data were available for $^{16}O^{18}O$ in the γ-band and line positions were determined from the atmospheric spectra and then fitted to provide new spectroscopic constants.

2.7.5. Future work

Recently, Yu et al. [137] carried out a global fit of all available experimental line positions for all the bands and isotopologues from the microwave to UV region. The constants derived in that fit may be used to update line positions and energy levels throughout the entire HITRAN oxygen line list in the future.

2.8. NO (molecule 8)

Unchanged.

2.9. SO_2 (molecule 9)

The line positions and intensities of the pure-rotational transitions (with $J<100$) in the ground and ν_2 states of $^{32}SO_2$ and in the ground state of $^{34}SO_2$ have been adopted from the Cologne Database for Molecular Spectroscopy [87].

Several bands of $^{34}SO_2$ (second isotopologue by abundance in HITRAN) have been added to the database in the 4 and 7.2–10 μm regions based on the recent high resolution work of Flaud et al. [138] and Lafferty et al. [139,140]. All the previous data that existed for $^{34}SO_2$ in HITRAN2008 have been replaced.

2.10. NO_2 (molecule 10)

The reference zero point energy was made consistent for all the bands.

2.11. NH_3 (molecule 11)

Ammonia is an important atmospheric trace species with global emissions having increased very significantly due to the spread of intensive agriculture based on the use of fertilizers which has augmented the natural sources of ammonia from oceans, animal respiration, and soil microbial processes. Livestock, waste management, biomass burning and industry also lead to anthropogenic contributions to atmospheric ammonia. However, the actual ammonia emission budget remains uncertain [141]. Successful ammonia retrievals have been performed with the IASI/MetOp [142], MIPAS [143] and TES [144] remote-sensing satellites. Such observations are heavily dependent on the availability of reliable spectroscopic data. The ammonia line list in HITRAN has not been revised since the HITRAN2000 edition [145] and, as discussed below, is in need of improvement. The present edition is based on a complete reanalysis of the previous $^{14}NH_3$ data [146], new

Table 7
Definition of quantum labels for ammonia.

Quantum label	Definition
v_1	Quanta in vibrational mode 1 (symmetry stretch)
v_2	Quanta in vibrational mode 2 (symmetric bend)
v_3	Quanta in degenerate vibrational mode 3 (asymmetric stretch)
L_3	$\|l_3\|$ absolute vibrational angular moment for mode 3
v_4	Quanta in degenerate vibrational mode 4 (asymmetric bend)
L_4	$\|l_4\|$ absolute vibrational angular moment for mode 4
L	$\|l\|$ absolute total vibrational angular momentum
Γ_{vib}	Vibrational symmetry
J	Total angular momentum
K	$\|k\|$ projection of **J**
i	*s* or *a* for symmetric or anti-symmetric inversion symmetry[a]
Γ_{rot}	Rotational symmetry
Γ_{tot}	Total symmetry

[a] Some of the unassigned levels are given an asterisk (*) in the inversion parity "*i*" field. Levels where labels are deemed unreliable are given an ampersand (&) in the inversion parity "*i*" field.

spectroscopic experiments [147], and some new bands generated using empirical lower-state energies and ab initio line intensities [146].

The lower-state energy levels up to $J=20$ have all been replaced by those derived by Chen et al. [148]; energies for states with $J=21$ and 22 were not changed and are in line with more recent measured values [149]. Down et al. [146] used these energy levels, combination differences, and direct comparison with the computed BYTe line list for ammonia [150] to re-analyze and re-assign the previous HITRAN data resulting in 229 newly assigned lines, 324 assigned lines, and a significant number of other corrections to the quantum number labels. Down et al. also recommended the use of a newly defined and consistent set of quantum numbers as most of the previous sets employed contained insufficient quantum numbers to uniquely identify all the levels. These new quantum labels are adopted in the present edition. The new quantum notation is given as follows. The symmetry quantum numbers can be A_1', A_1'', A_2', A_2'', E′ and E″ except for Γ_{tot} for which the A_1 states do not exist. For Γ_{vib},′ and ″ denote even or odd inversion symmetry respectively (see Table 7 for definitions).

A number of recent experimental studies [151–154] observed intensities differing significantly from those in the previous editions of HITRAN for the ν_2 band. Comparisons performed by Down et al. [146] found that the newer intensities agreed closely with the BYTe intensities [150] which are based on the use of ab initio dipole moments [155]. Intensities for the ν_2 band have therefore been replaced by the newly measured values, where available, or by the values from BYTe. Down et al. found that both the frequencies and the intensities for the $2\nu_2-\nu_2$ hot band were not reliable and lines for this band have been replaced with a new line list generated using frequencies from empirical energy levels and BYTe transition intensities. These new intensities agree well with the measured values of Chu et al. [156]. Down et al. employed the same technique to synthesize line lists for the $\nu_2+\nu_4-\nu_4$, $\nu_4-\nu_2$, $\nu_4-\nu_4$, and $2\nu_2-2\nu_2$ bands, all of which are included in HITRAN for the first time. Further details of all the above changes can be found in the paper by Down et al. [146] included in this issue.

Sung et al. [147] recently measured ammonia spectra in the 6300–7000 cm^{-1}, a region not previously considered in HITRAN. These data have been included in HITRAN with the quantum number labels, where available, changed to the form recommended by Down et al. [146]. Two studies were combined to provide an ammonia HITRAN database for the first time in this region. Sung et al. [147] reported an extensive empirical line list of about 4800 $^{14}NH_3$ lines (positions, intensities, empirical lower-state energies with some quantum assignments) from 6300 to 7000 cm^{-1}; this study used FTIR to characterize 99.7% of observed opacity in this region. Concurrently, Cacciani et al. [157] reported 313 line positions with empirical lower-state energies between 6626 and 6669 cm^{-1} using laser spectra recorded at temperatures down to 130 K. Lacking near-IR pressure broadening studies (see Ref. [158]), information for the ν_2 band from Nemtchinov et al. [153] was applied. Details about the sources of parameters and the ascribed uncertainties are given below.

Almost all of the line positions listed in the 6300–7000 cm^{-1} region are adopted from Sung et al. [147], who analyzed a series of Kitt Peak FTS spectra recorded at temperatures 296–185 K. Among them, however, positions for six lines were replaced with values from Cacciani et al. [157], namely 6626.6553, 6628.2738, 6629.2148, 6635.6400, 6635.6602, and 6642.7091 cm^{-1}. There are another three lines (6650.9102, 6662.8051, 6667.3572 cm^{-1}), whose positions and intensities were adopted from Cacciani [159]. There are another three lines (6634.5034, 6644.7300, 6667.3554 cm^{-1}) listed in the Supplement of Ref. [157], but not observed by Sung et al. [147]. We have not included them in this update since we have no intensity information for them.

Line position uncertainties were estimated by taking into account multiple aspects that included root-mean-square of individual measurements of line positions, the number of the spectra averaged, and their line intensity range. For instance, the best uncertainty of 0.0005 cm^{-1} (HITRAN error code=4) was given to strong lines (whose line intensity $S \geq 1\times10^{-22}$ cm^{-1}/(molecule cm^{-2})) and well-measured unblended lines. Worse values were selected for blends or lines retrieved in less than 4 different laboratory spectra as shown in Table 8.

In this 1.5-μm region, all the line intensities were adopted exclusively from Sung et al. [147]. For intensity uncertainty estimates, similar factors were considered: (1) the rms of the averaged intensity, (2) the number of individual spectra averaged, and (3) the level of strength itself (associated with peak height of the absorption features in the observed spectrum), as listed in Table 9. For instance, for a line whose intensity is averaged over only two spectra, no better than 10% uncertainty is assumed. For unblended strong lines, $S \geq 1\times10^{-22}$ cm^{-1}/(molecule cm^{-2}), uncertainties are expected to be as good as 2%, while the uncertainties for most of the other lines are in the range of 5–10%.

Sung et al. [147] reported quantum assignments for ~1000 transitions by (J, K, l_3, l_4, s/a), almost doubling the

Table 8
Three factors considered in the estimation of ammonia line position uncertainties.

rms of ν_{obs} (cm^{-1})	Number. of spectra averaged	Line intensities cm^{-1}/(molecule cm^{-2})	Uncertainties assumed (cm^{-1})	Error codes
< 0.01	1	$S \le 5 \times 10^{-24}$	< 0.01	3
< 0.005	2 or 3	$1 \times 10^{-23} \le S < 1 \times 10^{-22}$	< 0.01	3
< 0.0005	4 or more	$S \ge 1 \times 10^{-22}$	< 0.001	4

Table 9
Three factors considered in the estimation of ammonia line intensity uncertainty estimates.

rms of S_{obs} (%)	Number of spectra averaged	Line intensities cm^{-1}/(molecule cm^{-2})	Uncertainties claimed (%)	Error codes
> 5	1	$S < 5 \times 10^{-24}$	< 20	4
≤5	2	$5 \times 10^{-24} \le S < 1 \times 10^{-23}$	< 10	5
≤2	3 or more	$1 \times 10^{-23} \le S < 1 \times 10^{-22}$	< 5	6

Table 10
Sources of lower-state energy, E'', for ammonia line list from Refs. [147,157].

Transitions	Quantum numbers	E'' used	Number of lines	References
Fully assigned	J', K', l', a/s' J'', K'', l'', a/s''	Calculated by Urban et al. [164]	1048	[147]
Only lower state assigned	J'', K''	Empirical values rounded to nearest calculated E''	146	[157]
Unassigned, with inferred E''		Empirical values rounded to nearest calculated E''	2497	[147, 157]
Unassigned, no inferred E''		Crude default set to 333 cm^{-1}	1387	

number of transitions whose assignments are available from early work, including Lundsberg-Nielson et al. [160], Xu et al. [161], Li et al. [162], Lees et al. [163], and references therein. Recently, additional assignments for lower state J and K were suggested by Cacciani et al. [157] for 313 transitions between 6626 and 6669 cm^{-1} in the supplement. They exploited very cold spectra (130 K) to substantially diminish interferences or blending by neighboring high-J features and reveal transitions belonging to low-J transitions. As in Sung et al., they also reported empirical lower-state energies and used that information to assign the lower-state quantum numbers, J and K.

For the new HITRAN list, composite assignments and measured lower-state energies from Refs. [147,157] were selectively adopted after comparing synthetic spectra based on the lists against selected cold and room temperature FTIR spectra. If lower-state assignments were validated, the empirical lower-state energies were replaced by corresponding calculated ground-state energies from Urban et al. [164]. For unassigned features for which empirical lower-state energies were given by either Ref. [147] or Ref. [157], the closest values among the calculated ground-state energies [164] replaced the estimates, as summarized along with their sources in Table 10. Some of the empirical lower-state energies may later be found to be inaccurate.

The vibrational dependence of the pressure broadened widths is expected to be smaller than measurement uncertainties for NH_3 line widths currently available. Therefore, the pressure broadening coefficients and their temperature dependence exponents measured in the ν_2 band by Nemtchinov et al. [153] were extrapolated for the 1.5-μm region. In cases where their quantum assignments are suggested in Ref. [147], air- and self-broadening half widths, γ_{air} and γ_{self}, for given rotational quantum numbers, J and K, were computed by

$$\gamma(J,\ K) = \beta_0 + \beta_1 m + \beta_2 K + \beta_3 m^2 + \beta_4 K^2 + \beta_5 mK. \tag{2}$$

Here $m = -J$, J, $J+1$ for the P, Q, and R branches, respectively, and β_i are the polynomial coefficients by Nemtchinov et al. [153] derived from the asymmetric ν_2 state. Uncertainties for the widths of assigned transitions were assumed to be 10% by taking into account their measurement and modeling uncertainties. For unassigned transitions or those assigned only in part, a best set of quantum numbers (i.e., J, K, a/s), at which the calculated ground-state energy by Urban et al. [164] is nearest to the empirical lower-state energy estimates, was employed to compute the broadening coefficients in Eq. (2) with uncertainties being no better than 10%. Finally, γ_{air} and γ_{self} were assumed to be 0.065 and 0.45 $cm^{-1}\,atm^{-1}$, respectively, for transitions whose E'' are not determined or derived.

Temperature dependence exponents are also adopted from Nemtchinov et al. [153]. Taking their temperature dependence exponents for N_2 and O_2 broadening given at J and K less than 8 in the ν_2 band, we have computed air-pressure broadening temperature exponents, n_{air}, by

$$n_{air} = 0.79 \times n_{N_2} + 0.21 \times n_{O_2} \tag{3}$$

Finally, the range of computed exponents was confined to be either greater than 0.51 or less than 0.95 for all other J and K. The uncertainty of the temperature exponent, 0.11, was adopted by taking their realistic estimate from Ref. [153].

To summarize, the uncertainties and temperature dependence exponents are listed in Table 11 along with their error codes.

Table 11
Uncertainty determination for ammonia pressure-broadened widths.

Transitions	Empirical lower-state E''	Quantum number	Pressure-broadened width (cm^{-1} atm^{-1})	Uncertainties	Code
Assigned	Assigned	J, K determined	Computed	< 10%	4
Unassigned	E'' estimate	J, K candidates	Estimated	< 20%	3
Unassigned	E'' estimates not available		$\gamma_{air}=0.065$ $\gamma_{self}=0.45$	Constant	1

Table 12
Comparison of air-broadened widths and air-pressure frequency shifts of NH_3 measured by Bell et al. [158] in the 1.5-μm region to those adopted in this work.

Transitions	Ref. [158]	Ref. [147]	Ref. [158]	HITRAN2012	Ref. [158]	HITRAN2012
	ν_{obs} (cm^{-1})	ν_{obs} (cm^{-1})	γ_{air} (cm^{-1} atm^{-1})	γ_{air} (cm^{-1} atm^{-1})	δ_{air} (cm^{-1} atm^{-1})	δ_{air} (cm^{-1} atm^{-1})
RQ(4, 1)a	6595.923	6595.9272	0.0803(7)	0.0856(86)	–0.009(1)	–0.009
QP(10, 6)s[a]	6595.616	6595.6206	0.0627(7)	0.0858(86)	–0.014(1)	–0.009
RQ(5, 1)s	6595.241	6595.2459	0.0774(5)	0.0786(79)	–0.008(1)	–0.008
RQ(5, 1)a	6595.063	6595.0682	0.0801(5)	0.0786(79)	–0.009(1)	–0.008

[a] Assigned by Lundsberg-Nielsen et al. [160], but not confirmed in Sung et al. [147].

Highly reliable pressure-shift measurements are rare because these are challenging parameters to measure for transitions found in the dense NH_3 manifolds. Moreover, the line positions are perturbed by line mixing effects at higher pressures; the presence of an intrinsic limitation in measured pressure shifts based on the Voigt line-shape model cannot be overestimated. This being said, we estimated a crude magnitude of pressure shifts by applying a "rule-of-thumb" notion that shifts are smaller than line width coefficients at the corresponding J and K by an order of magnitude. In observing that pressure shifts are more likely to be red shifts (i.e., negative shifts) in the near infrared region for isolated lines of polyatomic molecules, we assumed the pressure shifts by the following expression [147]:

$$\delta_{air}(J,\ K) = -0.1\gamma_{air}(J,\ K), \tag{4}$$

where $\gamma_{air}(J,\ K)$ was obtained as described above. Uncertainty for the assumed pressure shifts should be no better than 0.005 cm^{-1}. It should be noted, however, that the true sign of the shift is not known until their measurements are available.

Finally, in Table 12, these computed air-broadening and air-pressure shifts are compared to four measured shifts reported by Bell et al. [158]. Such agreement may not be true for the whole line list, however, so an error code of 3 was selected for the shifts.

Some caveats are in order. The supplemental line list file in Sung et al. [147] includes *empirical adjustment* of line positions and intensities of blended features if some quantum assignments are known. On occasion, the two asymmetry components of the same J and K were reset to have equal intensity and line width. An additional sanity check was also made to obtain a decent set of positions and intensities in ensemble representing the observed spectra well in the 296–185 K temperature range. This permitted further improvement and consistency in the line parameters, but still left some of severely blended regions less characterized, such as for the $PQ(J, 1)$ branch near 6612 cm^{-1}. Further details on the quality of the individual line positions and strengths can be found in Ref. [147].

The updated $^{14}NH_3$ line list contains 45,302 lines which replace the 27,994 lines in previous editions.

2.12. HNO_3 (molecule 12)

For nitric acid, we have updated the pure-rotational band of the ground state and added hyperfine structure from the JPL catalog [165] in the microwave region. Pure-rotational bands of ν_6, ν_7, ν_8, ν_9, $\nu_5/2\nu_9$ (mixed) states have also been added using the JPL catalog, which is largely based on the work of Petkie et al. [166,167]. The total partition sum, Q_{total} (296 K) = 214,120, was used for the conversion to HITRAN format. As mentioned in the introduction, the line positions for this molecule in the MW region are provided in a way that allows accommodation of more decimal places. The usual HITRAN line position uncertainty code has been extended to incorporate more significant digits from the JPL catalog. Three more numbers have been added, namely 7 (≥0.0000001 and ≤0.000001 cm^{-1}), 8 (≥0.00000001 and ≤0.0000001 cm^{-1}), and 9 (better than 0.00000001 cm^{-1}). The air- and self- broadened half widths were adopted from the work of Gomez et al. [168].

New to HITRAN is the second-most abundant isotopologue of nitric acid, $H^{15}NO_3$. The ν_5 and $2\nu_9$ vibrational bands (in the 11-μm region) for this isotopologue were added using the work of Perrin and Mbiaké [169]. The total partition sum, Q_{total} (296 K) = 141,872, was adopted from the same reference. Air- and self-broadened half widths and temperature dependence were adopted from the work of Flaud et al. [170]. The line list for the pure rotational band of the ground state of $H^{15}NO_3$ was adapted from the JPL catalog and is based on the work of Drouin et al. [171].

Table 13
The maximum ν, J range of the calculation for hydrogen halides.

	$H^{19}F$	$D^{19}F$	$H^{35,37}Cl$	$D^{35,37}Cl$	$H^{79,81}Br$	$D^{79,81}Br$	$H^{127}I$	$D^{127}I$
ν_{max}	19	26	17	22	7	5	7	5
J_{max}	40	40	40	80	40	40	40	40

2.13. OH (molecule 13)

Some errors in the quantum notation of the line list for the hydroxyl radical were identified in HITRAN2008 and were corrected in this edition.

2.14. HF (molecule 14)

A thorough evaluation of all the hydrogen halide line parameters that have existed in previous HITRAN editions was carried out at the HITRAN project. Accurate line positions, line intensities and Einstein *A*-coefficients were calculated for all ro-vibrational transitions (fundamental, overtone, and hot bands) for hydrogen halides in HITRAN. In addition, the deuterated isotopologues of these species have been entered into HITRAN for the first time. It should be noted that besides the terrestrial atmospheric and environmental issues that knowledge of the spectroscopy of the hydrogen halides addresses, the deuterated species have implications for planetary research, see for example Ref. [172]. Many of the updates are similar for the hydrogen halides (HF, HCl, HBr, HI); we give an overview in this section on HF. Some specifics to the other hydrogen halides are given in their respective Sections (2.15–2.17). More details about the updates to the hydrogen halides can be found in Li et al. [173].

The new calculation employs the recently developed semi-empirical dipole moment functions and very accurate potential energy functions that include the parameters characterizing the Born–Oppenheimer breakdown effects [166]. Table 13 shows the choice of the maximum ν, J levels for the different hydrogen halides, mainly based on the highest ro-vibrational level that is measured experimentally in high resolution. For example, $\nu=22$, $J=80$ for $D^{35,37}Cl$ means the nearby ν, J level was measured experimentally for $D^{35,37}Cl$. The evaluation of the calculated line position and intensities can be found in Refs. [173–175].

For the fundamental band of HF, the air-broadening parameters, γ_{air}, in the HITRAN2008 compilation turned out to be fitted not with a Voigt profile, but with the Galatry profile based on the Pine and Looney [176] measurements. However, the Dicke narrowing parameter was not provided in the previous database. The corresponding collisional, or Dicke, narrowing parameters have been cast into a separate columnar table that is easily linked to the main part of HITRAN using the unique combination of molecule number, isotopologue number, and quantum identifications. A header is supplied at the top of the columns to further clarify the quantities in the table. For the pure rotational bands ($\Delta\nu=0$), γ_{air} values from the HITRAN2008 listing were retained.

For the 2-0 band and beyond, N_2-and self-broadening measurements for the P(3) and P(6) lines of the 2-0 band by Chou et al. [177] were used to calibrate the Meredith and Smith measurements [178] for the 2-0 band. In the case of N_2-broadening, the calibrated results were then scaled to air by

$$\gamma_{air}=0.9\gamma_{N_2}. \tag{5}$$

The self-broadening parameters, γ_{self}, of HF in the HITRAN2008 listing, which were based on Pine et al. [179], were retained for the fundamental and $\Delta\nu=1$ bands. Linear extrapolation in the vibrational level ν were made using the measurements of Pine et al. [179] and Chou et al. [177] to obtain γ_{self} for the other bands. The same γ_{air} and γ_{self} were applied to the corresponding bands of DF.

For the $\Delta\nu=0$, 1 bands, the temperature-dependence of γ_{air}, n, retained values from the HITRAN2008 listing. A default value of 0.5 was used for bands with $\Delta\nu\geq2$. The pressure shift, δ_{air}, also retained values from HITRAN2008 for the $\delta\nu=0$, 1 bands. Measurements by Guelachvili and Smith [180] were used for the bands with $\Delta\nu\geq2$.

2.15. HCl (molecule 15)

The hyperfine structure (hfs) components for the $X^1\Sigma^+$ 0–0 $H^{35}Cl$, $H^{37}Cl$ bands were regenerated for $J\leq15$ with improved ground-state parameters from Cazzoli and Puzzarini [181]. Similarly, hyperfine structure components for the $X^1\Sigma^+$ 0–0 $D^{35}Cl$, $D^{37}Cl$ bands were calculated using the ground-state parameters from Cazzoli and Puzzarini [182]. The sum of the relative line intensities of the HCl and DCl hfs components, calculated with the PGOPHER program [183], was normalized to the intensity of the corresponding rotational line from the study by Li et al. [174,175].

For the air-broadening parameters, γ_{air}, the same remarks as for HF above apply to HCl concerning the profiles of the fundamental band in HITRAN2008. Pine and Looney N_2-measurements were multiplied by a factor of 0.960 to obtain the air broadening parameters for the 0–0 band. Only the R(3) transition measurement by Park et al. [184] was applied directly. In a similar fashion, high-accuracy measurements ($\pm1\%$ for N_2- and O_2-broadening) for the P(4) and R(3) lines of 2-0 band by De Rosa et al. [185] were used to scale Pine and Looney measurements with a factor of 1.089. The scaled values were used for bands with $\Delta\nu\geq2$.

For γ_{self} in the $\Delta\nu=0$, 1 bands, Pine et al. [179] measurements were combined with the Hurtmans et al. [186] accurate measurement for the P(14) line to extrapolate to high-*J* lines. For the $\Delta\nu=2$ bands, Pine et al. measurements were scaled with measurements ($\pm3\%$ uncertainty) of Ortwein et al. [187] and De Rosa et al.

[185]. Ogilvie and Lee [188] and Zughul et al. [189] measurements were used for the $\Delta\nu=3$ and $\Delta\nu\geq4$ bands, respectively. Tudorie et al. [190] refitting of the γ_{self} measurements by Eaton and Thompson [191] were used for all bands of DCl.

Pine and Looney [176] values of the temperature-dependence exponent, n, were used for all the bands.

2.16. HBr (molecule 16)

The line positions of the hfs components for the $X^1\Sigma^+$ (0–0) and (1–0) $H^{79}Br$, $H^{81}Br$ bands were retained from the HITRAN2008 listing. However, the high-J rotational line positions without hfs structure of the same bands were recalculated using the semi-empirical potential from Coxon and Hajigeorgiou [192]. The sum of the relative line intensities of the hfs components was normalized to the intensity of the corresponding rotational line from the study by Li et al. [175].

Values of γ_{air} from the HITRAN2008 listing were retained for hydrogen bromide. The same values were applied to DBr. However, Benedict and Herman [193] calculated values of γ_{self} were used for all bands of DBr. No data were available for the temperature dependence of the half widths of hydrogen bromide; a default value of 0.5 was used. No data were available for the shift as well.

2.17. HI (molecule 17)

There was a complete revision of line positions of HI compared with HITRAN2008. Some details are given below.

The calculated line positions for the 0–0 $D^{127}I$ band, including the hyperfine structure components, were adopted from the work by Varberg et al. [194]. The sum of the relative line intensities of the hfs components of HI and DI, calculated using the PGOPHER program, was normalized to the intensity of the corresponding rotational line from the study by Li et al. [175].

For the fundamental, first, second, third overtone bands (corresponding to $\Delta\nu=1$, 2, 3, 4), γ_{N_2} from Domanskaya et al. [195] was scaled to air by Eq. (5). For the pure rotational band, the values from the fundamental band were used. For $\Delta\nu\geq1$ bands, the values from the 4-0 band were used. Values of γ_{air} for HI were used for DI.

Hartmann et al. [196] measurements for γ_{self} were used for the $\Delta\nu=1$, 2 bands. Bulanin et al. [197] recent γ_{self} measurements were used for $\Delta\nu\geq3$ bands. Values of γ_{self} for HI were used for DI. No data were available for the temperature dependence of the half width of hydrogen bromide; a default value of 0.5 was used. Domanskaya et al. [195] measurements for the N_2 shift were adopted for HI. No data were found for the DI air shifts.

2.18. ClO (molecule 18)

Previous HITRAN intensities for the fundamental band of chlorine monoxide were introduced in a paper by Goldman et al. [198] and were based on the measurements of Burkholder et al. [199]. The intensities of all the fundamental band lines from both HITRAN isotopologues (^{35}ClO and ^{37}ClO) were adding up to a total band strength of 9.68 cm^{-2} atm^{-1} with a linear Hermann–Wallis (HW) rotational distribution ($1+0.00563m$), where m is equal to $-J''$ for the P branch, J'' for the Q branch, and $J''+1$ for the R branch. In a later experimental work, Birk and Wagner [200] derived number densities of the unstable ClO from pure rotational line intensities by consecutive mid- and far-infrared measurements. The mid infrared line strength analysis yielded a band strength of 9.01 cm^{-2} atm^{-1}. They have also shown that a quadratic expression ($1+0.00684m$ $+1.56\times10^{-4}m^2$) is more appropriate to account for HW vibration-rotation interaction (see Fig. 4 of Ref. [200]). Consequently, the HITRAN2012 intensities have been corrected to match the results of Ref. [200].

In addition, the air-broadened half widths and their temperature dependence in the fundamental band were changed using the same method that was applied in HITRAN2008 [1] to the pure rotational band. A rough estimate for the self-broadening half width (0.1 cm^{-1} atm^{-1}) was assigned to all ClO lines in the database.

2.19. OCS (molecule 19)

The line positions and intensities in the pure rotational band for all of the HITRAN carbonyl sulfide isotopologues were updated using parameters from the Cologne Database for Molecular Spectroscopy [87]. The intensities were converted using the procedure described in the Appendix of the HITRAN2008 paper, which includes scaling of the partition functions.

It was found that due to a programming error, some of the air- and self-broadening half widths for all isotopologues of carbonyl sulfide were in error by as much as 50% in the HITRAN2008 edition. In addition, a typographical error in the b_3 coefficient for the O_2-broadening Padé approximant given in Ref. [201] was found. These errors have now been fixed, yielding much improved broadening parameters.

2.20. H_2CO (molecule 20)

The pure-rotational data for formaldehyde was updated with the most recent entries in the CDMS catalog [87]. These values are largely based on the fit of experimental data for the three most abundant isotopologues from Refs. [202–205]. The intensities were converted using the procedure described in the Appendix of the HITRAN2008 paper, which includes scaling of the partition functions.

In addition, the line-shape parameters throughout the entire H_2CO line list were updated based on the data from Jacquemart et al. [206].

2.21. HOCl (molecule 21)

Unchanged.

2.22. N_2 (molecule 22)

It was discovered that the HITRAN2008 quadrupole line-intensities for the nitrogen molecule had not been correctly converted from the ab initio work of Li and Le Roy [207].

The correction applied here yielded about a 2% change in intensities. We have also updated the line positions to the ones derived from the semi-empirical potential energy function of Le Roy et al. [208]. New parameters have been validated using retrievals from the ACE satellite [209] and proved to be an improvement [210].

In addition, based on the works of Refs. [207] and [208], we have also added vibrational bands up to 4–0 for the principal isotopologue and pure rotational and fundamental bands of $^{14}N^{15}N$. It may be interesting to determine the $^{14}N/^{15}N$ ratios in different astrophysical objects using molecular nitrogen directly rather than rely on the ammonia spectra.

The excellent quality of the ab initio intensities of Ref. [207] and line positions derived from Ref. [208] has also been validated in CRDS experiments [118] where S-branch transitions of the second overtone were measured. From the work of Li and Le Roy one can, in principle, obtain the complete database for $^{14}N_2$, $^{14}N^{15}N$ and $^{15}N_2$ lines for the transitions involving $v \le 4$ [207].

2.23. HCN (molecule 23)

Unchanged.

2.24. CH_3Cl (molecule 24)

The pure-rotational band of methyl chloride was converted from the JPL catalog [165] into the HITRAN format. HITRAN2008 intensities in the 640–2600 cm^{-1} region, that originate from Nikitin et al. [211], were rescaled to be in a better agreement with existing experimental [212–214] data. Theoretical data were used [215] when no experimental values were available, and for some of the hot bands that were not measured or calculated, the PNNL cross-sections were used to estimate the band strengths [216] to provide quantitative information. The scaling factors for band strengths ranged from 5 to 650 and were isotopologue dependent. Thus this update results in a significant change to the CH_3Cl data in this region in comparison with HITRAN2008. The 3-μm region was completely replaced using data from Bray et al. [217].

Finally the representation of the rotational quanta was changed to accommodate not just magnitude but also the sign of *l*-quantum number which is now given for all transitions of CH_3Cl.

2.25. H_2O_2 (molecule 25)

Unchanged.

2.26. C_2H_2 (molecule 26)

The 7.7 μm region was completely updated based on the work of Gomez et al. [218,219]. In addition, the line positions of most of the $\nu_1+\nu_3$ band of the principal isotopologue were updated using the recommended values from the web site http://www.bipm.org/utils/common/pdf/mep/M-e-P_C2H2_1.54.pdf as well as Ref. [220].

The C_2HD isotopologue was introduced into HITRAN for the first time with microwave values originating from the CDMS catalog [87], while parameters in the 416-789 cm^{-1} region were taken from the work of Jolly et al. [221].

Finally, some minor corrections were applied: the vibrational assignment of the line at 735.54341 cm^{-1} was corrected, and quantum assignments were corrected for the 23 Q-branch lines of the $3\nu_4+\nu_5-\nu_5$ band at 1950 cm^{-1}.

2.27. C_2H_6 (molecule 27)

Ethane is an important constituent not only in the atmosphere of the earth and comets, but also in the atmospheres of Jupiter, Saturn, Neptune, and Titan as revealed by its 12-μm emission features (e.g., see Ref. [222]). The ν_9 fundamental of ethane is the strongest band seen in Titan observed in the 10-μm terrestrial window and is often used to detect and monitor its abundance in planetary atmospheres. In the HITRAN2008 database [1], the previously existing spectral line parameters for this band were replaced by Vander Auwera et al. [223] with a new line list for the ν_9, $3\nu_4$, $\nu_4+\nu_9-\nu_4$, and$+2\nu_4+\nu_9-2\nu_4$ bands. The line positions and intensities in Ref. [1] were generated based upon the global fit analysis of the four lowest vibrational states of ethane [224,225].

Since the release of HITRAN2008 [1], two new high-resolution experimental line-parameters measurements [226,227] have been reported in the region of the ν_9 band of $^{12}C_2H_6$. The results from Refs. [226,227] confirmed that while the line positions agreed to within 1×10^{-4} cm^{-1} with values in Ref. [1], the line intensities were on average 15% lower. This observation was verified by comparisons made in several measured sub-band intensities between Ref. [1] and Refs. [226,227]. Therefore, in the new HITRAN database, the line positions were retained to be the same as in HITRAN2008, while the intensities have been reduced by 15% compared to HITRAN2008.

Constant default values assumed for all transitions for air- and self-broadened half-width coefficients in Ref. [1] have been replaced with calculated values using the linear expressions for the ν_9 *Q* branch transitions [226,227] for all branches in all bands. The Lorentz air-broadened half-width coefficients are computed from the reported N_2-broadened Lorentz half-width coefficients [226,227] by assuming Eq. (5). The constant temperature dependence exponent of unity that was assumed for all lines in Ref. [1] has been replaced with calculated values based upon the new measurements [226,227] and corrected to air by

$$n_{air} = 0.9 n_{N_2}. \qquad (6)$$

The accuracy code for line positions in the aforementioned update is 4 (0.0001–0.001 cm^{-1}), 5% for the intensities, 10–15% for the half width coefficients, and 10–20% for the temperature dependence exponents. A short spectral region in the $^{r}Q(J, K=0)$ sub-band near the band head region is shown in Fig. 8 as an example to illustrate the quality of the fit obtained for retrieving the various spectral line parameters in Ref. [227].

Calculated C_2H_6 line positions, intensities, and quantum assignments between 1330 and 1610 cm^{-1} (7-μm region) from di Lauro et al. [228] have also now been included in HITRAN. The spectrum is very complex, and there are a

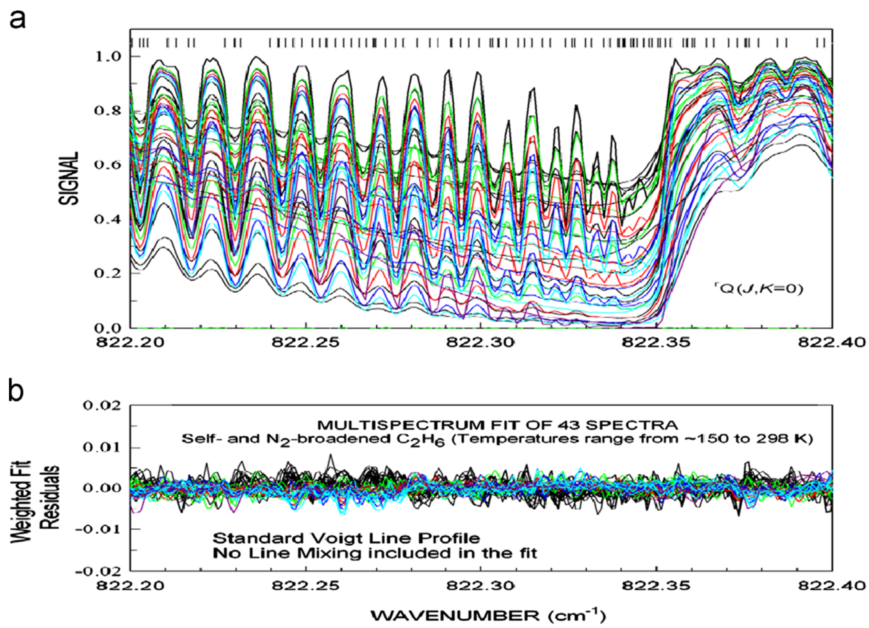

Fig. 8. Example of multispectrum fit (top panel) near the band head of ν_9 ^rQ and the excellent residuals (bottom panel).

Table 14
Band-by-band summary of the 12- and 7-μm line list for ethane.

Band	ν_0 (cm^{-1})	ν_{min} (cm^{-1})	ν_{max} (cm^{-1})	Number of lines	$\sum_{int}$	J_{max}	K_{max}
12-μm region							
$3\nu_4$	790.9	706.8572	775.3455	43	0.0000566	45	2
ν_9	821.3	706.6015	942.1680	7188	641.548	45	22
$\nu_9+\nu_4-\nu_4$	832.2	717.8110	951.5441	7188	159.381	45	22
$\nu_9+2\nu_4-2\nu_4$	843.9	727.2776	961.1450	7188	46.923	45	22
7-μm region							
ν_6	1379.2	1330.2862	1604.5903	2252	117.044	44	19
$2\nu_4+\nu_9$	1388.2	1371.3452	1604.6207	42	0.440	40	18
ν_8	1471.8	1330.7725	1610.7034	8443	1331.374	45	20
$\nu_4+\nu_8-\nu_4$	1471.9	1330.3300	1610.3803	5093	341.043	45	20
$2\nu_4+\nu_{12}-\nu_4$		1373.9485	1567.3138	781	19.044	37	14
$\nu_4+\nu_{12}$	1480.6	1379.8273	1591.0744	3263	165.200	46	12

Note: ν_0 is the band center, ν_{min} and ν_{max} are the beginning and the ending wavenumber range of the transitions included in each band, and $\sum_{int}$ is the summed intensities in units of 10^{-21} cm^{-1}/(molecule cm^{-2}) at 296 K.

multitude of resonances and interactions that must be included in order to analyze high resolution spectra. The accuracies of many predicted positions at 7 μm are enhanced using *empirical* upper state energies, E', tabulated as a function of the ethane quantum numbers by adding to the measured positions of assigned lines the corresponding lower state energies E''. The altered positions have the HITRAN accuracy code=4 (0.0001–0.001 cm^{-1}). A more conservative accuracy code=2 (0.01–0.1 cm^{-1}) is set for the remaining predicted positions. At 7 μm, relative intensities are predicted and normalized to match the available laboratory spectra used by di Lauro et al. [228]. Self- and N_2-broadened C_2H_6 half widths and N_2-broadened temperature dependences have been added using the linear expressions for ν_9 Q-branch transitions reported by Devi et al. [226,227] for all types of transitions (P, Q, R) of both the parallel and perpendicular bands. The accuracies for widths are conservatively set to 10–20% (HITRAN code=4). The accuracies for the temperature dependence exponents of the widths are thought to be 10–25%.

Table 14 is an overview of the 12- and 7-μm bands of ethane in the new line list.

In this edition of HITRAN, IR cross-sections for the 3.3-μm region have been added. See Section 3.1 for the discussion and available pseudo-line list option. There has been some additional recent work on line assignments [229] and band models [230] in the 3.3-μm region, but these results are not yet ready for inclusion in the HITRAN database.

It should be noted that the $^{13}C^{12}CH_6$ isotopologue had not been added to the official release of HITRAN2008

Table 15
Overview of the positions and intensities for higher polyads of H_2S.

Polyad (cm^{-1})	Source of data	Number of isotopologues	Number of lines	Position accuracies (cm^{-1})	Intensity accuracies[a]	Vibrational bands	
1st hexad 4471 –5665	Kitt Peak FTS	3	11,678	0.0005–0.005	5–10%, 10–20% and worse	200–000 002–000 021–000 210–010	101–000 120–000 040–000 111–010
2nd hexad 5671–6695	Kitt Peak FTS	3	7016	0.0005–0.005	5–10%, 10–20% and worse	210–000 012–000 031–000 121–010	111–000 130–000 050–000 220–010
1st decade 7053–8039	Kitt Peak FTS	1	3343	0.0005–0.005	15–20% and worse	300–000 102–000 220–000	201–000 003–000 121–000
1st pentadecad 9385–10,266	ICLAS–VECSEL	3	4071	Better than 0.01	25–30% and worse	301–000 221–000 141–000	202–000 122–000
2nd pentadecad 10,777–11,329	ICLAS	3	2865	0.005	15–20% and worse	311–000 212–000 330–000	

[a] "Worse" accuracies (meaning different by a factor of two) apply to the weakest lines.

despite the text in Ref. [1]; this additional isotopologue has now been included (for the 12-μm region). Finally, the symmetry labeling of some of the ethane lines in the official HITRAN2008 release were found to be erroneous. This situation has now been remedied.

2.28. PH_3 (molecule 28)

Phosphine FIR line parameters have been introduced into HITRAN for the first time and originate from the CDMS catalog [87]. The dataset is slightly different from the one uploaded to CDMS in October 2008. The creation of the 2008 version was prompted by the very accurate Lamb-dip and Doppler-limited measurements up to 534 GHz and near 800 GHz, respectively [231]. The Lamb-dip measurements resolved the H and P hyperfine structure to a very large extent. Also included in the fit were transitions between the A_1 and A_2 components of $K=3,6,9,\ldots$ transitions with hyperfine information as far as available [232], $\Delta K=3$ transitions [233–236] as well as regular $\Delta K=0$ rotational transitions measured at sub-millimeter [236] and far-infrared wavelengths [237]. The entry was deemed to be satisfactory for radio-astronomical observations in the interstellar medium, but may not be extensive enough for studies of giant planets or brown dwarfs or for benchmarking against large-scale quantum-chemical calculations [238]. Therefore, the same dataset was used in HITRAN2012 to create an entry with considerably lowered intensity cut-offs. It is superior to the fit published in Ref. [231] which only employed data from that work as well as $\Delta K=0$ additional rotational transitions from Ref. [235]. The details of the present fit which results in this HITRAN2012 edition are given in Ref. [239]. As mentioned in the introduction, the line positions for this molecule in the MW region are provided with more decimal places.

Current quantum notation existing in HITRAN will be reconsidered in the future to provide unique assignments of rotational levels and avoid assignments that appear identical for different lines or seemingly contradicting selection rules. This problem, however, does not affect the actual spectroscopic data and simulations that employ them.

2.29. COF_2 (molecule 29)

A simultaneous fit of high-resolution THz and infrared spectra of carbonyl fluoride [240] allowed us to improve the line positions in HITRAN and, more importantly, create a more complete line list for this molecule. Apart from fundamentals, the dataset now also includes hot bands in the ν_6 band region (12.9 μm) as well as ν_6 lines of the $^{13}COF_2$ isotopologue, which have been introduced into HITRAN for the first time.

2.30. SF_6 (molecule 30)

Unchanged.

2.31. H_2S (molecule 31)

The knowledge of reliable reference spectral data for hydrogen sulfide is important for the monitoring of the quality of air [241], especially near oil refineries. H_2S can also serve as a biomarker on exoplanets [242]. A substantial update of the pure-rotational transitions and introduction of the NIR transitions was carried out to aid these research fields.

2.31.1. Pure-rotational transitions in the 45–360 cm^{-1} region

New room-temperature, Fourier transform measurements performed by Azzam et al. [243] have been used to replace and augment the pure-rotational transitions of hydrogen sulfide in the 45–360 cm^{-1} region. These measurements significantly extended previous experimental studies in this region [244–246] for the isotopologues $H_2{}^{32}S$, $H_2{}^{33}S$ and $H_2{}^{34}S$. Pure-rotational transitions within the excited ν_2 vibrational state of $H_2{}^{32}S$ were observed for the first time and assigned using an ab initio line list [247] with most assignments confirmed by combination differences based on the HITRAN data for the ν_2 vibrational band. The new experimental data were combined with lower frequency measurements to obtain new sets of Hamiltonian parameters which were used to generate a line list for the entire 45–360 cm^{-1} region giving a total of 4794 transitions which replace the existing data for this region. See the paper by Azzam et al. [243] in this issue for further details. Note however that the data provided in HITRAN2012 correspond to the preliminary analyses performed by Azzam et al. In the near future we plan to update the database to the more up-to-date analyses by Azzam et al.

2.31.2. Addition of new transitions in the 4472 and 11,330 cm^{-1} regions

The compilation for hydrogen sulfide has been extended by adding 28,973 transitions between 4471.7 and 11,329.6 cm^{-1}. All the new transitions fall into specific spectral regions (polyads) corresponding to the first and second hexads (4471–6695 cm^{-1}), the first decade (7053–8039 cm^{-1}), and the first and second pentadecades (9385–11,330 cm^{-1}). Two minor isotopologues are also included. The new information is summarized in Table 15 which gives the spectrometer used for the measurements, the numbers of studied isotopologues and included absorption lines, the estimated accuracies for positions and intensities, and the vibrational bands included for $H_2{}^{32}S$.

The extended line list contains both pure experimental and calculated line positions and intensities. The calculated positions are obtained only from the experimental upper-state energy levels based on known quantum assignments and have accuracies comparable to the experimental ones. The intensities were measured and predicted with a range of accuracies that depend on the spectral region (see Table 15). Consistent with earlier versions of HITRAN, constant broadening coefficients are applied: γ_{air}, γ_{self}, and δ_{air} of 0.074, 0.158 and 0.0 cm^{-1} atm^{-1} at 296 K, respectively; 0.75 was adopted for the temperature dependence of the air-broadened half width. Detailed laboratory investigations are needed to characterize the variation of air and self broadening as a function of the ro-vibrational quantum numbers for the range of atmospheric temperatures.

2.31.2.1. Data obtained by Fourier transform spectrometer. The new H_2S analyses between 4450 and 8050 cm^{-1} were based on the high-resolution (0.0056 and 0.011 cm^{-1}) laboratory spectra recorded with the McMath Fourier transform spectrometer located at Kitt Peak National Solar Observatory. The resulting peak list was assigned and modeled using the Watson-type effective Hamiltonian. Accurate line intensities for about 2900 lines were retrieved for the 1st and 2nd hexads from a dozen spectra recorded using path lengths of 1.5–433 m and pressures ranging from 1.5 to 30 Torr. For the strongest transitions in the two hexad regions, the averaged observed intensities were based on 6–10 individual spectra. These were then modeled with the effective transition moment series using 34 and 20 parameters to achieve RMS agreement close to experimental accuracy: 2.9% and 3.6%, respectively. For the 1st decade region above 7050 cm^{-1}, line intensities were either retrieved from only a few spectra, or were estimated from the peak absorption for weak lines. Of these, 920 measured intensities of transitions belonging to the 003–000, 201–000, 121–000, 102–000, 300–000, and 220–000 vibrational bands were modeled within 12% by using 21 transition moment parameters. In the case of the $H_2{}^{34}S$ and $H_2{}^{33}S$ isotopologues, the calculated intensities were based on the transition moment parameters for the main isotopologue and true rotational–vibrational wavefunctions obtained from the energy level fitting for isotopologues.

Some details about energy levels and transition intensity modeling can be found in Refs. [248–250]. A review of all published information on the $H_2{}^{32}S$, $H_2{}^{33}S$, and $H_2{}^{34}S$ infrared spectra is given in Ref. [251]. In particular, the $H_2{}^{32}S$ spectra in the 2nd hexad (5700–6650 cm^{-1}) and 1st decade (7300–7900 cm^{-1}) regions have been investigated in recent papers by Ulenikov et al. [252,253]; however, no information about line positions and intensities has been published. In any case, the $H_2{}^{32}S$ transitions included in this issue of HITRAN involve a considerably large number of upper-state energy levels compared to those published in Refs. [252,253].

The resulting list of transitions consists of 16,288 transitions between 4450 and 8050 cm^{-1} belonging to 22 vibrational bands of $H_2{}^{32}S$, including four hot bands (see Table 15). There also are 4098 lines of $H_2{}^{34}S$ and 1116 lines of $H_2{}^{33}S$ included between 4700 and 6600 cm^{-1}. In total, the new H_2S line list contains 22,037 transitions derived from the analysis of FTIR spectra.

The accuracies of the positions and intensities vary. The position accuracy of stronger isolated lines that dominate the spectrum is estimated to be 0.001 cm^{-1} and better, as confirmed by the combination difference analysis. For blended features and those that are 500 times weaker than the strongest lines in the region, the accuracy may degrade to 0.005 cm^{-1} and worse. The accuracy of presented intensities can vary within a wide interval. The most accurate data are in both hexads where experimental uncertainties vary from 1% to 7%. For the 1st decade the accuracy of experimental intensities is 10–20% for stronger lines but worse for all experimental transitions with intensities less than 5.0×10^{-25} cm^{-1}/(molecule cm^{-2}) at 296 K. The calculated intensities are thought to be accurate within 10–20% for intensities larger than 2.0×10^{-24} cm^{-1}/(molecule cm^{-2}) at 296 K and worse for weaker lines. In the case of the two hexads, the calculated intensities obtained from the modeling of accurate experimental data are believed to be more reliable than those for the 1st decade region.

Very few near infrared experimental intensities of H_2S have been previously published near 1.6 μm for direct comparison. One recent paper [241] reported intensities of four lines near 6341 cm^{-1} using a laser spectrometer. As seen in Table 16, their new values are ~12% higher than the present intensities. Thus, further investigation is needed.

Table 16
Comparison of the present observed H_2S intensities with literature data.

Position (cm^{-1})	Vibrational band	$J'K_a'K_c'$–$J''K_a''K_c''$	H_2S intensity[a]		Intensity ratio Ref. [241]/present
			HITRAN	Ref. [241]	
6339.24518	(111)–(000)	423–322	2.67 ± 2.1%	2.9 ± 17%	1.09
6340.43196	(111)–(000)	413–312	10.7 ± 1.5%	11.6 ± 2.6%	1.08
6342.80948	(210)–(000)	606–515 616–505	4.45 ± 1.6%	5.1 ± 7.8%	1.15
6344.00001	(111)–(000)	606–515 616–505	17.4 ± 1.3%	20.0 ± 1.0%	1.15

[a] In units of 10^{-23} cm^{-1}/(molecule cm^{-2}) at 296 K. Values in percent are experimental precisions of the measured intensities. Where two assignments are listed, the intensity represents the sum.

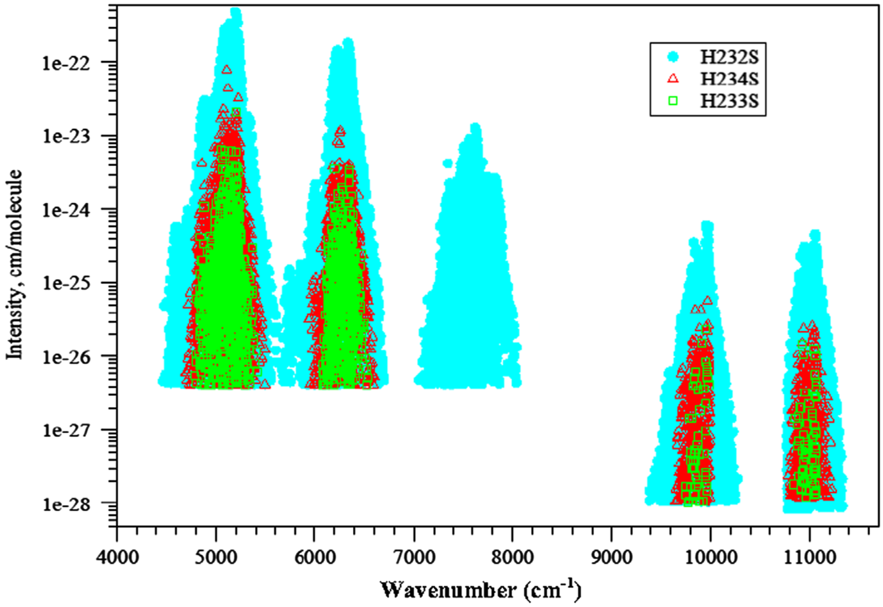

Fig. 9. New absorption lines of hydrogen sulfide added for the HITRAN2012 database. Transitions of $H_2{}^{32}S$, $H_2{}^{34}S$, and $H_2{}^{33}S$ are shown, respectively, by circles (in cyan), triangles (in red), and squares (in green). Intensities in cm^{-1}/(molecule cm^{-2}) at 296 K are given for natural abundance.

2.31.2.2. Data obtained by intra-cavity laser absorption spectroscopy. High sensitive ICLAS—VECSEL (Intra-Cavity Laser Absorption Spectroscopy with a Vertical External Cavity Surface Emitting laser) and ICLAS systems were used to record weak absorption lines of hydrogen sulfide in the 9385–10,200 [254] and the 10,780–11,330 cm^{-1} [255] spectral regions, respectively. In total, 3385 transitions involving eight highly excited upper states were recorded and assigned. The relative experimental intensities were approximately derived from the peak absorption and then scaled to the FTS data of Ref. [256].

The accuracy of line positions in the 9385–10,200 cm^{-1} region was estimated to be better than 0.01 cm^{-1}. The experimental intensities are believed to be accurate within 25–30% for stronger lines, while for the weakest lines the uncertainty in measured intensities can reach up to 100%. The transition moment parameters were obtained by fitting to 1183 observed transition intensities. An rms deviation of 18% was achieved by varying 25 parameters.

For the 10,780–11,330 cm^{-1} interval, the position accuracy of 0.005 cm^{-1} was estimated in the process of spectra calibration and then confirmed by the combination differences analysis. Six transition moment parameters were derived by fitting to 337 relatively strong, well isolated line intensities, which reproduce 82% of the fitted intensities within 15%.

Finally a line list including 3385 experimentally measured lines was combined with 3551 weaker transitions whose intensities were predicted using the derived transition moment parameters; the calculated positions were estimated from the experimental upper-state energy levels.

The graphical summary of the new information on hydrogen sulfide absorption included in HITRAN2012 is shown in Fig. 9.

This extension of the H_2S parameters can enable more in situ and remote sensing in the near-IR, particularly with sensitive laser-based techniques. As seen in the characterization of accuracies, the listed line positions are usually well within the full Doppler widths of H_2S so that the quantum assignments should be unambiguous. However, the line intensities may not be sufficiently reliable for applications desiring to measure atmospheric abundances with the highest accuracies. Much more is needed to characterize accurate pressure broadening at all wavelengths for hydrogen sulfide.

2.32. HCOOH (molecule 32)

Unchanged.

2.33. HO_2 (molecule 33)

Unchanged.

2.34. O (“molecule” 34)

Unchanged.

2.35. $ClONO_2$ (molecule 35)

Unchanged.

2.36. NO^+ (molecule 36)

Unchanged.

2.37. HOBr (molecule 37)

Unchanged.

2.38. C_2H_4 (molecule 38)

Unchanged.

2.39. CH_3OH (molecule 39)

Unchanged.

2.40. CH_3Br (molecule 40)

Unchanged.

2.41. CH_3CN (molecule 41)

Unchanged.

2.42. CF_4 (molecule 42)

Unchanged.

2.43. C_4H_2 (molecule 43)

Diacetylene, the simplest member of the polyacetylene family, is a molecule of relevant astrophysical interest. In the interstellar medium, it plays a major role in the synthesis of complex hydrocarbons and cyanopolyynes through ion–neutral or neutral–neutral reactions with C^+ or CN [257]. C_4H_2 is also a well known constituent of the stratosphere of the giant planets and their moons [104,258,259], where it acts as a UV shield and is thought to take part in the photochemical reaction network initiating the organic aerosols (tholines) present in the atmospheres of these solar system bodies [260].

The ν_8 perpendicular band of diacetylene at 16 μm has been detected in the proto-planetary nebulae CRL 618 and CRL 2688 by ISO [261], and also outside our galaxy in a similar object embedded in the Large Magellanic Cloud (SMP LMC 11) using the IRS spectrograph on board Spitzer [262]. As concerns our Solar System, the first identification of diacetylene dates back to 1981, in Titan's atmosphere by Voyager with its IRIS spectrometer [263]. Subsequently, its detection was made in the atmospheres of Saturn [258], Jupiter [264], Uranus [265], and Neptune [266]. All these detections were made through the ν_8 band observed by ISO/SWS, Spitzer/IRS and Cassini/CIRS.

The infrared spectrum of diacetylene is dominated by three strong features at 3300 cm^{-1} (ν_4), 1240 cm^{-1} ($\nu_6+\nu_8$), and 627 cm^{-1} (ν_8) [267–269]. This latter band is particularly relevant for astrophysical and planetary studies as it is detectable in emission in a large variety of environments. Despite this, the region below 1000 cm^{-1} was the subject of only one high-resolution study [269] until very recently, when comprehensive investiga tions of the low-energy band system were undertaken [270–272].

The C_4H_2 line positions and relative intensities presented here were calculated from the results of the high-resolution analysis of the ν_8 fundamental, the $\nu_7+\nu_9$ combination band, the $\nu_3-\nu_9$ and $\nu_8-\nu_6$ difference bands, plus the hot bands $\nu_8+\nu_9-\nu_9$, $\nu_7+2\nu_9-\nu_9$ and $\nu_8+\nu_9-\nu_6-\nu_9$ [271,272]. Over 1200 infrared lines measured in Ref. [272] were fitted together with the ro-vibrational transitions recorded in the millimeter-wave range [271] for the bend-bend difference bands. The model adopted for the analysis includes the rotational and vibrational *l*-type resonances active between the various *l*-sublevels of the multiple bending excited states, and also considers the two anharmonic interactions which couple $\nu_3=1$ with the $\nu_8=\nu_9=1$ combination state and the $\nu_3=2$ overtone states through the normal coordinate cubic potential constants ϕ_{389} and ϕ_{377}. The resulting Hamiltonian matrix was block-factorized and diagonalized to derive the energy eigenvalues and the relative transition intensities.

The C_4H_2 relative line intensities of the bands in the microwave region were scaled to the band intensities calculated from the transition dipole moments measured by Matsumura et al. [273]. We note that in the microwave region, the line list presented here is the first compilation available for scientists, and should prove useful in searching for this molecule in different astrophysical objects with instruments including the submillimeter array (SMA) [274] and Herschel [275].

Band intensities in the ν_8 region were scaled to those reported by Jolly et al. [270]. Lines from the bands involving vibrational states that were not observed in Refs. [271,272] were taken from Jolly et al. [270]. The new line list spans the region 0–758 cm^{-1} and contains 124,126 transitions (for only the principal isotopologue).

For the line-shape parameters, no broadening measurements nor calculations were available; for this edition default constant values were adopted ($\gamma_{air}=0.10\ cm^{-1}\ atm^{-1}$, $\gamma_{self}=0.20\ cm^{-1}\ atm^{-1}$, $n=0.75$, $\delta_{air}=0\ cm^{-1}\ atm^{-1}$).

2.44. HC_3N (molecule 44)

Cyanoacetylene is present in the atmosphere of Titan [263] and in molecular clouds [276]. It is therefore important to have reliable spectroscopic reference data for this molecule. The line list of HC_3N covering the spectral regions of the ν_5 (460–550 cm^{-1}) and ν_6 (620–750 cm^{-1}) fundamentals has been adapted from Jolly et al. [277]. The line list also contains some of the hot bands.

The transitions with $\Delta\nu=0$ in the ground, $\nu_6=1$ and $\nu_7=1$ states (in the microwave region) have been adopted from the CDMS catalog [87]. Interestingly, the ro-vibrational energy levels in the $\nu_7=1$ states in the CDMS catalog are systematically shifted by $+0.5863\ cm^{-1}$ with respect to the energy levels from Ref. [277], while there is no difference between the rotational energy levels in the ground state. Since in the work of Jolly et al. spectroscopic constants for all vibrational levels were derived in a global fit which included unpublished lines from the $\nu_6+\nu_7-\nu_7$ and $\nu_6+\nu_7$ bands which allows determination of the position of the $\nu_7=1$ with respect to the ground state accurately, we have made the energy levels from CDMS database consistent with the ones from Jolly et al. [277].

To accommodate representation of seven vibrational modes, three of which are doubly degenerate (ν_5, ν_6 and ν_7) in the fifteen-field "global" quanta space in post-HITRAN2004 format, vibrational quantum numbers are given as follows. In FORTRAN notation it is 2x, 7I1, 3I2. Here each of the integers (I1) corresponds to ν_1, ν_2,…,ν_7, whereas each of the integers (I2) corresponds to ℓ_5, ℓ_6 and ℓ_7. The line list so far is limited to the principal isotopologue and contains 180,332 lines.

2.45. H_2 (molecule 45)

Molecular hydrogen (H_2) is the most abundant gas in the atmosphere of gaseous giants. The quadrupole fundamental and overtone transitions needed to be incorporated into the database. The rotational lines of these bands are very sparse and relatively weak which makes them good candidates for probing very deep and dense Jovian atmospheres. The two most abundant isotopologues of the hydrogen molecule are making their debut in HITRAN. The details of the compilation of these line lists are given below.

The "non-local", non-adiabatic effects are important for H_2 and HD; thus there is no natural way to present the energy as a simple 1-D potential. Fortunately, the theoretical approach developed by Komasa et al. [278] has proved to be very effective. The line positions of the electric quadrupole-allowed transitions for H_2 in the ground electronic state were generated using the dissociation energies calculated by Komasa et al. [278]. The line positions of electric dipole-allowed transitions for HD in the electronic ground state were generated using the dissociation energies calculated by Pachucki et al. [279]. A summary of the spectral range and the number of lines is given in Table 2. The maximum vibrational levels for H_2 and HD are 14 and 17, respectively; the maximum rotational levels, J_{max}, are 30 and 35 respectively for H_2 and HD.

Combining the isotopologue-dependent "best adiabatic" point-wise potential of Schwartz and Le Roy [280] (downloaded from http://leroy.uwaterloo.ca/potentials.html) and an ab initio electric quadrupole moment function of Wolniewicz et al. [281], the matrix elements of quadrupole allowed transitions were calculated for H_2 using Le Roy's LEVEL program [see web site, http://leroy.uwaterloo.ca/programs/%7D.]. Similarly, the dipole matrix elements of HD were calculated, based on the dipole moment function from Ref. [282]. The corresponding line intensities were subsequently calculated from these matrix elements.

The theoretical results we used here had been in excellent agreement with recent cavity ring down experiments [283–286], but in fact surpass them in accuracy and, more importantly, in the extent of the data. Therefore these ab initio results have been adopted for hydrogen line positions in HITRAN. The same discussion applies to the calculation of the intensities.

In the future, electric quadrupole lines of HD will be added to the database.

The Voigt line shape is known to be particularly inadequate for the case of broadening of hydrogen lines [287,288]. Nevertheless, no complete sets of broadening parameters are currently available for either Voigt or non-Voigt line shapes. So far only default Voigt values are used in HITRAN: $\gamma_{air}=0.05\ cm^{-1}\ atm^{-1}$; $\gamma_{self}=0.05\ cm^{-1}\ atm^{-1}$; and $n=0.75$. One should also keep in mind that no shifts are provided at the present time.

2.46. CS (molecule 46)

Carbon monosulfide is a new addition to the HITRAN database. CS detection has been a source of interest for the study of comets and planetary atmospheres. The abundance has been measured, for instance, in the Hyakutake and Hale–Bopp comets [289]. It has also been detected in the atmosphere of Jupiter after the collision with the Shoemaker–Levy comet [290]. Data for four isotopologues ($^{12}C^{32}S$, $^{12}C^{33}S$, $^{12}C^{34}S$, $^{13}C^{32}S$) are now included in the HITRAN database in the microwave region, while infrared data are provided only for the first two isotopologues. The line positions and lower-state energies were obtained from the Cologne Database for Molecular Spectroscopy (CDMS) catalog [87] which are derived from the global fit from the experimental data including that from Refs. [291–293]. Intensities were calculated from theoretical Einstein A-coefficients that were provided in the paper by Chandra et al. [294]. The conversion from Einstein A-coefficients to HITRAN intensities is described in the paper by Šimecková et al. [3].

To the best of our knowledge, no experimental broadening parameters exist for carbon monosulfide, so rough estimates of their values had to be made. To make reasonable estimates of the behavior and values of the broadening parameters of carbon monosulfide, a comparison between carbon dioxide and carbon monoxide broadening parameters (found in the HITRAN database [1]) were made. Using the J-dependent scaling factors obtained for the carbon oxides, the experimental values for nitrogen [295] and self-broadening [296] of carbon disulfide were scaled to obtain broadening parameters for CS. The temperature-dependence exponent for the nitrogen-broadening was estimated to be a standard 0.75, as no experimental data exist.

2.47. SO_3 (molecule 47)

Sulfur trioxide spectroscopic line parameters have been included for the first time in the 2012 HITRAN edition. SO_3 occurs naturally in volcanic emissions and is also a pollutant emitted by smoke-stacks and other industrial exhausts [297]. In the terrestrial atmosphere, SO_3 rapidly forms sulfuric acid with its association with acid rain. SO_3 is also thought to be present in the atmosphere of Venus [298].

SO_3 is a planar, non-polar molecule. However with sufficient rotational excitation the molecule can distort and undergo pure rotational transitions. Lines in this centrifugally-induced pure rotational spectrum were observed by Meyer et al. [299]; in this case the ab initio transition intensities of Underwood et al. [300] have been used as there is no intensity information in the experiment.

Parameters in the infrared region are based on a series of infrared spectra recorded by Maki and co-workers [301–305]. These spectra, which in general were recorded at two pressures, only provide relative intensities. Recently Underwood et al. [300] performed detailed ab initio electronic structure and variational nuclear motion calculations for $^{32}S^{16}O_3$. Comparisons between their absolute, calculated intensities and the measured, relative intensities give good agreement for the strong bands and reasonable agreement for the weaker ones. The line parameters provided have therefore used the ab initio calculations to scale the measured intensities to absolute values. Details of this scaling procedure can be found in Underwood et al. [300].

No measurements or calculations for the line-shape parameters were available, therefore the usual default values were chosen. The new line list for SO_3 contains 10,881 lines covering the region up to 2825 cm^{-1}. Only the main $^{32}S^{16}O_3$ isotopologue has been considered.

3. Infrared absorption cross-sections

Infrared absorption cross sections for this edition of the HITRAN compilation are listed in Table 17. This portion of the database supplies cross sections of molecules for which high-resolution (line-by-line) spectral line parameters are incomplete or unavailable; generally these are large polyatomic molecules for which generating line parameters is very difficult or undesirable at this time due to the lack of detail concerning hot bands and/or characterization of other relevant phenomena such as pressure-induced effects. It is important to point out that the sets of absorption cross sections in HITRAN are far from complete and may not include some additional useful sets; within our resources, the HITRAN committee continues to evaluate and recommend additional sets. Note that all absorption cross sections in this portion of HITRAN have units of cm^2 $molecule^{-1}$.

The cross section format remains the same as HITRAN2008. Absorption cross sections are contained in files by molecule appended with the extension ".xsc", and named by the molecular formula followed by "_IRxx", where xx indicates the last two digits of the year in which the data were first introduced or updated. Files may contain many temperature–pressure sets over a number of spectral regions, as indicated by headers throughout the file. Headers provide the molecule name, the wavenumber range (cm^{-1}), the number of data points, the temperature (K) and pressure (Torr) of the laboratory measurement, the maximum value of the cross section (cm^2 $molecule^{-1}$), and the resolution (cm^{-1}) of the measurement. Absorption cross sections with negative values (generally occurring when there is measurement noise close to the baseline) are set to zero. For a number of datasets, the original experimental files are also provided with "_alt" appended to the filename.

There have been significant additions to the IR-absorption-cross-section section of HITRAN2008, in particular data for a number of important organic molecules are now included, largely from the work of Harrison et al. [306–313]. Updates to the database are indicated in the last 10 entries to Table 17, and are described below.

3.1. C_2H_6

Ethane is the second most abundant hydrocarbon after methane in the atmosphere and a strong absorber in the troposphere. Its line parameters have been present in the HITRAN database for a number of years; however the line parameters in the 3-μm region (ν_7 band) are incomplete, in particular many P and R branch lines are absent. The ν_7 band has been identified as the most desirable for remote-sensing of ethane because it occurs in a reasonably uncongested spectral region and is associated with a C–H stretch vibrational mode (C–H stretches correspond to the most intense features in the IR spectra of aliphatic hydrocarbons). The ν_7 band is particularly accessible to remote-sensing instruments that measure atmospheric absorption using the sun as a light source. On the other hand, instruments detecting in the thermal infrared can only make use of the weaker ν_9 band (780–868 cm^{-1}).

Infrared absorption cross sections for ethane that cover the spectral range 2545–3315 cm^{-1} have been added to the database [306]. Spectra of ethane/dry synthetic air mixtures inside a 26-cm cell were recorded at a number of pressure–temperature combinations using a high-resolution FTIR spectrometer (Bruker IFS 125 HR) at 0.015 cm^{-1} resolution (calculated as the Bruker instrument resolution of 0.9/MOPD). These cross sections include the structure that is missing from the line list and provides a higher degree of accuracy for tropospheric sounding than can currently be obtained using a line-by-line calculation. These cross sections have been used to create a set of "pseudo-lines", effective spectral lines that empirically reproduce the pressure- and temperature-dependencies of spectral absorption without any recourse to quantum-mechanical assignments. They provide a convenient means of interpolating (and extrapolating) cross sections such that the derived absorption varies smoothly with temperature and pressure. The user will find these more useful for remote sensing purposes until the line list

Table 17
Summary of molecules represented by IR cross-section data in HITRAN.

Molecule	Common name	Temperature range (K)	Pressure range (Torr)	Number of *T*,*P* sets	Spectral coverage (cm^{-1})
SF_6	Sulfur hexafluoride	180–295	20–760	32	925–955
$ClONO_2$	Chlorine nitrate	189–297	0–117	25	750–830
		189–297	0–117	25	1260–1320
		213–296	0	2	1680–1790
CCl_4	Carbon tetrachloride	208–297	8–760	32	750–812
N_2O_5	Dinitrogen pentoxide	205–293	0	5	540–1380
HNO_4	Peroxynitric acid	220	0	1	780–830
C_2F_6	Hexafluoroethane, CFC-116	181–296	25–760	43	1061–1165
		181–296	25–760	43	1220–1285
CCl_3F	CFC-11	190–296	8–760	55	810–880
		190–296	8–760	55	1050–1120
CCl_2F_2	CFC-12	190–296	8–760	52	850–950
		190–296	8–760	52	1050–1200
$CClF_3$	CFC-13	203–293	0	6	765–805
		203–293	0	6	1065–1140
		203–293	0	6	1170–1235
CF_4	CFC-14	180–296	8–761	55	1250–1290
$C_2Cl_2F_3$	CFC-113	203–293	0	6	780–995
		203–293	0	6	1005–1232
$C_2Cl_2F_4$	CFC-114	203–293	0	6	815–860
		203–293	0	6	870–960
		203–293	0	6	1030–1067
		203–293	0	6	1095–1285
C_2ClF_5	CFC-115	203–293	0	6	955–1015
		203–293	0	6	1110–1145
		203–293	0	6	1167–1260
$CHCl_2F$	HCFC-21	296	1	1	785–840
$CHClF_2$	HCFC-22	181–297	0–765	29	760–860
		181–296	22–761	31	1070–1195
		253–287	0	3	1060–1210
		253–287	0	3	1275–1380
$CHCl_2CF_3$	HCFC-123	253–287	0	3	740–900
		253–287	0	3	1080–1450
$CHClFCF_3$	HCFC-124	287	0	1	675–715
		287	0	1	790–920
		287	0	1	1035–1430
CH_3CCl_2F	HCFC-141b	253–287	0	3	710–790
		253–287	0	3	895–1210
		253–287	0	3	1325–1470
$CHCl_2CF_2CF_3$	HCFC-225ca	253–287	0	3	695–865
		253–287	0	3	1010–1420
$CClF_2CF_2CHClF$	HCFC-225cb	253–287	0	3	715–1375
CH_2F_2	HFC-32	203–297	0–750	17	995–1236
		203–297	0–750	17	1385–1475
CHF_2CF_3	HFC-125	203–293	0–600	16	494–1503
CHF_2CHF_2	HFC-134	203–297	0–750	9	600–1700
CFH_2CF_3	HFC-134a	253–287	0	3	815–865
		190–296	20–760	32	1035–1130
		190–296	20–760	33	1135–1340
		253–287	0	3	935–1485
CF_3CH_3	HFC-143a	203–297	0–750	9	580–630
		203–297	0–750	9	750–1050
		203–297	0–750	9	1100–1500
CH_3CHF_2	HFC-152a	253–287	0	3	840–995
		253–287	0	3	1050–1205
		253–287	0	3	1320–1490
SF_5CF_3	Trifluoromethyl sulfur pentafluoride	213–323	760	5	599–624
		213–323	760	5	676–704
		213–323	760	5	740–766
		213–323	760	5	860–920
		213–323	760	5	1150–1280
		213–323	760	5	1280–2600
$CH_3C(O)OONO_2$	PAN	295	0.08	1	1650–1901
CH_3CN	Acetonitrile (methyl cyanide)	276–324	760	3	624–784
		276–324	760	3	867–1159
		276–324	760	3	1175–1687
		276–324	760	3	2217–2343
		276–324	760	3	2786–3261

Table 17 (*continued*)

Molecule	Common name	Temperature range (K)	Pressure range (Torr)	Number of *T,P* sets	Spectral coverage (cm^{-1})
		276–324	760	3	3881–4574
C_6H_6	Benzene	278–323	760	3	600–6500
New data introduced since HITRAN2008 [1]					
C_2H_6	Ethane	194–297	49–763	14	2545–3315
CH_3OH	Methanol	204–295	50–761	12	877–1167
		204–296	51–761	12	2600–3250
CH_3CN	Acetonitrile	203–297	50–760	12	880–1700
		208–296	50–760	11	2550–3300
C_3H_8	Propane	195–296	40–763	12	2540–3300
CH_3COCH_3	Acetone	194–298	50–700	19	830–1950
		195–296	49–759	12	2615–3300
$CH_3C(O)OONO_2$	PAN	250–295	0	3	560–1400
		250	0	1	1590–2200
CH_3CHO	Acetaldehyde	200–297	50–762	16	2400–3400
CH_3CClF_2	HCFC-142b	223–283	0	7	650–1500
$BrONO_2$	Bromine nitrate	218–296	0	2	770–843
ClOOCl	Chlorine peroxide	225–250	15–33	4	500–835

Note: These data are in the main directory. Additional redundant data for CFC-11, CFC-12, HFC-125, and HFC-143a are stored in a supplemental subdirectory. Rescaling of data for HCFC-141b for the 1325–1470 cm^{-1} region at 270 K has been performed as described in Section 3.8.

near 3 μm is greatly improved. Visit http://mark4sun.jpl.nasa.gov/pseudo.html to obtain the pseudo-line list.

3.2. CH_3OH

Methanol is the second most abundant organic molecule in the terrestrial atmosphere after methane. Around two-thirds of methanol emissions arise from plant growth, with the rest coming from plant decay, atmospheric oxidation of methane and other hydrocarbons, biomass burning and biofuels, and vehicles and industrial activities.

Two new infrared absorption cross section datasets have been added to the database, covering the spectral ranges 877–1167 cm^{-1} and 2600–3250 cm^{-1} [312]. Spectra of methanol/dry synthetic air were recorded with a high-resolution FTIR spectrometer (Bruker IFS 125 HR) at 0.015 cm^{-1} resolution (≡0.9/MOPD) using a coolable White cell with a maximum path length of 19.32 m. Methanol data near 3.4 μm are included in HITRAN for the first time. Line parameters near 10 μm have been included in HITRAN since 2004; this band system is principally associated with the strong fundamental ν_8 mode at 1033 cm^{-1} (CO stretch). The new cross sections near 10 μm provide a higher level of accuracy at lower temperatures and reveal a number of problems with the line list, which was derived from a set of room-temperature spectra. When simulating spectra using the HITRAN line list, the integrated intensity of the band system drops by about one quarter from 300 to 200 K. This is at odds with the new 10 μm data, which provide no evidence for temperature dependence. Therefore, using the existing HITRAN line list for remote sensing will impact the accuracy of the retrievals. A methanol pseudo-line list near 10 μm, using the same procedure described above for ethane near 3 μm, is currently planned.

3.3. CH_3CN

Acetonitrile (CH_3CN) is a minor constituent of the Earth's atmosphere, with the majority of emissions arising from biomass burning. The lifetime of acetonitrile is of the order of 6 months, making this molecule a useful tracer for troposphere–stratosphere transport.

In addition to line parameters for the ν_4 band, HITRAN2008 contained a number of acetonitrile absorption cross sections between 624 and 4574 cm^{-1} recorded at a resolution of 0.112 cm^{-1} and a pressure of 760 Torr nitrogen at 276, 298, and 323 K. On their own, these are not useful for retrieving concentrations from spectra recorded in the upper troposphere/lower stratosphere (UTLS) because they do not cover the appropriate range of atmospheric temperatures and pressures. This problem has been remedied by the addition of a number of new pressure–temperature sets of infrared absorption cross sections to HITRAN. These datasets cover the spectral ranges 880–1700 cm^{-1} [311] and 2550–3300 cm^{-1} [310]. Spectra of acetonitrile/dry synthetic air were recorded by a high-resolution FTIR spectrometer (Bruker IFS 125 HR) at 0.015 cm^{-1} resolution (≡0.9/MOPD) using a coolable White cell with a maximum path length of 19.32 m. The cross sections in the MWIR region, in particular the $^rQ_0$ branch of the ν_6 band at 1462.96–1463.60 cm^{-1}, have recently been used as the basis for an ACE-FTS (Atmospheric Chemistry Experiment) acetonitrile research product [313].

3.4. $CH_3CH_2CH_3$

Propane is the third most abundant hydrocarbon after methane in the atmosphere. However, thus far there have been no global measurements using IR remote-sensing techniques. Infrared absorption cross sections for propane have been introduced for the first time into HITRAN; they cover the spectral range 2540–3300 cm^{-1} [307], where propane has its strongest-intensity vibrational modes (C–H stretch). Spectra of propane/dry synthetic air mixtures inside a 26-cm cell were recorded at 12 pressure–temperature combinations using a high-resolution FTIR spectrometer (Bruker IFS 125 HR) at 0.015 cm^{-1} resolution (≡0.9/MOPD).

3.5. CH_3COCH_3

Infrared absorption cross sections for propanone (acetone) have been introduced for the first time into HITRAN. Acetone is the simplest member of the ketone family, and one of the most abundant volatile organic compounds (VOCs) in the free troposphere. The largest source of atmospheric acetone is the oxidation of organic precursors, e.g. alkanes. Other sources include biomass burning and biogenic emissions, including plant growth and decay, and a minor contribution from anthropogenic emissions.

Two new datasets have been added to the database, covering the spectral ranges 830–1950 cm^{-1} [309] and 2615–3300 cm^{-1}[308]; the mid-IR cross sections have been combined with older measurements taken by Waterfall [314] to create a combined dataset. For the new measurements, spectra of acetone/dry synthetic air were recorded by a high-resolution FTIR spectrometer (Bruker IFS 125 HR) at 0.015 cm^{-1} resolution (≡0.9/MOPD) using a coolable White cell with a maximum path length of 19.32 m. These mid-IR data have been used, for example, to retrieve acetone concentrations from spectra recorded by the MIPAS (Michelson Interferometer for Passive Atmospheric Sounding) instrument onboard Envisat [315]. Additionally, an ACE research product has recently been developed [316].

3.6. $CH_3C(O)OONO_2$

Infrared absorption data at 295 K for peroxyacetyl nitrate (abbreviated as PAN) became available in HITRAN2008. PAN, a reservoir for reactive NO_x, has a number of sources, including photochemical smog and biomass burning. Due to thermal stability of PAN at lower temperatures, it can be transported over long distances in the middle and upper troposphere; the consequence of this is the long-distance transport of pollution.

Additional infrared absorption cross sections for PAN (560–1400 cm^{-1}) have been included in HITRAN. The original data [317,318] have been adapted to correct the baselines so that they agree better with each other and the intensities have been normalized to the room temperature value [319]; the data in HITRAN (at 250, 273 and 295 K), therefore, differ slightly from those in the original references. PAN cross sections are also available over the range 1590–2200 cm^{-1} at 250 K and 1650–1900 cm^{-1} at 295 K. The user should use these two cross sections with care due to an obvious discrepancy in the baseline between the two measurements.

3.7. CH_3CHO

Ethanal, also known as acetaldehyde, is a trace molecular species found in the terretrial atmosphere. Sources include photochemical production, the oxidation of hydrocarbons, biogenic emission from plant decay, anthropogenic combustion and biomass burning. So far there have been no measurements using IR remote-sensing techniques. Infrared absorption cross sections for acetaldehyde in the 3 μm region [320] have been introduced for the first time into HITRAN. The spectra were recorded at a number of temperatures and pressures appropriate for atmospheric conditions.

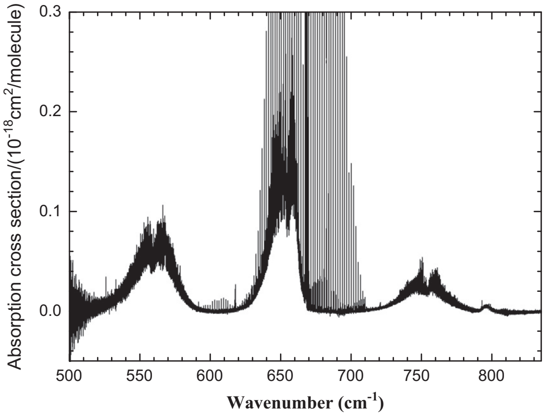

Fig. 10. Absorption cross sections of ClOOCl at 213 K and 20 hPa.

3.8. HCFC-141b

HITRAN infrared cross-sections for the hydrochlorofluorocarbon HCFC-141b (1,1-dichloro-1-fluoroethane) originate from Clerbaux et al. [321]. It was found recently that the set of cross-sections in the 1325–1470 cm^{-1} region at 270 K differed from the ones in the original publication. The reason for this discrepancy is unclear. The HITRAN cross-sections in this pressure–temperature set have now been multiplied by 1.75 to bring them into consistency with the original publication.

3.9. HCFC-142b

New temperature-dependent absorption cross-sections of HCFC-142b (1-chloro-1,1-difluoroethane) have been added to the HITRAN compilation. The data cover the 650–1500 cm^{-1} spectral region, and come from the work of Le Bris and Strong [322]. These data replace the sets of HCFC-142b IR cross-sections that previously existed in HITRAN.

3.10. $BrONO_2$

IR absorption cross sections for bromine nitrate were recently introduced into HITRAN. $BrONO_2$ is an important species in stratospheric bromine chemistry and is part of the photochemistry in stratospheric ozone depletion. It is the most important reservoir species for inorganic stratospheric bromine.

The cross-sections are given at 218 K and 296 K. The latter set is based on laboratory measurements, whereas the set for 218 K was obtained by scaling the 296 K experimental data. The values are explained in more detail in the paper about the atmospheric detection of $BrONO_2$ by the MIPAS instrument [323].

3.11. ClOOCl

Chlorine peroxide (ClOOCl) is known to play an important role in the antarctic and arctic perturbed chemistry leading to the well-known ozone hole [324]. The first proof that ClOOCl, being a product of the ClO self reaction, has a peroxide like structure which is the only Cl_2O_2 isomer capable of destroying ozone in a catalytic cycle was shown by Birk et al. [325]. The first direct observation of this species by balloon-borne mid-infrared limb sounding in the Arctic [326] is based on the absorption cross sections now entered into the HITRAN database. This latter paper also contains details about the laboratory measurements of the absorption cross-sections. The agreement of the total chlorine budget using these absorption cross-sections with the total inorganic chlorine load of the atmosphere indicates the validity of the data.

Four sets of absorption cross sections are given for combinations of temperatures 213 K and 243 K and total pressures 20 hPa and 40 hPa in the mixture of nitrogen and helium. The total uncertainty of the absorption cross sections is 12%. Fig. 10 shows the absorption cross sections for 213 K and 20 hPa. There are three bands that have been observed. So far the weakest band in the range 720–790 cm^{-1} was used for retrieval. The middle band is blended by CO_2 and cannot be used for atmospheric measurements. In the absorption cross sections, this band is contaminated by CO_2 arising from the technical-grade chlorine used in the synthesis. Best suited for atmospheric measurements would be the band between 500 and 600 cm^{-1} since this band is three times stronger than the band at 720–790 cm^{-1}. So far no limb sounder is available covering this region.

Table 18
Refractive indices included in HITRAN2012.

Compound	Measurement specifics	References
Water	27°C, 10–5000 cm^{-1}	[329]
Water	0.67–2.5 μm	[330]
Ice	266 K, 0.04 μm–2 m	[330]
Ice	0.67–2.5 μm	[331]
Water, ice, sodium chloride, sea salt, water soluble aerosol, ammonium sulfate, carbonaceous aerosol, volcanic dust, sulfuric acid, meteoric dust, quartz, hematite, sand	Room temperature, 0.2–40 μm	[332]
Sulfuric acid (H_2SO_4/H_2O)	Room temperature, 25–96% H_2SO_4	[333]
Sulfuric acid (H_2SO_4/H_2O)	Room temperature, 75 and 90% H_2SO_4	[334]
Sulfuric acid (H_2SO_4/H_2O)	215 K, 499–6996 cm^{-1}	[335]
Sulfuric acid (H_2SO_4/H_2O)	200–300 K, 825–4700 cm^{-1}	[336]
Sulfuric acid (H_2SO_4/H_2O)	213–293 K, 432–5028 cm^{-1}	[337]
Nitric acid (H_2SO_4/HNO_3)	Room temperature, 250–2987 cm^{-1}	[338]
Nitric acid (H_2SO_4/HNO_3)	220 K, 754–4700 cm^{-1}	[339]
Nitric acid (H_2SO_4/HNO_3)	213–293 K, 432–5028 cm^{-1}	[337]
Amorphous nitric acid (NAM, NAD, NAT)	153 K, 482–7000 cm^{-1}	[340]
NAM	179 K, 482–6002 cm^{-1}	[340]
NAD	184 K, 482–6981 cm^{-1}	[340]
NAD	160–190 K, 700–4700 cm^{-1}	[341]
αNAT	181 K, 482–6989 cm^{-1}	[340]
βNAT	196 K, 482–6364 cm^{-1}	[340]
NAT	160 K, 711–4004 cm^{-1}	[342]
Burning vegetation	525–5000 cm^{-1}	[343]
Burning vegetation	0.35–1.5 μm	[344]
Carbon flame	0.4–0.7 μm, 25–600 °C	[345]
Flame soot	0.2–38 μm	[346]
Brown carbon	0.2–1.2 μm	[347]
Organic acids (oxalic, malonic, succinic, pinonic, pyruvic, phthalic)	0.25–1.1 μm	[348]
Organic haze	0.525 nm	[349]
SOA (proxy)	0.525 nm	[350]
Minerals (clay, illite, kaolin, montmorillonite)	2.5–200 μm	[351]
Minerals (granite, montmorillonite)	5–40 μm	[352]
Saharan dust	0.30–0.95 μm	[353]
Saharan dust	0.35–0.65 μm	[354]
Volcanic ash	0.45–25 μm	[355]

4. Ultraviolet datasets

4.1. H_2CO

A study of the previous ultraviolet absorption cross sections for formaldehyde in HITRAN was carried out as recommended by the HITRAN Advisory Committee. The cross sections introduced into the new edition of HITRAN have been derived from two existing sets, one using a Fourier transform spectrometer, and one using a grating instrument. The new re-scaled data are based on the work of Chance and Orphal [327].

5. Aerosol refractive indices

Aerosols and clouds influence radiative transfer in the terrestrial atmosphere [328], participate in chemistry reactions in both the liquid and solid phases [324], and complicate remote-sensing retrievals of gaseous species. Light scattering and absorption by aerosols and clouds is dependent upon how particle size distributions are distributed in a three-dimensional manner, the compositions (i.e. refractive indices) of the aerosols and cloud particles, and by the shapes of the particles. HITRAN2012 contains refractive indices in the visible, infrared, and millimeter spectral ranges of many of the materials which comprise the compositions of aerosols and clouds. Table 18 lists the HITRAN2012 indices.

Additions to HITRAN2012 focus upon absorptive aerosol species. Absorptive aerosol is of interest since it can perturb the radiation field close to the Earth's surface, thereby perturbing the temperature profile structure and convective processes [356]. The dimensionless complex refractive index

$$m = m_{\mathrm{real}} + i m_{\mathrm{imag}} \tag{7}$$

has positive real m_{real} and imaginary m_{imag} components. A plane light wave of wavelength λ is attenuated along the propagation x axis according to

$$E = E_0 \exp(-2\pi m_{imag} x/\lambda)\, \exp(i2\pi m_{real} x/\lambda - i2\pi ct/\lambda) \tag{8}$$

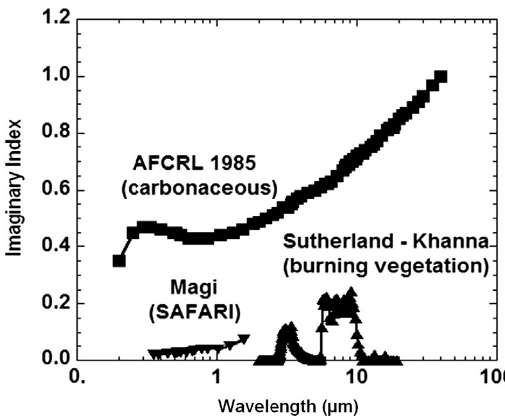

Fig. 11. Imaginary indices of three carbon containing materials that illustrate the wide range of absorptive characteristics of naturally occurring combustion products.

with time t and the speed of light c. Thus, it is the imaginary refractive index which determines the amount of light absorption in a medium.

New HITRAN indices include secondary organic acid (proxy) [350], carbonaceous indices [345,346] mineralogical indices, Saharan dust (as a function of hematite content) [353], brown carbon [347], volcanic ash indices [355], and vegetation-fire indices derived from field measurements [344]. Organic acids, which scatter primarily and are precursors to secondary organic aerosols, are also tabulated [347].

HITRAN2012 contains indices based upon field measurements of aerosols in their natural setting in addition to laboratory measurements. Since the composition of aerosol is chemically very diverse and evolves daily, it is useful to include field measurements of aerosol refractive indices in HITRAN. Fig. 11 illustrates this point by presenting the composite AFCRL carbonaceous aerosol indices [332], Sutherland-Khana burning vegetation indices [343], and the Magi indices of biomass fires inferred from aircraft measurements during the SAFARI 2000 field experiment [344]. Since the imaginary refractive index is responsible for light absorption, differences in the imaginary index of various materials are of primary interest. The range in the imaginary indices in Fig. 11—a factor of 10—is considerable.

A new development for HITRAN2012 is the introduction of the HITRAN-RI program [357] that will reside on the HITRAN website. This program, written in the IDL (Interactive Design Language) and Fortran 90 programming languages, allows the user to access and use the HITRAN2012 indices in Mie calculations. Output ASCII files of the indices, particle size distributions, and spectra (extinction, scattering, absorption, single scattering albedo, backscattering, and asymmetry parameters) are created by the program. The IDL version of the program also produces output Postscript graphics files. The user specifies the size distribution and the indices of the particles by editing a simple ASCII input file. The wavelength dependence of the refractive indices of two datasets can be compared to each other. The user can obtain composite indices of multiple-component aerosols by applying one of several available mixing rules. There are test cases which serve an instructional purpose for those not familiar with Mie calculations. Subdirectories associated with HITRAN-RI contain pdfs of the reference papers, and the indices are specified in both ASCII and netCDF formats. The ASCII files are useful to quickly obtain the real and imaginary indices at a specific wavelength, while the netCDF files are used by the HITRAN-RI program in user friendly calculations.

6. Collision-induced absorption

Collision-induced absorption (CIA) is caused by a transient dipole moment being created during collisions of molecules. The absorption features underlie many of the traditional electric dipole, magnetic dipole, and quadrupole transitions that have been the traditional mainstay of HITRAN. They not only are valuable for radiative-transfer calculations for the terrestrial atmosphere, but are applicable to simulations of radiance in planetary and stellar

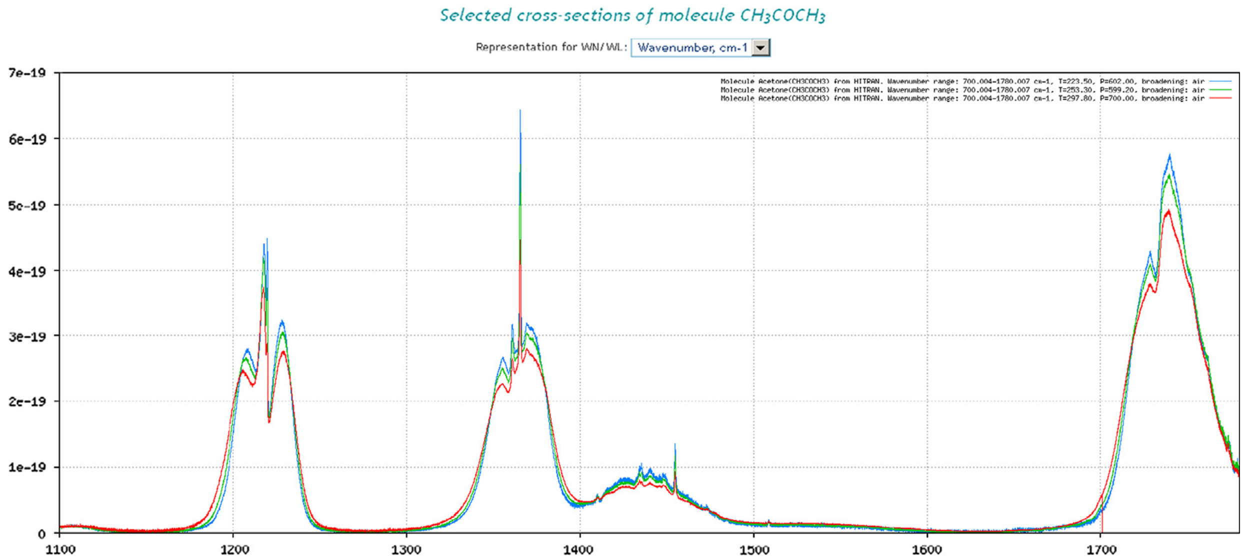

Fig. 12. HITRAN on the web plot of selected cross-sections of acetone (CH_3COCH_3). *Y* axis in absorption (cm^2 molecule^{-1}).

atmospheres. Experimental and theoretical sources have now been assembled and cast into a consistent format of cross-sections for this new edition of HITRAN. The details of the sets of collision pairs, their spectral and temperature ranges, and their sources are described in Ref. [132].

In this first presentation of CIA in the HITRAN compilation, fourteen different collisional pairs are given, N_2-N_2, N_2-H_2, N_2-CH_4, H_2-H_2, H_2-He, H_2-CH_4, H_2-H, He-H, O_2-O_2, O_2-N_2, O_2-CO_2, CO_2-CO_2, CH_4-CH_4, and CH_4-Ar. In the future, other complexes of interest will be included, improved data will replace less accurate data, and the CIA datasets will be extended to cover other spectral regions and temperature domains when possible.

7. Global data and software

7.1. Options for accessing, filtering, and managing HITRAN data

The Java-based JavaHawks software that accompanied previous editions of HITRAN is no longer maintained and, although one can still use it for most of the molecules, it will not be able to handle new molecules or new isotopologues that have been recently introduced. It will also fail to select vibrational bands which were introduced into HITRAN after the year 2004.

HITRAN on the Web (hitran.iao.ru) is an efficient online HITRAN browsing and plotting tool developed at the V.E. Zuev Institute of Atmospheric Optics and the Harvard-Smithsonian Center for Astrophysics taking advantage of the S&MPO ozone database software [79] and adapted functionalities of the JavaHawks software. Inside HITRAN on the web, the HITRAN data are treated as a relational database under control of the MySQL database management system. The site software is written in the PHP language using the Zend Framework. The modules for spectra simulations are written on C. Application software was developed using the Model-View-Controller (MVC) approach. Within MVC, the data model of an application, the user interface, and the operating logic are considered as separate components, so that updating of one of the components has minimum influence on others.

The HITRAN on the Web browsing tool allows selections and manipulations with HITRAN data that are most desired by the users of the database. The “HITRAN survey” option allows selecting lines of chosen molecules within a desired spectral range. A more sophisticated interactive system is provided in the individual “Molecules” section. In particular, it allows for the selection of multiple spectral bands and their plotting in different colors, predicting spectra at different temperatures, and implementation of user-selected isotopic abundances. Other important features include (1) easy access to the abstracts of publications used as sources of data for the spectroscopic parameters and absorption cross-sections in HITRAN; (2) selection of data based on the uncertainty index; (3) advanced plotting options that are also applicable to the cross-sections (see Fig. 12, for example, that was generated using this online tool); (4) convenient presentation of relative band intensities and the spectral range they cover and many other important features. One of the presentations, describing the use of the database, is given as supplementary material to this paper.

Another development for accessing the HITRAN database is the development of a user interface based on the relational database discussed in the next section.

7.2. Database structures

Under the auspices of the Virtual Atomic and Molecular Data Centre (VAMDC) project [358], an initiative was created to cast the HITRAN database into a relational database structure that would be interoperable with other major databases in the fields of atomic, molecular, and plasma physics. This structure has many advantages over the fixed-field, text-based format that has existed since the inception

Table 19
Values of isotopic abundance chosen for isotopologues in HITRAN.

Molecule	Isotopologue	Abundance	Q (296 K)	g_j	Mass (g)
(1) H_2O	161	9.973×10^{-1}	1.74×10^{2}	1	18.01056
	181	1.999×10^{-3}	1.75×10^{2}	1	20.01481
	171	3.719×10^{-4}	1.04×10^{3}	6	19.01478
	162	3.107×10^{-4}	8.59×10^{2}	6	19.01674
	182	6.230×10^{-7}	8.75×10^{2}	6	21.02098
	172	1.158×10^{-7}	5.22×10^{3}	36	20.02096
(2) CO_2	626	9.842×10^{-1}	2.87×10^{2}	1	43.98983
	636	1.106×10^{-2}	5.78×10^{2}	2	44.99319
	628	3.947×10^{-3}	6.09×10^{2}	1	45.99408
	627	7.340×10^{-4}	3.55×10^{3}	6	44.99405
	638	4.434×10^{-5}	1.23×10^{3}	2	46.99743
	637	8.246×10^{-6}	7.16×10^{3}	12	45.99740
	828	3.957×10^{-6}	3.24×10^{2}	1	47.99832
	827	1.472×10^{-6}	3.78×10^{3}	6	46.99829
	727	1.368×10^{-7}	1.10×10^{4}	1	45.998262
	838	4.446×10^{-8}	6.54×10^{2}	2	49.00168
	837[a]	1.654×10^{-8}	7.62×10^{3}	12	48.00165
(3) O_3	666	9.929×10^{-1}	3.48×10^{3}	1	47.98475
	668	3.982×10^{-3}	7.47×10^{3}	1	49.98899
	686	1.991×10^{-3}	3.65×10^{3}	1	49.98899
	667	7.405×10^{-4}	4.33×10^{4}	6	48.98896
	676	3.702×10^{-4}	2.14×10^{4}	6	48.98896
(4) N_2O	446	9.903×10^{-1}	5.00×10^{3}	9	44.00106
	456	3.641×10^{-3}	3.36×10^{3}	6	44.9981
	546	3.641×10^{-3}	3.46×10^{3}	6	44.9981
	448	1.986×10^{-3}	5.31×10^{3}	9	46.00531
	447	3.693×10^{-4}	3.10×10^{4}	54	45.00528
(5) CO	26	9.865×10^{-1}	1.07×10^{2}	1	27.99492
	36	1.108×10^{-2}	2.24×10^{2}	2	28.99827
	28	1.978×10^{-3}	1.12×10^{2}	1	29.99916
	27	3.679×10^{-4}	6.59×10^{2}	6	28.99913
	38	2.223×10^{-5}	2.36×10^{2}	2	31.00252
	37	4.133×10^{-6}	1.38×10^{3}	12	30.00249
(6) CH_4	211	9.883×10^{-1}	5.90×10^{2}	1	16.0313
	311	1.110×10^{-2}	1.18×10^{3}	2	17.03466
	212	6.158×10^{-4}	4.79×10^{3}	3	17.03748
	312	6.918×10^{-6}	9.60×10^{3}	6	18.04083
(7) O_2	66	9.953×10^{-1}	2.16×10^{2}	1	31.98983
	68	3.991×10^{-3}	4.52×10^{2}	1	33.99408
	67	7.422×10^{-4}	2.64×10^{3}	6	32.99405
(8) NO	46	9.940×10^{-1}	1.14×10^{3}	3	29.99799
	56	3.654×10^{-3}	7.89×10^{2}	2	30.99502
	48	1.993×10^{-3}	1.20×10^{3}	3	32.00223
(9) SO_2	626	9.457×10^{-1}	6.34×10^{3}	1	63.9619
	646	4.195×10^{-2}	6.37×10^{3}	1	65.9577
(10) NO_2	646	9.916×10^{-1}	1.36×10^{4}	3	45.9929
(11) NH_3	4111	9.959×10^{-1}	1.73×10^{3}	3	17.02655
	5111	3.661×10^{-3}	1.15×10^{3}	2	18.02358
(12) HNO_3	146	9.891×10^{-1}	2.14×10^{5}	6	62.99564
	156	3.636×10^{-3}	1.42×10^{5}	4	63.99268
(13) OH	61	9.975×10^{-1}	8.04×10^{1}	2	17.00274
	81	2.000×10^{-3}	8.09×10^{1}	2	19.00699
	62	1.554×10^{-4}	2.09×10^{2}	3	18.00892
(14) HF	19	9.998×10^{-1}	4.15×10^{1}	4	20.00623
	29	1.557×10^{-4}	1.16×10^{2}	6	21.0124
(15) HCl	15	7.576×10^{-1}	1.61×10^{2}	8	35.97668
	17	2.423×10^{-1}	1.61×10^{2}	8	37.97373
	25	1.180×10^{-4}	4.63×10^{2}	12	36.98285
	27	3.774×10^{-5}	4.64×10^{2}	12	38.9799
(16) HBr	19	5.068×10^{-1}	2.00×10^{2}	8	79.92616
	11	4.931×10^{-1}	2.00×10^{2}	8	81.92412
	29	7.894×10^{-5}	5.86×10^{2}	12	80.93234
	21	7.680×10^{-5}	5.87×10^{2}	12	82.93029
(17) HI	17	9.998×10^{-1}	3.89×10^{2}	12	127.9123
	27	1.557×10^{-4}	1.15×10^{3}	18	128.9185
(18) ClO	56	7.559×10^{-1}	3.27×10^{3}	4	50.96377
	76	2.417×10^{-1}	3.33×10^{3}	4	52.96082
(19) OCS	622	9.374×10^{-1}	1.22×10^{3}	1	59.96699
	624	4.158×10^{-2}	1.25×10^{3}	1	61.96278

Table 19 (*continued*)

Molecule	Isotopologue	Abundance	Q (296 K)	g_j	Mass (g)
	632	1.053×10^{-2}	2.48×10^{3}	2	60.97034
	623	7.399×10^{-3}	4.95×10^{3}	4	60.96637
	822	1.880×10^{-3}	1.31×10^{3}	1	61.97123
(20) H_2CO	126	9.862×10^{-1}	2.85×10^{3}	1	30.01057
	136	1.108×10^{-2}	5.84×10^{3}	2	31.01392
	128	1.978×10^{-3}	2.99×10^{3}	1	32.01481
(21) HOCl	165	7.558×10^{-1}	1.93×10^{4}	8	51.97159
	167	2.417×10^{-1}	1.96×10^{4}	8	53.96864
(22) N_2	44	9.927×10^{-1}	4.66×10^{2}	1	28.00615
	45	7.478×10^{-3}	3.86×10^{2}	6	29.00318
(23) HCN	124	9.851×10^{-1}	8.95×10^{2}	6	27.0109
	134	1.107×10^{-2}	1.84×10^{3}	12	28.01425
	125	3.622×10^{-3}	6.21×10^{2}	4	28.00793
(24) CH_3Cl	215	7.489×10^{-1}	5.79×10^{4}	4	49.99233
	217	2.395×10^{-1}	5.88×10^{4}	4	51.98938
(25) H_2O_2	1661	9.950×10^{-1}	9.82×10^{3}	1	34.00548
(26) C_2H_2	1221	9.776×10^{-1}	4.14×10^{2}	1	26.01565
	1231	2.197×10^{-2}	1.66×10^{3}	8	27.01901
	1222	3.046×10^{-4}	1.58×10^{3}	6	27.02183
(27) C_2H_6	1221	9.770×10^{-1}	7.09×10^{4}	1	30.04695
	1231	2.195×10^{-2}	3.62×10^{4}	2	31.05031
(28) PH_3	1111	9.995×10^{-1}	3.25×10^{3}	2	33.99724
(29) COF_2	269	9.865×10^{-1}	7.00×10^{4}	1	65.99172
	369	1.108×10^{-2}	3.78×10^{4}	2	66.99508
(30) SF_6	29	9.502×10^{-1}	1.62×10^{6}	1	145.9625
(31) H_2S	121	9.499×10^{-1}	5.03×10^{2}	1	33.98772
	141	4.214×10^{-2}	5.04×10^{2}	1	35.98352
	131	7.498×10^{-3}	2.01×10^{3}	4	34.98711
(32) HCOOH	126	9.839×10^{-1}	3.91×10^{4}	4	46.00548
(33) HO_2	166	9.951×10^{-1}	4.30×10^{3}	2	32.99766
(34) O	6	9.976×10^{-1}	6.72	1	15.99492
(35) $ClONO_2$	5646	7.496×10^{-1}	4.79×10^{6}	12	96.95667
	7646	2.397×10^{-1}	4.91×10^{6}	12	98.95372
(36) NO^+	46	9.940×10^{-1}	3.12×10^{2}	3	29.99799
(37) HOBr	169	5.056×10^{-1}	2.83×10^{4}	8	95.92108
	161	4.919×10^{-1}	2.82×10^{4}	8	97.91903
(38) C_2H_4	2211	9.773×10^{-1}	1.10×10^{4}	1	28.0313
	2311	2.196×10^{-2}	4.52×10^{4}	2	29.03466
(39) CH_3OH	2161	9.859×10^{-1}	3.53×10^{4}	2	32.02622
(40) CH_3Br	219	5.010×10^{-1}	8.30×10^{4}	4	93.94181
	211	4.874×10^{-1}	8.34×10^{4}	4	95.93976
(41) CH_3CN	2124	9.739×10^{-1}	8.87×10^{4}	3	41.02655
(42) CF_4	29	9.889×10^{-1}	1.21×10^{5}	1	87.99362
(43) C_4H_2	2211	9.560×10^{-1}	9.82×10^{3}	6	50.01090
(44) HC_3N	1224	9.633×10^{-1}	2.48×10^{4}	6	51.0109
(45) H_2	11	9.997×10^{-1}	7.67×10^{0}	1	2.01565
	12	3.114×10^{-4}	2.99×10^{1}	6	3.02182
(46) CS	22	9.396×10^{-1}	2.54×10^{2}	1	43.97104
	24	4.168×10^{-2}	2.53×10^{2}	1	45.96679
	32	1.056×10^{-2}	5.37×10^{2}	2	44.97437
	23	7.417×10^{-3}	1.02×10^{3}	4	44.97040
(47) SO_3	26	9.434×10^{-1}	7.96×10^{3}	1	79.95682

[a] This eleventh isotopologue could not be entered into HITRAN under the standard format.

of HITRAN four decades ago. First of all it addresses some of the deficiencies encountered by the old structure, including (1) the limited ability to expand the fields to account for the quantum identification of complex states, for example polyatomic molecules with many vibrational modes, dynamic molecules with torsional modes, hyperfine coupling to more than one nucleus, etc.; (2) the limited ability to expand the line shape parameters, including line broadening by other collisional partners, their temperature dependences, line-shape formalisms other than Voigt profile, line mixing, etc.; (3) the inconvenient methods of flagging unavailable data (for example setting the lower-state energy to negative unity to flag an unassigned transition); and (4) the restriction of field length that prevents accommodating parameters with a greater number of significant figures. The advantages of a relational database for HITRAN are myriad. It is easy to extend. More complex molecular states can be represented with as many quantum numbers as necessary. Parameters for alternative line shapes (for example Galatry) can easily be implemented. Additional broadeners, now needed for planetary atmospheres, can be efficiently added. Field size is not an issue, so all significant digits of a parameter can be stored.

Other advantages of the relational database for HITRAN include the ability to simply establish a data provenance, that is, each parameter can be given a time stamp; it is not removed when replaced by newer data and can easily be reproduced at a later time if necessary. The database allows for a structured query language which greatly facilitates validation and data mining for semantic information. References to sources of data, which have previously been stored in a separate file, are now part of the database and easily accessed (this is similar to the feature available in the HITRAN on the Web system discussed in Section 7.1).

Under continued development, the new database structure has the ability to filter and return HITRAN data in different output formats, including the older ones familiar to many users. Details of this endeavor can be found in Hill et al. [359].

7.3. Global data

Certain data that are general in scope to HITRAN appear in a separate folder of the compilation that we call Global Data. These data are necessary information including: (1) the isotopic abundance values chosen for the HITRAN intensities (required by the user to normalize their values); and (2) the partition sums of the isotopologues as used by HITRAN. Table 19 is the table of chosen molecular quantities provided with the HITRAN compilation.

Besides giving the value of the partition sum at the HITRAN standard temperature of 296 K, a program is provided with the compilation to compute the partition sum of the isotopologues at temperatures from 70 to 3000 K. Note that the definition of partition sums in HITRAN is very general and includes state-independent statistical weights. Thus the values themselves may appear rather large; however, the partition sums usually appear as ratios, so extra factors in the definitions cancel out. Descriptions of the methodology for deriving the HITRAN partition sums can be found in Refs. [360,361].

8. Conclusions

The improvements to a new HITRAN database release have been elaborated upon. The new edition has incorporated improved line position, intensity, and line-shape parameters for many of the previously existing molecules and isotopologues. Several new molecules and isotopologues have been added to the compilation, with special consideration for applications beyond those associated with the terrestrial atmosphere.

Applications over the past few years, especially high-resolution, high signal-to-noise satellite remote-sensing missions, have put new demands on the standard database. Thus one can see in this new edition of HITRAN a concentrated effort to not only provide more accurate data, but to expand the database to include more vibration-rotation bands, weaker transitions, and refined line-shape parameters and formalisms. The compilation also includes for the first time sets of collision-induced absorption data.

HITRAN is also evolving in terms of structure. A new relational database structure has been established that allows for many expansions that would be prohibitive in the old fixed-length ASCII format of previous HITRAN editions. Interfaces on the internet have also been established that provide the diverse group of HITRAN users with much power to filter, extract, plot, and query the database.

The compilation is free; access instructions can be obtained at http://www.cfa.harvard.edu/HITRAN.

Acknowledgments

The management and development of the HITRAN molecular database has been supported by NASA AURA mission Grant NNX11AF91G, and NASA Planetary Atmosphere Grant NNX10AB94G.

We gratefully acknowledge the many researchers who provided data, experimental and/or theoretical: M. Abel, N.D.C. Allen, A.A.A. Azzam, A. Borysow, C. Bray, P. Cacciani, A. Coustenis, J. Coxon, A. Császár, L. Daumont, M.-R. De Backer, M. Down, L. Frommhold, T. Furtenbacher, M. Gustaffson, P. Hadjigeorgiou, M. Herman, C. Hermans, S. Kassi, I. Kleiner, N. Lacome, W.J. Lafferty, A. Laraia, K. LeBris, O. Leshchishina, L. Lodi, C.E. Miller, D. Mondelain, G. Orton, L. Régalia, K.M. Smith, K. Strong, K.A. Terezschuk, H. Tran, J. Vander Auwera, L. Wang, S. Yu, S. Yurchenko.

We also wish to acknowledge the many colleagues who provided independent validation of the line lists: B. Bonev, C.D. Boone, M. Cich, S.A. Clough, E. Gibb, A. Goldman, M. Koshelev, V.A. Krasnopolsky, Q. Ma, E. Mlawer, V. Paine, D. Pliutau, G. Villanueva, B. Voronin.

NCAR is sponsored by the National Science Foundation. Part of the research at the College of William and Mary, Langley Research Center, and the Jet Propulsion Laboratory (JPL), California Institute of Technology, was performed under contract with the National Aeronautics and Space Administration.

Appendix A. Supporting information

Supplementary data associated with this article can be found in the online version at http://dx.doi.org/10.1016/j.jqsrt.2013.07.002.

References

[1] Rothman LS, Gordon IE, Barbe A, Benner DC, Bernath PF, Birk M, et al. The HITRAN 2008 molecular spectroscopic database. J Quant Spectrosc Radiat Transfer 2009;110:533–72.

[2] Rothman LS, Jacquemart D, Barbe A, Chris Benner D, Birk M, Brown LR, et al. The HITRAN 2004 molecular spectroscopic database. J Quant Spectrosc Radiat Transfer 2005;96:139–204.

[3] Simecková M, Jacquemart D, Rothman LS, Gamache RR, Goldman A. Einstein *A*-coefficients and statistical weights for molecular absorption transitions in the *HITRAN* database. J Quant Spectrosc Radiat Transfer 2006;98:130–55.

[4] Oudot C, Wang L, Thomas X, Von der Heyden P, Daumont L, Régalia L. Intensity measurements of $H_2{}^{16}O$ lines in the spectral region 8000–9350 cm^{-1}. J Mol Spectrosc 2010;262:22–9.

[5] Lodi L, Tennyson J, Polyansky OL. A global, high accuracy ab initio dipole moment surface for the electronic ground state of the water molecule. J Chem Phys 2011;135 (034113-10).

[6] Shillings AJL, Ball SM, Barber MJ, Tennyson J, Jones RL. An upper limit for water dimer absorption in the 750 nm spectral region and a revised water line list. Atmos Chem Phys 2011;11:4273–87.

[7] Tallis L, Coleman M, Gardiner T, Ptashnik IV, Shine KP. Assessment of the consistency of H_2O line intensities over the near-infrared using sun-pointing ground-based Fourier transform spectroscopy. J Quant Spectrosc Radiat Transfer 2011;112:2268–80.

[8] Coudert LH, Wagner G, Birk M, Baranov YI, Lafferty WJ, Flaud J-M. The $H_2{}^{16}O$ molecule: line position and line intensity analyses up to the second triad. J Mol Spectrosc 2008;251:339–57.
[9] Ptashnik IV, Smith KM. Water vapour line intensities and self-broadening coefficients in the 5000–5600 cm^{-1} spectral region. J Quant Spectrosc Radiat Transfer 2010;111:1317–27.
[10] Jenouvrier A, Daumont L, Régalia-Jarlot L, Tyuterev VG, Carleer M, Vandaele AC, et al. Fourier transform measurements of water vapor line parameters in the 4200–6600 cm^{-1} region. J Quant Spectrosc Radiat Transfer 2007;105:326–55.
[11] Toth RA. Linelists of water vapor parameters from 500 to 8000 cm^{-1}. ⟨http://mark4sun.jpl.nasa.gov/data/spec/⟩.
[12] Wunch D, Toon GC, Blavier J-FL, Washenfelder RA, Notholt J, Connor BJ, et al. The total carbon column observing network. Philos Trans R Soc A: Math Phys Eng Sci 2011;369:2087–112.
[13] Gordon IE, Rothman LS, Gamache RR, Jacquemart D, Boone C, Bernath PF, et al. Current updates of the water-vapor line list in HITRAN: a new "diet" for air-broadened half-widths. J Quant Spectrosc Radiat Transfer 2007;108:389–402.
[14] Gamache RR, Laraia AL. N_2-, O_2-, and air-broadened half-widths, their temperature dependence, and line shifts for the rotation band of $H_2{}^{16}O$. J Mol Spectrosc 2009;257:116–27.
[15] Gamache RR. Lineshape parameters for water vapor in the 3.2–17.76 μm region for atmospheric applications. J Mol Spectrosc 2005;229:9–18.
[16] Jacquemart D, Gamache R, Rothman LS. Semi-empirical calculation of air-broadened half-widths and air pressure-induced frequency shifts of water-vapor absorption lines. J Quant Spectrosc Radiat Transfer 2005;96:205–39.
[17] Ma Q, Tipping RH, Gamache RR. Uncertainties associated with theoretically calculated N_2-broadened half-widths of H_2O lines. Mol Phys 2010;108:2225–52.
[18] Birk M, Wagner G. Temperature-dependent air broadening of water in the 1250–1750 cm^{-1} range. J Quant Spectrosc Radiat Transfer 2012;113:889–928.
[19] Rothman LS, Gordon IE, Barber RJ, Dothe H, Gamache RR, Goldman A, et al. HITEMP, the high-temperature molecular spectroscopic database. J Quant Spectrosc Radiat Transfer 2010;111:2139–50.
[20] Barber RJ, Tennyson J, Harris GJ, Tolchenov RN. A high-accuracy computed water line list. Mon Not Astr R Soc 2006;368:1087–94.
[21] Tennyson J, Bernath PF, Brown LR, Campargue A, Császár AG, Daumont L, et al. IUPAC critical evaluation of the rotational–vibrational spectra of water vapor, Part III: Energy levels and transition wavenumbers for $H_2{}^{16}O$. J Quant Spectrosc Radiat Transfer 2013;117:29–58.
[22] Furtenbacher T, Császár AG, Tennyson J. MARVEL: measured active rotational–vibrational energy levels. J Mol Spectrosc 2007;245:115–25.
[23] Furtenbacher T, Császár AG. MARVEL: measured active rotational–vibrational energy levels. II. Algorithmic improvements. J Quant Spectrosc Radiat Transfer 2012;113:929–35.
[24] Martin MA, Coudert L, Pirali O, Balcon O. Positions and intensities of water vapor transitions in 0–6000 cm^{-1} region. J Chem Phys 2013 [in preparation].
[25] Gordon IE, Rothman LS, Lodi L, Tennyson J, Toon GC, Brown LR. In: Proceedings of the 67th international symposium on molecular spectroscopy, Columbus, OH, USA, 2012.
[26] Wagner G, Birk M. Water line intensities in the 1 μm region. J Quant Spectrosc Radiat Transfer 2013 [in preparation].
[27] Lisak D, Hodges JT. Low-uncertainty H_2O line intensities for the 930 nm region. J Mol Spectrosc 2008;249:6–13.
[28] Lodi L, Tennyson J. Line lists for $H_2{}^{18}O$ and $H_2{}^{17}O$ based on empirical line positions and ab initio intensities. J Quant Spectrosc Radiat Transfer 2012;113:850–8.
[29] Shirin SV, Polyansky OL, Zobov NF, Ovsyannikov RI, Császár AG, Tennyson J. Spectroscopically determined potential energy surfaces of the $H_2{}^{16}O$, $H_2{}^{17}O$, and $H_2{}^{18}O$ isotopologues of water. J Mol Spectrosc 2006;236:216–23.
[30] Tennyson J, Bernath PF, Brown LR, Campargue A, Carleer MR, Császár AG, et al. IUPAC critical evaluation of the rotational–vibrational spectra of water vapor. Part I—Energy levels and transition wavenumbers for $H_2{}^{17}O$ and $H_2{}^{18}O$. J Quant Spectrosc Radiat Transfer 2009;110:573–96.
[31] Ma Q, Tipping RH, Lavrentieva NN. Pair identity and smooth variation rules applicable for the spectroscopic parameters of H_2O transitions involving high-J states. Mol Phys 2011;109:1925–41.
[32] Brown LR, Humphrey CM, Gamache RR. CO_2-broadened water in the pure rotation and ν_2 fundamental regions. J Mol Spectrosc 2007;246:1–21.
[33] Clough SA. Private communication; 2012.
[34] Voronin BA, Tennyson J, Tolchenov RN, Lugovskoy AA, Yurchenko SN. A high accuracy computed line list for the HDO molecule. Mon Not Astr R Soc 2010;402:492–6.
[35] Tennyson J, Bernath PF, Brown LR, Campargue A, Császár AG, Daumont L, et al. IUPAC critical evaluation of the rotational–vibrational spectra of water vapor, Part II: Energy levels and transition wavenumbers for $HD^{16}O$, $HD^{17}O$, and $HD^{18}O$. J Quant Spectrosc Radiat Transfer 2010;111:2160–84.
[36] Scheepmaker RA, Frankenberg C, Galli A, Butz A, Schrijver H, Deutscher NM, et al. Improved water vapour spectroscopy in the 4174–4300 cm^{-1} region and its impact on SCIAMACHY HDO/H2O measurements. Atmos Meas Tech Discuss 2012;5:8539–78.
[37] Thompson DR, Benner DC, Brown LR, Crisp D, Devi VM, Jiang YB, et al. Atmospheric validation of high accuracy CO_2 absorption coefficients for the OCO-2 mission. J Quant Spectrosc Radiat Transfer 2012;113:2265–76.
[38] Yokomizo M. Greenhouse gases Observing SATellite (GOSAT) ground systems. Fujitsu Sci Tech J 2008;44:410–7;
Nikitin AV, Lyulin OM, Mikhailenko SN, Perevalov VI, Filippov NN, Grigoriev IM, et al. GOSAT-2009 methane spectral linelist in the 5550–6236 cm^{-1} range. J Quant Spectrosc Radiat Transfer 2010;111:2211–24.
[39] Bézard B, Fedorova A, Bertaux JL, Rodin A, Korablev O. The 1.10- and 1.18-μm nightside windows of Venus observed by SPICAV-IR aboard Venus Express. Icarus 2011;216:173–83.
[40] Toth RA, Brown LR, Miller CE, Malathy Devi V, Benner DC. Spectroscopic database of CO_2 line parameters: 4300–7000 cm^{-1}. J Quant Spectrosc Radiat Transfer 2008;109:906–21.
[41] Perevalov VI, Tashkun SA. In: Proceedings of the 10th HITRAN database conference, Cambridge, MA, USA, 2008.
[42] Tashkun SA, Perevalov VI, Teffo JL, Bykov AD, Lavrentieva NN. In: Proceedings of the 14th international symposium on high resolution molecular spectroscopy, Krasnoyarsk, Russia, 2003.
[43] Jacquemart D, Gueye F, Lyulin OM, Karlovets EV, Baron D, Perevalov VI. Infrared spectroscopy of CO_2 isotopologues from 2200 to 7000 cm^{-1}: characterizing experimental uncertainties of positions and intensities. J Quant Spectrosc Radiat Transfer 2012;113:961–75.
[44] Lyulin OM, Karlovets EV, Jacquemart D, Lu Y, Liu AW, Perevalov VI. Infrared spectroscopy of ^{17}O- and ^{18}O-enriched carbon dioxide in the 1700–8300 cm^{-1} wavenumber region. J Quant Spectrosc Radiat Transfer 2012;113:2167–81.
[45] Borkov YG, Jacquemart D, Lyulin OM, Tashkun SA, Perevalov VI. Infrared spectroscopy of ^{17}O- and ^{18}O-enriched carbon dioxide. Line positions and intensities in 3200–4700 cm^{-1} region. J Quant Spectrosc Radiat Transfer 2013 ([submitted]).
[46] Karlovets EV, Campargue A, Mondelain D, Béguier S, Kassi S, Tashkun SA, et al.. High sensitivity cavity ring down spectroscopy of ^{18}O enriched carbon dioxide between 5850 and 7000 cm^{-1}: I. Analysis and theoretical modeling of the $^{16}O^{12}C^{18}O$ spectrum. J Quant Spectrosc Radiat Transfer 2013 [this issue], http://dx.doi.org/10.1016/j.jqsrt.2013.05.019.
[47] Depraz S, Perrin MY, Rivière P, Soufiani A. Infrared emission spectroscopy of CO_2 at high temperature. Part II: Experimental results and comparisons with spectroscopic databases. J Quant Spectrosc Radiat Transfer 2012;113:14–25.
[48] Song KF, Kassi S, Tashkun SA, Perevalov VI, Campargue A. High sensitivity CW-cavity ring down spectroscopy of $^{12}CO_2$ near 1.35 μm (II): new observations and line intensities modeling. J Quant Spectrosc Radiat Transfer 2010;111:332–44.
[49] Durry G, Li JS, Vinogradov I, Titov A, Joly L, Cousin J, et al. Near infrared diode laser spectroscopy of C_2H_2, H_2O, CO_2 and their isotopologues and the application to TDLAS, a tunable diode laser spectrometer for the Martian PHOBOS-GRUNT space mission. Appl Phys B 2010;99:339–51.
[50] Casa G, Wehr R, Castrillo A, Fasci E, Gianfrani L. The line shape problem in the near-infrared spectrum of self-colliding CO_2 molecules: experimental investigation and test of semiclassical models. J Chem Phys 2009;130:4306.
[51] Villanueva GL, Mumma MJ, Novak RE, Hewagama T. Identification of a new band system of isotopic CO_2 near 3.3 μm: implications for remote sensing of biomarker gases on Mars. Icarus 2008;195:34–44.
[52] Villanueva GL, Mumma MJ, Novak RE, Hewagama T. Discovery of multiple bands of isotopic CO_2 in the prime spectral regions used when searching for CH_4 and HDO on Mars. J Quant Spectrosc Radiat Transfer 2008;109:883–94.

[53] Joly L, Marnas F, Gibert F, Bruneau D, Grouiez B, Flamant PH, et al. Laser diode absorption spectroscopy for accurate CO_2 line parameters at 2 μm: consequences for space-based DIAL measurements and potential biases. Appl Opt 2009;48:5475–83.
[54] Cai TD, Wang GS, Chen WD, Zhang WJ, Gao XM. Study of CO_2 spectroscopic parameters at high hemperature near 1.57 μm. Spectros Spectral Ana 2009;29:1463–7.
[55] Castrillo A, de Tommasi E, Gianfrani L, Sirigu L, Faist J. Doppler-free saturated-absorption spectroscopy of CO_2 at 4.3 μm by means of a distributed feedback quantum cascade laser. Opt Lett 2006;31:3040–2.
[56] Lu Y, Liu AW, Pan H, Li XF, Perevalov VI, Tashkun SA, et al. High sensitivity cavity ring down spectroscopy of $^{13}C^{16}O_2$ overtone bands near 806 nm. J Quant Spectrosc Radiat Transfer 2012;113:2197–204.
[57] Pan H, Li XF, Lu Y, Liu AW, Perevalov VI, Tashkun SA, et al. Cavity ring down spectroscopy of ^{18}O and ^{17}O enriched carbon dioxide near 795 nm. J Quant Spectrosc Radiat Transfer 2013;114:42–4.
[58] Robert S, Borkov YG, Vander Auwera J, Drummond R, Mahieux A, Wilquet V, et al. Assignment and rotational analysis of new absorption bands of carbon dioxide isotopologues in Venus spectra. J Quant Spectrosc Radiat Transfer 2013;114:29–41.
[59] Giusfredi G, Bartalini S, Borri S, Cancio P, Galli I, Mazzotti D, et al. Saturated-absorption cavity ring-down spectroscopy. Phys Rev Lett 2010;104:110801.
[60] Cancio P, Bartalini S, Borri S, Galli I, Gagliardi G, Giusfredi G, et al. Frequency-comb-referenced mid-IR sources for next-generation environmental sensors. Appl Phys B 2011;102:255–69.
[61] Tashkun SA, Velichko TI, Mikhailenko SN. Critical evaluation of measured pure-rotation and rotation–vibration line positions and an experimental dataset of energy levels of $^{12}C^{16}O$ in $X^1\Sigma^+$ state. J Quant Spectrosc Radiat Transfer 2010;111:1106–16.
[62] Lamouroux J, Gamache RR, Laraia AL, Hartmann J-M, Boulet C. Semiclassical calculations of half-widths and line shifts for transitions in the 30012–00001 and 30013–00001 bands of CO_2 II: collisions with O_2 and air. J Quant Spectrosc Radiat Transfer 2012;113:991–1003.
[63] Lamouroux J, Gamache RR, Laraia AL, Hartmann J-M, Boulet C. Semiclassical calculations of half-widths and line shifts for transitions in the 30012–00001 and 30013–00001 bands of CO_2. III: Self collisions. J Quant Spectrosc Radiat Transfer 2012;113:1536–46.
[64] Gamache RR, Lamouroux J. The vibrational dependence of half-widths of CO_2 transitions broadened by N_2, O_2, air, and CO_2. J Quant Spectrosc Radiat Transfer 2013;117:93–103.
[65] Gamache RR, Lamouroux J. Predicting accurate line shape parameters for CO_2 transitions. J Quant Spectrosc Radiat Transfer 2013 [this issue], http://dx.doi.org/10.1016/j.jqsrt.2013.05.021.
[66] Lamouroux J, Tran H, Laraia AL, Gamache RR, Rothman LS, Gordon IE, et al. Updated database plus software for line-mixing in CO_2 infrared spectra and their test using laboratory spectra in the 1.5–2.3 μm region. J Quant Spectrosc Radiat Transfer 2010;111:2321–31.
[67] Tyuterev VG, Tashkun SA, Schwenke DW, Jensen J, Cours T, Barbe A, et al. Variational EKE-calculations of rovibrational energies of the ozone molecules from an empirical potential function. Chem Phys Lett 2000;316:271–9.
[68] Tyuterev VG, Tashkun SA, Schwenke DW, Barbe A. Variational calculations of high-J rovibrational states of the ozone molecule from empirically determined isotopically invariant potential energy surface. SPIE Proc Ser 2004;5311:176–84.
[69] Funke B, López-Puertas M, García-Comas M, Kaufmann M, Höpfner M, Stiller GP. GRANADA: a Generic RAdiative traNsfer AnD non-LTE population algorithm. J Quant Spectrosc Radiat Transfer 2012;113:1771–817.
[70] Bouazza S, Barbe A, Mikhailenko S, Plateaux JJ. Line positions and intensities of the $\nu_1+2\nu_2+\nu_3$ and $2\nu_2+2\nu_3$ bands of $^{16}O_3$. J Mol Spectrosc 1994;166:365–71.
[71] Barbe A, De Backer MR, Starikova E, Tashkun SA, Thomas X, Tyuterev VG. FTS high resolution spectra of $^{16}O_3$ in 3500 and 5500 cm^{-1} regions. First example of new theoretical modelling for a polyad of strongly coupled states. J Quant Spectrosc Radiat Transfer 2012;113:829–39.
[72] Mikhailenko S, Barbe A, Tyuterev VG, Régalia L, Plateaux JJ. Line positions and intensities of the $\nu_1+\nu_2+3\nu_3$, $\nu_2+4\nu_3$, and $3\nu_1+2\nu_2$ bands of ozone. J Mol Spectrosc 1996;180:227–35.
[73] Barbe A, Chichery A, Tyuterev VG, Plateaux JJ. Analysis of high resolution measurements of the $\nu_1+5\nu_3$ band of ozone: Coriolis interactions with the $6\nu_3$ and $3\nu_1+\nu_2+2\nu_3$ bands. Mol Phys 1998;94:751–7.
[74] Campargue A, Barbe A, De Backer-Barilly MR, Tyuterev VG, Kassi S. The near infrared spectrum of ozone by CW-cavity ring down spectroscopy between 5850 and 7000 cm^{-1}: new observations and exhaustive review. Phys Chem Chem Phys 2008;10:2925–46.
[75] Kassi S, Campargue A, De Backer-Barilly MR, Barbe A. The $\nu_1+3\nu_2+3\nu_3$ and $4\nu_1+\nu_2+\nu_3$ bands of ozone by CW-cavity ring down spectroscopy between 5900 and 5960 cm^{-1}. J Mol Spectrosc 2007;244:122–9.
[76] Campargue A, Kassi S, Romanini D, Barbe A, De Backer-Barilly MR, Tyuterev VG. CW-cavity ring down spectroscopy of the ozone molecule in the 6625–6830 cm^{-1} region. J Mol Spectrosc 2006;240:1–13.
[77] Barbe A, De Backer-Barilly MR, Tyuterev VG, Campargue A, Romanini D, Kassi S. CW-cavity ring down spectroscopy of the ozone molecule in the 5980–6220 cm^{-1} region. J Mol Spectrosc 2007;242:156–75.
[78] Barbe A, De Backer-Barilly MR, Tyuterev VG, Kassi S, Campargue A. CW-cavity ring down spectroscopy of the ozone molecule in the 6220–6400 cm^{-1} region. J Mol Spectrosc 2007;246:22–38.
[79] Mikhailenko SN, Babikov YL, Tyuterev VG, Barbe A. The databank of ozone spectroscopy on WEB (S&MPO). J Comput Technol 2002;7:64–70.
[80] Tyuterev VG, Tashkun SA, Seghir H. High-order contact transformations: general algorithm, computer implementation and triatomic tests. SPIE Proc Ser 2004;5311:164–75.
[81] Barbe A, Mikhailenko S, Starikova E, De Backer MR, Tyuterev VG, Mondelain D, et al.. Ozone spectroscopy in the electronic ground state: high-resolution spectra analyses and update of line parameters since 2003. J Quant Spectrosc Radiat Transfer 2013 [this issue], http://dx.doi.org/10.1016/j.jqsrt.2013.06.007.
[82] Malathy Devi V, Chris Benner D, Smith MAH, Mantz AW, Sung K, Brown LR, et al. Spectral line parameters including temperature dependences of self- and air-broadening in the 2←0 band of CO at 2.3 μm. J Quant Spectrosc Radiat Transfer 2012;113:1013–33.
[83] Malathy Devi V, Chris Benner D, Smith MAH, Mantz AW, Sung K, Brown LR. Spectral line parameters including temperature dependences of air-broadening in the 2←0 bands of $^{13}C^{16}O$ and $^{12}C^{18}O$ at 2.3 μm. J Mol Spectrosc 2012;276–277:33–48.
[84] Levy A, Lacome N, Chackerian C. Collisional line mixing. In: Rao KN, Weber A, editors. Spectroscopy of the earth's atmosphere and interstellar medium. Boston, MA: Academic Press; 1992. p. 261–337 [Chapter 2].
[85] Rosenkranz PW. Shape of 5 mm oxygen band in atmosphere. IEEE Trans Antennas Propag 1975;AP-23:498–506.
[86] Hartmann J-M, Boulet C. Line shape parameters for HF in a bath of argon as a test of classical path models. J Chem Phys 2000;113:9000.
[87] Müller HSP, Schlöder F, Stutzki J, Winnewisser G. The Cologne Database for Molecular Spectroscopy, CDMS: a useful tool for astronomers and spectroscopists. J Mol Struct 2005;742:215.
[88] Klapper G, Surin L, Lewen F, Müller HSP, Pak I, Winnewisser G. Precision measurements of the rotational spectrum of $^{12}C^{17}O$ and $^{13}C^{17}O$. Astrophys J 2003;582:262–8.
[89] Gendriesch R, Lewen F, Klapper G, Menten KM, Winnewisser G, Coxon JA, et al. Accurate laboratory rest frequencies of vibrationally excited CO up to $v=3$ and up to 2 THz. Astron Astrophys 2009;497:927–30.
[90] Brown LR, Sung K, Benner DC, Devi VM, Boudon V, Gabard T, et al. Methane line parameters in the HITRAN2012 database. J Quant Spectrosc Radiat Transfer 2013 [this issue], http://dx.doi.org/10.1016/j.jqsrt.2013.06.020.
[91] Daumont L, Nikitin AV, Thomas X, Régalia L, Von der Heyden P, Tyuterev VG, et al. New assignments in the 2 μm transparency window of the $^{12}CH_4$ octad band system. J Quant Spectrosc Radiat Transfer 2013;116:101–9.
[92] Niederer HM, Albert S, Bauerecker S, Boudon V, Champion JP, Quack M. Global analysis of the infrared spectrum of $^{13}CH_4$: lines in the region 0 to 3200 cm^{-1}. Chimia 2008;62:273–6.
[93] Niederer HM, Albert S, Bauerecker S, Boudon V, Champion JP, Quack M. Analysis of the rovibrational spectrum of methane $^{13}CH_4$ in the octad range. J Mol Spectrosc 2013 [in press]. http://dx.doi.org/10.1016/j.jms.2013.06.003.
[94] Nikitin AV, Daumont L, Thomas X, Régalia L, Rey M, Tyuterev VG, et al. Preliminary assignments of $2\nu_3-\nu_4$ hot band of $^{12}CH_4$ in the 2 μm transparency window from long-path FTS spectra. J Mol Spectrosc 2011;268:93–106.
[95] Nikitin AV, Brown LR, Sung K, Rey M, Tyuterev VG, Smith MAH, et al. Preliminary modeling of CH_3D from 4000 to 4550 cm^{-1}. J Quant Spectrosc Radiat Transfer 2013;114:1–12.
[96] Wishnow EH, Orton GS, Ozier I, Gush HP. The distortion dipole rotational spectrum of CH_4: a low temperature far-infrared study. J Quant Spectrosc Radiat Transfer 2007;103:102–17.

[97] Boudon V, Pirali O, Roy P, Brubach J-B, Manceron L, Vander Auwera J. The high-resolution far-infrared spectrum of methane at the SOLEIL synchrotron. J Quant Spectrosc Radiat Transfer 2010;111: 1117–29.

[98] Brown LR. Empirical line parameters of methane from 1.1 to 2.1 μm. J Quant Spectrosc Radiat Transfer 2005;96:251–70.

[99] Campargue A, Leshchishina O, Wang L, Mondelain D, Kassi S. The WKLMC empirical linelists (5852–7919 cm^{-1}) for methane between 80 K and 296 K: "final" lists in HITRAN format for atmospheric and planetary applications. J Mol Spectrosc 2013 [in press], http://dx.doi.org/10.1016/j.jms.2013.03.001.

[100] Benner DC, Devi VM, O'Brien JJ, Shaji S, Spickler PT, Houck CP, et al. Empirical line parameters of CH_4 from 10923 to 11502 cm^{-1}. Icarus 2013 [in preparation].

[101] Abe M, Iwakuni K, Okubo S, Sasada H. Accurate transition frequency list of the ν_3 band of methane from sub-Doppler resolution comb-referenced spectroscopy. J Opt Soc Am B 2013;30: 1027–35.

[102] Zolot AM, Giorgetta FR, Baumann E, Swann WC, Coddington I, Newbury NR. Broad-band frequency references in the near-infrared: accurate dual comb spectroscopy of methane and acetylene. J Quant Spectrosc Radiat Transfer 2013;118:26–39.

[103] Sanzharov M, Vander Auwera J, Pirali O, Roy P, Brubach J-B, Manceron L, et al. Self and N_2 collisional broadening of far-infrared methane lines measured at the SOLEIL synchrotron. J Quant Spectrosc Radiat Transfer 2012;113:1874–86.

[104] Coustenis A, Achterberg RK, Conrath BJ, Jennings DE, Marten A, Gautier D, et al. The composition of Titan's stratosphere from Cassini/CIRS mid-infrared spectra. Icarus 2007;189:35–62.

[105] Mackie CJ, Gordon IE, Rothman LS, Leshchishina O, Kassi S, Campargue A, et al. Revision of spectral parameters for the bands of oxygen that involve ground $X^3\Sigma_g^-$ and first excited $a^1\Delta_g$ electronic states. J Quant Spectrosc Radiat Transfer 2013 [in preparation].

[106] Leshchishina O, Kassi S, Gordon IE, Rothman LS, Wang L, Campargue A. High sensitivity CRDS of the $a^1\Delta_g - X^3\Sigma_g^-$ band of oxygen near 1.27 μm: extended observations, quadrupole transitions, hot bands and minor isotopologues. J Quant Spectrosc Radiat Transfer 2010;111:2236–45.

[107] Leshchishina O, Kassi S, Gordon IE, Yu S, Campargue A. The $a^1\Delta_g$–$X^3\Sigma_g^-$ band of $^{16}O^{17}O$, $^{17}O^{18}O$ and $^{17}O_2$ by high sensitivity CRDS near 1.27 μm. J Quant Spectrosc Radiat Transfer 2011;112:1257–65.

[108] Tretyakov MY, Koshelev MA, Dorovskikh VV, Makarov DS, Rosenkranz PW. 60-GHz oxygen band: precise broadening and central frequencies of fine-structure lines, absolute absorption profile at atmospheric pressure, and revision of mixing coefficients. J Mol Spectrosc 2005;231:1–14.

[109] Golubiatnikov GY, Krupnov AF. Microwave study of the rotational spectrum of oxygen molecule in the range up to 1.12 THz. J Mol Spectrosc 2003;217:282–7.

[110] Park K, Nolt IG, Steele TC, Zink LR, Evenson KM, Chance KV, et al. Pressure broadening of the 50.873 and 83.469 cm^{-1} molecular oxygen lines. J Quant Spectrosc Radiat Transfer 1996;56:315–6.

[111] Jennings DA, Evenson KM, Vanek MD, Nolt IG, Radostitz JV, Chance KV. Air- and oxygen-broadening coefficients for the O_2 rotational line at 60.46 cm^{-1}. Geophys Res Lett 1987;14:722–5.

[112] Drouin BJ. Temperature dependent pressure induced linewidths of $^{16}O_2$ and $^{16}O^{18}O$ transitions in nitrogen, oxygen and air. J Quant Spectrosc Radiat Transfer 2007;105:450–8.

[113] Newman SM, Orr-Ewing AJ, Newnham DA, Ballard J. Temperature and pressure dependence of line widths and integrated absorption intensities for the O_2 $a^1\Delta_g - X\,^3\Sigma_g^-$ (0,0) transition. J Phys Chem A 2000;104:9467–80.

[114] Washenfelder RA, Toon GC, Blavier J-F, Yang Z, Allen NT, Wennberg PO, et al. Carbon dioxide column abundances at the Wisconsin tall tower site. J Geophys Res [Atmos] 2006;111:22305.

[115] Gordon IE, Kassi S, Campargue A, Toon GC. First identification of the $a^1\Delta_g - X^3\Sigma_g^-$ electric quadrupole transitions of oxygen in solar and laboratory spectra. J Quant Spectrosc Radiat Transfer 2010;111: 1174–83.

[116] Kassi S, Leshchishina O, Gordon IE, Yu S, Campargue A. Hyperfine structure of the $a^1\Delta_g - X\,^3\Sigma_g^-$ transitions of $^{16}O^{17}O$, $^{17}O^{18}O$ and $^{17}O_2$ by CRDS at 80 K. Chem Phys Lett 2011;502:37–41.

[117] Mishra AP, Balasubramanian TK, Shetty BJ. Generalized electric quadrupole branch linestrengths for the infrared atmospheric oxygen bands. J Quant Spectrosc Radiat Transfer 2011;112:2303–9.

[118] Kassi S, Campargue A. Cavity ring down spectroscopy with 5×10^{-13} cm^{-1} sensitivity. J Chem Phys 2012;137:4201.

[119] Robichaud DJ, Hodges JT, Brown LR, Lisak D, Maslowski P, Yeung LY, et al. Experimental intensity and lineshape parameters of the oxygen A-band using frequency-stabilized cavity ring-down spectroscopy. J Mol Spectrosc 2008;248:1–13.

[120] Robichaud DJ, Hodges JT, Lisak D, Miller CE, Okumura M. High-precision pressure shifting measurement technique using frequency-stabilized cavity ring-down spectroscopy. J Quant Spectrosc Radiat Transfer 2008;109:435–44.

[121] Robichaud DJ, Hodges JT, Masłowski P, Yeung LY, Okumura M, Miller CE, et al. High-accuracy transition frequencies for the O_2 A-band. J Mol Spectrosc 2008;251:27–37.

[122] Robichaud DJ, Yeung LY, Long DA, Okumura M, Havey DK, Hodges JT, et al. Experimental line parameters of the $b^1\Sigma_g^+ \leftarrow X^3\Sigma_g^-$(0,0) band of oxygen isotopologues at 760 nm using frequency-stabilized cavity ring-down spectroscopy. J Phys Chem A 2009;113: 13089–99.

[123] Havey DK, Long DA, Okumura M, Miller CE, Hodges JT. Ultra-sensitive optical measurements of high-J transitions in the O_2 A-band. Chem Phys Lett 2009;483:49–54.

[124] Long DA, Havey DK, Okumura M, Miller CE, Hodges JT. O_2 A-band line parameters to support atmospheric remote sensing. J Quant Spectrosc Radiat Transfer 2010;111:2021–36.

[125] Long DA, Havey DK, Yu SS, Okumura M, Miller CE, Hodges JT. O_2 A-band line parameters to support atmospheric remote sensing. Part II: The rare isotopologues. J Quant Spectrosc Radiat Transfer 2011;112:2527–41.

[126] Galatry L. Simultaneous effect of Doppler and foreign gas broadening on spectral lines. Phys Rev 1961;122:1218–23.

[127] Ritter KJ, Wilkerson TD. High-resolution spectroscopy of the oxygen A-band. J Mol Spectrosc 1987;121:1–19.

[128] Long DA, Hodges JT. On spectroscopic models of the O_2 A-band and their impact upon atmospheric retrievals. J Geophys Res-Atmos 2012;117:D12309.

[129] Tran H, Boulet C, Hartmann JM. Line mixing and collision-induced absorption by oxygen in the A band: laboratory measurements, model, and tools for atmospheric spectra computations. J Geophys Res-Atmos 2006;111:D15210.

[130] Tran H, Hartmann JM. An improved O_2 A band absorption model and its consequences for retrievals of photon paths and surface pressures. J Geophys Res-Atmos 2008;113:D18104.

[131] Long DA, Robichaud DJ, Hodges JT. Frequency-stabilized cavity ring-down spectroscopy measurements of line mixing and collision-induced absorption in the O_2 A-band. J Chem Phys 2012;137.

[132] Richard C, Gordon IE, Rothman LS, Abel M, Frommhold L, Gustafsson M, et al. New section of the HITRAN database: collision-induced absorption (CIA). J Quant Spectrosc Radiat Transfer 2012;113: 1276–85.

[133] Long DA, Havey DK, Okumura M, Pickett HM, Miller CE, Hodges JT. Laboratory measurements and theoretical calculations of O_2 A-band electric quadrupole transitions. Phys Rev A 2009;80:042513.

[134] Gordon IE, Rothman LS, Toon GC. Revision of spectral parameters for the B- and gamma-bands of oxygen and their validation against atmospheric spectra. J Quant Spectrosc Radiat Transfer 2011;112: 2310–22.

[135] Miller CE, Wunch D. Fourier transform spectrometer remote sensing of O_2 A-band electric quadrupole transitions. J Quant Spectrosc Radiat Transfer 2012;113:1043–50.

[136] Brault JW. Detection of electric quadrupole transitions in the oxygen A-band at 7600 Å. J Mol Spectrosc 1980;80:384–7.

[137] Yu S, Miller CE, Drouin BJ, Müller HSP. High resolution spectral analysis of oxygen. I. Isotopically invariant Dunham fit for the $X^3\Sigma_g^-$, $a^1\Delta_g$, $b^1\Sigma_g^+$ states. J Chem Phys 2012;137:4304.

[138] Flaud JM, Lafferty WJ, Sams RL. Line intensities for the ν_1, ν_3 and $\nu_1+\nu_3$ bands of $^{34}SO_2$. J Quant Spectrosc Radiat Transfer 2009;110: 669–74.

[139] Lafferty WJ, Flaud JM, Ngom EHA, Sams RL. $^{34}S^{16}O_2$: High-resolution analysis of the (0 3 0), (1 0 1), (1 1 1), (0 0 2) and (2 0 1) vibrational states; determination of equilibrium rotational constants for sulfur dioxide and anharmonic vibrational constants. J Mol Spectrosc 2009;253:51–4.

[140] Lafferty WJ, Flaud J-M, Sams RL, Abib Ngom EH. High resolution analysis of the rotational levels of the (0 0 0), (0 1 0), (1 0 0), (0 0 1), (0 2 0), (1 1 0) and (0 1 1) vibrational states of $^{34}S^{16}O_2$. J Mol Spectrosc 2008;252:72–6.

[141] Galloway JN, Aber JD, Erisman JW, Seitzinger SP, Howarth RW, Cowling EB, et al. The nitrogen cascade. BioScience 2003;53:341.

[142] Clarisse L, Clerbaux C, Dentener F, Hurtmans D, Coheur P-F. Global ammonia distribution derived from infrared satellite observations. Nat Geosci 2009;2:479–83.

[143] Burgess AB, Dudhia A, Grainger RG, Stevenson D. Progress in tropospheric ammonia retrieval from the MIPAS satellite instrument. Adv Space Res 2006;37:2218–21.
[144] Beer R, Shephard MW, Kulawik SS, Clough SA, Eldering A, Bowman KW, et al. First satellite observations of lower tropospheric ammonia and methanol. Geophys Res Lett 2008;35:L09801.
[145] Rothman LS, Barbe A, Chris Benner D, Brown LR, Camy-Peyret C, Carleer MR, et al. The HITRAN molecular spectroscopic database: edition of 2000 including updates through 2001. J Quant Spectrosc Radiat Transfer 2003;82:5–44.
[146] Down MJ, Hill C, Yurchenko SN, Tennyson J, Brown LR, Kleiner I. Re-analysis of ammonia spectra: updating the HITRAN $^{14}NH_3$ database. J Quant Spectrosc Radiat Transfer 2013 [this issue], http://dx.doi.org/10.1016/j.jqsrt.2013.05.027.
[147] Sung K, Brown LR, Huang X, Schwenke DW, Lee TJ, Coy SL, et al. Extended line positions, intensities, empirical lower state energies and quantum assignments of NH_3 from 6300 to 7000 cm^{-1}. J Quant Spectrosc Radiat Transfer 2012;113:1066–83.
[148] Chen P, Pearson JC, Pickett HM, Matsuura S, Blake GA. Measurements of $^{14}NH_3$ in the $\nu_2=1$ state by a solid-state, photomixing, THz spectrometer, and a simultaneous analysis of the microwave, terahertz, and infrared transitions between the ground and ν_2 inversion–rotation levels. J Mol Spectrosc 2006;236:116–26.
[149] Yu S, Pearson JC, Drouin BJ, Sung K, Pirali O, Vervloet M, et al. Submillimeter-wave and far-infrared spectroscopy of high-J transitions of the ground and $\nu_2=1$ states of ammonia. J Chem Phys 2010;133 (174317-14).
[150] Yurchenko SN, Barber RJ, Tennyson J. A variationally computed line list for hot NH_3. Mon Not Astr R Soc 2011;413:1828–34.
[151] Guinet M, Jeseck P, Mondelain D, Pepin I, Janssen C, Camy-Peyret C, et al. Absolute measurements of intensities, positions and self-broadening coefficients of R branch transitions in the ν_2 band of ammonia. J Quant Spectrosc Radiat Transfer 2011;112:1950–60.
[152] Fabian M, Yamada KMT. Absolute intensity of the NH_3 ν_2 band. J Mol Spectrosc 1999;198:102–9.
[153] Nemtchinov V, Sung K, Varanasi P. Measurements of line intensities and half-widths in the 10 μm bands of $^{14}NH_3$. J Quant Spectrosc Radiat Transfer 2004;83:243–65.
[154] Aroui H, Nouri S, Bouanich JP. NH_3 self-broadening coefficients in the ν_2 and ν_4 bands and line intensities in the ν_2 band. J Mol Spectrosc 2003;220:248–58.
[155] Yurchenko SN, Barber RJ, Yachmenev A, Thiel W, Jensen P, Tennyson J. A variationally computed $T=300$ K line list for NH_3. J Phys Chem A 2009;113:11845–55.
[156] Chu Z, Chen L, Cheo PK. Absorption spectra of NH_3 using a microwave sideband CO_2-laser spectrometer. J Quant Spectrosc Radiat Transfer 1994;51:591–602.
[157] Cacciani P, Cermak P, Cosléou J, Khelkhal M, Jeseck P, Michaut X. New progress in spectroscopy of ammonia in the infrared 1.5 μm range using evolution of spectra from 300 K down to 122 K. J Quant Spectrosc Radiat Transfer 2012;113:1084–91.
[158] Bell CL, Dhib M, Hancock G, Ritchie GAD, van Helden JH, van Leeuwen NJ. Cavity enhanced absorption spectroscopy measurements of pressure-induced broadening and shifts coefficients in the $\nu_1+\nu_3$ combination band of ammonia. Appl Phys B 2009;94:327–36.
[159] Cacciani P. Private communication; 2012.
[160] Lundsberg-Nielsen L, Hegelund F, Nicolaisen FM. Analysis of the high-resolution spectrum of ammonia ($^{14}NH_3$) in the near-infrared regions, 6400–6900 cm^{-1}. J Mol Spectrosc 1993;162:230–45.
[161] Xu L-H, Liu Z, Yakovlev I, Tretyakov MY, Lees RM. External cavity tunable diode laser NH_3 spectra in the 1.5 μm region. Infra Phys Tech 2004;45:3–45.
[162] Li L, Lees RM, Xu L-H. External cavity tunable diode laser spectra of the $\nu_1+2\nu_4$ stretch-bend combination bands of $^{14}NH_3$ and $^{15}NH_3$. J Mol Spectrosc 2007;243:219–26.
[163] Lees RM, Li L, Xu L-H. New VISTA on ammonia in the 1.5 μm region: assignments for the $\nu_3+2\nu_4$ of $^{14}NH_3$ and $^{15}NH_3$ by isotopic shift labeling. J Mol Spectrosc 2008;251:241–51.
[164] Urban Š, D'Cunha R, Rao NK, Papoušek D. The $\Delta K=\pm 2$ forbidden band and inversion rotation energy-levels of ammonia. Can J Phys 1984;62:1775–91.
[165] Pickett HM, Poynter RL, Cohen EA, Delitsky ML, Pearson JC, Müller HSP. Submillimeter, millimeter and microwave spectral line catalog. J Quant Spectrosc Radiat Transfer 1998;60:883–90.
[166] Petkie DT, Helminger P, Winnewisser BP, Winnewisser M, Butler RAH, Jucks KW, et al. The simulation of infrared bands from the analyses of rotational spectra: the $2\nu_9-\nu_9$ and $\nu_5-\nu_9$ hot bands of HNO_3. J Quant Spectrosc Radiat Transfer 2005;92:129–41.
[167] Petkie DT, Helminger P, Butler RAH, Albert S, De Lucia FC. The millimeter and submillimeter spectra of the ground state and excited ν_9, ν_8, ν_7, and ν_6 vibrational states of HNO_3. J Mol Spectrosc 2003;218:127–30.
[168] Gomez L, Tran H, Perrin A, Gamache RR, Laraia A, Orphal J, et al. Some improvements of the HNO_3 spectroscopic parameters in the spectral region from 600 to 950 cm^{-1}. J Quant Spectrosc Radiat Transfer 2009;110:675–86.
[169] Perrin A, Mbiaké R. The ν_5 and $2\nu_9$ bands of the ^{15}N isotopic species of nitric acid ($H^{15}NO_3$): line positions and intensities. J Mol Spectrosc 2006;237:27–35.
[170] Flaud J-M, Brizzi G, Carlotti M, Perrin A, Ridolfi M. MIPAS database: validation of HNO_3 line parameters using MIPAS satellite measurements. Atmos Chem Phys 2006;6:5037–48.
[171] Drouin BJ, Miller CE, Fry JL, Petkie DT, Helminger P, Medvedev I. Submillimeter measurements of isotopes of nitric acid. J Mol Spectrosc 2006;236:29–34.
[172] Krasnopolsky VA, Belyaev DA, Gordon IE, Li G, Rothman LS. Observations of D/H ratios in H_2O, HCl, and HF on Venus and new DCl and DF line strengths. Icarus 2013;224:57–65.
[173] Li G, Gordon IE, Hajigeorgiou PG, Coxon JA, Rothman LS. Reference spectroscopic data for hydrogen halides. Part II: The line lists. J Quant Spectrosc Radiat Transfer, 10.1016/j.jqsrt.2013.07.019, this issue.
[174] Li G, Gordon IE, Bernath PF, Rothman LS. Direct fit of experimental ro-vibrational intensities to the dipole moment function: application to HCl. J Quant Spectrosc Radiat Transfer 2011;112:1543–50.
[175] Li G, Gordon IE, Le Roy RJ, Hajigeorgiou PG, Coxon JA, Bernath PF, et al. Reference spectroscopic data for hydrogen halides. Part I: Construction and validation of the ro-vibrational dipole moment functions. J Quant Spectrosc Radiat Transfer 2013;121:78–90.
[176] Pine AS, Looney JP. N_2 and air broadening in the fundamental bands of HF and HCl. J Mol Spectrosc 1987;122:41–55.
[177] Chou S-I, Baer DS, Hanson RK. Spectral intensity and lineshape measurements in the first overtone band of HF using tunable diode lasers. J Mol Spectrosc 1999;195:123–31.
[178] Meredith RE. Strengths and widths in the first overtone band of hydrogen fluoride. J Quant Spectrosc Radiat Transfer 1972;12:485–503.
[179] Pine AS, Fried A, Elkins JW. Spectral intensities in the fundamental bands of HF and HCl. J Mol Spectrosc 1985;109:30–45.
[180] Guelachvili G, Smith MAH. Measurements of pressure-induced shifts in the 1–0 and 2–0 bands of HF and in the 2–0 bands of $H^{35}Cl$ and $H^{37}Cl$. J Quant Spectrosc Radiat Transfer 1978;20:35–47.
[181] Cazzoli G, Puzzarini C. Hyperfine structure of the $J=1\leftarrow0$ transition of $H^{35}Cl$ and $H^{37}Cl$: improved ground state parameters. J Mol Spectrosc 2004;226:161–8.
[182] Cazzoli G, Puzzarini C. Hyperfine structure of the $J=1\leftarrow0$ and $J=2\leftarrow1$ transitions of $D^{35}Cl$ and $D^{37}Cl$. Phys Chem Chem Phys 2004;6:5133–9.
[183] Western CM. PGOPHER, a program for simulating rotational structure, University of Bristol, ⟨http://pgopher.chm.bris.ac.uk⟩.
[184] Park K, Chance KV, Nolt IG, Radostitz JV, Vanek MD, Jennings DA, et al. Pressure broadening of the 2.5 THz $H^{35}Cl$ rotational line by N_2 and O_2. J Mol Spectrosc 1991;147:521–5.
[185] De Rosa M, Nardini C, Piccolo C, Corsi C, D'Amato F. Pressure broadening and shift of transitions of the first overtone of HCl. Appl Phys B: Lasers Opt 2001;72:245–8.
[186] Hurtmans D, Henry A, Valentin A, Boulet C. Narrowing broadening and shifting parameters for R(2) and P(14) lines in the HCl fundamental band perturbed by N_2 and rare gases from tunable diode laser spectroscopy. J Mol Spectrosc 2009;254:126–36.
[187] Ortwein P, Woiwode W, Wagner S, Gisi M, Ebert V. Laser-based measurements of line strength, self- and pressure-broadening coefficients of the $H^{35}Cl$ R(3) absorption line in the first overtone region for pressures up to 1 MPa. Appl Phys B: Lasers Opt 2010;100:341–7.
[188] Ogilvie JF, Lee Y-P. Linestrengths in the 3–0 vibration–rotational band of gaseous $H^{35}Cl$ and the electric dipole moment function. Chem Phys Lett 1989;159:239–43.
[189] Zughul M, Gelfand J, Rabitz H, DePristo AE. Pressure broadening in the 0–4 through 0–7 overtone bands of $H^{35}Cl$ and $H^{37}Cl$. J Quant Spectrosc Radiat Transfer 1980;24:371–7.
[190] Tudorie M, Földes T, Vandaele AC, Vander Auwera J. CO_2 pressure broadening and shift coefficients for the 1–0 band of HCl and DCl. J Quant Spectrosc Radiat Transfer 2012;113:1092–101.
[191] Eaton DR, Thompson HW. Pressure broadening studies on vibration–rotation bands. II. The effective collision diameters. Proc R Soc London Ser A Math Phys Sci 1959;251:475–85.

[192] Coxon JA, Hajigeorgiou PG. Potential fitting analyses for the ground electronic state of hydrogen halides: HF/DF/TF. HCl/DCl/TCl, HBr/DBr/TBr and HI/DI/TI. J Quant Spectrosc Radiat Transfer 2013 [in preparation].

[193] Benedict WS, Herman R. The calculation of self-broadened line widths in linear molecules. J Quant Spectrosc Radiat Transfer 1963;3:265–78.

[194] Varberg TD, Roberts JC, Tuominen KA, Evenson KM. The far-infrared spectrum of deuterium iodide. J Mol Spectrosc 1998;191:384–6.

[195] Domanskaya AV, Asfin RE, Maul C, Kerl K, Bulanin MO. Nitrogen-induced broadening and shifts of rotation–vibrational lines in the fundamental, first, second and third overtone bands of HI. J Mol Spectrosc 2011;265:69–73.

[196] Hartmann JM, Bouanich JP, Boulet C, Bulanin MO, Domanskaya AV, Kerl K. Self-broadening and shifting of HI lines in the 1–0 and 2–0 infrared bands. J Quant Spectrosc Radiat Transfer 2005;95:151–63.

[197] Bulanin MO, Domanskaya AV, Kerl K, Maul C. Spectral line parameters in the (3←0) overtone band of the HI molecule and line-mixing in the band head. J Mol Spectrosc 2005;230:87–92.

[198] Goldman A, Gillis JR, Rinsland CP, Burkholder JB. Improved line parameters for the $X^2\Pi$–$X^2\Pi$ (1–0) bands of ^{35}ClO and ^{37}ClO. J Quant Spectrosc Radiat Transfer 1994;52:357–9.

[199] Burkholder JB, Howard CJ, Hammer PD, Goldman A. Infrared line intensity measurements in the $\nu=0$–1 band of the ClO radical. J Geophys Res 1989;94:2225–34.

[200] Birk M, Wagner G. Experimental line strengths of the ClO fundamental. J Geophys Res 1997;102:19199–206.

[201] Koshelev MA, Tretyakov MY. Collisional broadening and shifting of OCS rotational spectrum lines. J Quant Spectrosc Radiat Transfer 2009;110:118–28.

[202] Müller HSP, Gendriesch R, Lewen F, Winnewisser G. The submillimeter-wave spectrum of the formaldehyde isotopomer $H_2C^{18}O$ in its ground vibrational state. Z Naturforsch A 2000;55: 486–90.

[203] Müller HSP, Gendriesch R, Margulès L, Lewen F, Winnewisser G, Bocquet R, et al. Spectroscopy of the formaldehyde isotopomer $H_2{}^{13}CO$ in the microwave to terahertz region. Phys Chem Chem Phys 2000;2:3401–4.

[204] Brünken S, Müller HSP, Lewen F, Winnewisser G. High accuracy measurements on the ground state rotational spectrum of formaldehyde (H_2CO) up to 2 THz. Phys Chem Chem Phys 2003;5:1515–8.

[205] Bocquet R, Demaison J, Poteau L, Liedtke M, Belov S, Yamada KMT, et al. The ground state rotational spectrum of formaldehyde. J Mol Spectrosc 1996;177:154–9.

[206] Jacquemart D, Laraia A, Kwabia Tchana F, Gamache RR, Perrin A, Lacome N. Formaldehyde around 3.5 and 5.7 μm: measurement and calculation of broadening coefficients. J Quant Spectrosc Radiat Transfer 2010;111:1209–22.

[207] Li H, Le Roy RJ. Quadrupole moment function and absolute infrared quadrupolar intensities for N_2. J Chem Phys 2007;126:4301.

[208] Le Roy RJ, Huang Y, Jary C. An accurate analytic potential function for ground-state N_2 from a direct-potential-fit analysis of spectroscopic data. J Chem Phys 2006;125:164310–2.

[209] Bernath PF, McElroy CT, Abrams MC, Boone CD, Butler M, Camy-Peyret C, et al. Atmospheric chemistry experiment (ACE): mission overview. Geophys Res Lett 2005;32:5.

[210] Boone CD, Bernath PF. Spectroscopy for the atmospheric chemistry experiment (ACE). Presented at ASA/HITRAN meeting, Reims, France, August 2012.

[211] Nikitin A, Champion JP, Burger H. Global analysis of $^{12}CH_3{}^{35}Cl$ and $^{12}CH_3{}^{37}Cl$: simultaneous fit of the lower five polyads (0–2600 cm^{-1}). J Mol Spectrosc 2005;230:174–84.

[212] Chackerian C, Brown LR, Lacome N, Tarrago G. Methyl chloride ν_5 region lineshape parameters and rotational constants for the ν_2, ν_5, and $2\nu_3$ vibrational bands. J Mol Spectrosc 1998;191:148–57.

[213] Kondo S, Koga Y, Nakanaga T, Saëki S. Infrared intensities in methyl chloride. I. The fundamental bands. Bull Chem Soc Jpn 1983;56: 416–21.

[214] Kondo S, Koga Y, Nakanaga T, Saëki S. Infrared intensities in methyl chloride. II. Binary overtone and combination bands. Bull Chem Soc Jpn 1984;57:16–21.

[215] Kondo S, Koga Y, Nakanaga T. Infrared intensities in methyl chloride. III. Improvement of the anharmonic force field and the analysis of the overtone and combination band intensities. Bull Chem Soc Jpn 1985;58:65–72.

[216] Sharpe SW, Johnson TJ, Sams RL, Chu PM, Rhoderick GC, Johnson PA. Gas-phase databases for quantitative infrared spectroscopy. Appl Spectrosc 2004;58:1452–61.

[217] Bray C, Perrin A, Jacquemart D, Lacome N. The ν_1, ν_4 and $3\nu_6$ bands of methyl chloride in the 3.4 μm region: line positions and intensities. J Quant Spectrosc Radiat Transfer 2011;112:2446–62.

[218] Gomez L, Jacquemart D, Lacome N, Mandin JY. Line intensities of $^{12}C_2H_2$ in the 7.7 μm spectral region. J Quant Spectrosc Radiat Transfer 2009;110:2102–14.

[219] Gomez L, Jacquemart D, Lacome N, Mandin JY. New line intensity measurements for $^{12}C_2H_2$ around 7.7 μm and HITRAN format line list for applications. J Quant Spectrosc Radiat Transfer 2010;111: 2256–64.

[220] Nakagawa K, de Labachelerie M, Awaji Y, Kourogi M. Accurate optical frequency atlas of the 1.5 μm bands of acetylene. J Opt Soc Am 1996;13:2708–14.

[221] Jolly A, Benilan Y, Cané E, Fusina L, Tamassia F, Fayt A, et al. Measured integrated band intensities and simulated line-by-line spectra for $^{12}C_2HD$ between 25 and 2.5 μm, and new global vibration–rotation parameters for the bending vibrations. J Quant Spectrosc Radiat Transfer 2008;109:2846–56.

[222] Nixon CA, Achterberg RK, Conrath BJ, Irwin PGJ, Teanby NA, Fouchet T, et al. Meridional variations of C_2H_2 and C_2H_6 in Jupiter's atmosphere from Cassini CIRS infrared spectra. Icarus 2007;188:47–71.

[223] Vander Auwera J, Moazzen-Ahmadi N, Flaud J-M. Toward an accurate database for the 12 μm region of the ethane spectrum. Astrophys J 2007;662:750–7.

[224] Moazzen-Ahmadi N. A combined frequency analysis of the ν_3, ν_9, $3\nu_4$ and the far-infrared bands of ethane: a reassessment of the torsional parameters for the ground vibrational state. J Mol Spectrosc 2002;214:144–51.

[225] Cooper JR, Moazzen-Ahmadi N. Global fit analysis including the $\nu_9+\nu_4-\nu_4$ hot band of ethane: evidence of an interaction with the ν_{12} fundamental. J Mol Spectrosc 2006;239:51–8.

[226] Malathy Devi V, Rinsland CP, Chris Benner D, Sams RL, Blake TA. Multispectrum analysis of the ν_9 band of $^{12}C_2H_6$: positions, intensities, self- and N_2-broadened half-width coefficients. J Quant Spectrosc Radiat Transfer 2010;111:1234–51.

[227] Devi VM, Benner DC, Rinsland CP, Smith MAH, Sams RL, Blake TA, et al. Multispectrum measurements of spectral line parameters including temperature dependences of N_2- and self-bropadened half-width coefficients in the region of the ν_9 band of $^{12}C_2H_6$. J Quant Spectrosc Radiat Transfer 2010;111:2481–504.

[228] di Lauro C, Lattanzi F, Brown LR, Sung K, Vander Auwera J, Mantz AW, et al. High resolution investigation of the 7 μm region of the ethane spectrum. Planet Space Sci 2012;60:93–101.

[229] Lattanzi F, di Lauro C, Vander Auwera J. Toward the understanding of the high resolution infrared spectrum of C_2H_6 near 3.3 μm. J Mol Spectrosc 2011;267:71–9.

[230] Villanueva GL, Mumma MJ, Magee-Sauer K. Ethane in planetary and cometary atmospheres: transmittance and fluorescence models of the ν_7 band at 3.3 μm. J Geophys Res-Planets 2011;116:E08012.

[231] Cazzoli G, Puzzarini C. The Lamb-dip spectrum of phosphine: the nuclear hyperfine structure due to hydrogen and phosphorus. J Mol Spectrosc 2006;239:64–70.

[232] Davies PB, Neumann RM, Wofsy SC, Klemperer W. Radio-frequency spectrum of phosphine (PH_3). J Chem Phys 1971;55:3564–8.

[233] Belov SP, Burenin AV, Polyansky OL, Shapin SM. A new approach to the treatment of rotational spectra of molecules with small moments of inertia applied to the PH_3 molecule in the ground state. J Mol Spectrosc 1981;90:579–89.

[234] Chu FY, Oka T. "Forbidden" rotational spectra of phosphine and arsine. J Chem Phys 1974;60:4612–8.

[235] Helms DA, Gordy W. "Forbidden" rotational spectra of symmetric-top molecules: PH_3 and PD_3. J Mol Spectrosc 1977;66:206–18.

[236] Belov SP, Burenin AV, Gershtein LI, Krupnov AF, Markov VN, Maslovsky AV, et al. Rotational spectrum and spectroscopic constants of the phosphine molecule in the ground vibrational state. J Mol Spectrosc 1981;86:184–92.

[237] Fusina L, Carlotti M. The far-infrared spectrum and spectroscopic parameters of PH_3 in the ground state. J Mol Spectrosc 1988;130: 371–81.

[238] Sousa-Silva C, Tennyson J, Yurchenko SN. A computed room-temperature line list for phosphine. J Mol Spectrosc 2013;288: 28–37.

[239] Müller HSP. Spectroscopic parameters of phosphine. J Quant Spectrosc Radiat Transfer 2013 [this issue], http://dx.doi.org/10.1016/j.jqsrt.2013.05.002.

[240] Cohen EA, Drouin BJ, Brown LR, Oh JJ. Terahertz and infrared spectra of carbonyl fluoride, COF_2: vibration–rotation analyses of the four lowest bands, $2\nu_6$, and ν_6 hot bands; $^{13}COF_2$ ground state and ν_6 band. J Quant Spectrosc Radiat Transfer 2013;114:13–9.

[241] Ciaffoni L, Cummings BL, Denzer W, Peverall R, Procter SR, Ritchie GAD. Line strength and collisional broadening studies of hydrogen

sulphide in the 1.58 μm region using diode laser spectroscopy. Appl Phys B: Lasers Opt 2008;92:627–33.
[242] Kaltenegger L, Sasselov D. Detecting planetary geochemical cycles on exoplanets: atmospheric signatures and the case of SO_2. Astrophys J 2010;708:1162–7.
[243] Azzam AAA, Yurchenko SN, Tennyson J, Martin M-A, Pirali O. THz spectroscopy of hydrogen sulphide. J Quant Spectrosc Radiat Transfer 2013 [this issue], http://dx.doi.org/10.1016/j.jqsrt.2013.05.035.
[244] Flaud JM, Camy-Peyret C, Johns J. The far-infrared spectrum of hydrogen-sulfide—the (000) rotational–constants of $H_2{}^{32}S$, $H_2{}^{33}S$ and $H_2{}^{34}S$. Can J Phys 1983;61:1462–73.
[245] Yamada KMT, Klee S. Pure rotational spectrum of H_2S in the far-infrared region measured by FTIR spectroscopy. J Mol Spectrosc 1994;166:395–405.
[246] Belov SP, Yamada KMT, Winnewisser G, Poteau L, Bocquet R, Demaison J, et al. Terahertz rotational spectrum of H_2S. J Mol Spectrosc 1995;173:380–90.
[247] Azzam AAA, Yurchenko SN, Tennyson J. ExoMol line list: the rovibraional spectrum of H_2S. Mon Not R Astr Soc [in preparation].
[248] Brown LR, Naumenko OV, Polovtseva ER, Sinitsa LN. Hydrogen sulfide absorption spectrum in the 5700–6600 cm^{-1} spectral region. In: Sinitsa LN, Mikhailenko SN, editors. Proceedings of the SPIE 14th symposium on high-resolution molecular spectroscopy, 2003, vol. 5311. p. 59–67.
[249] Brown LR, Naumenko OV, Polovtseva ER, Sinitsa LN. Absorption spectrum of H_2S between 7200 and 7890 cm^{-1}. In: Matvienko GG, Krekov GM, editors. Proceedings of the SPIE tenth joint international symposium on atmospheric and ocean optics. Atmospheric Physics. Part I: Radiation propagation in the atmosphere and ocean, July 2004, vol. 5396. p. 42–48; February 2004, Krasnoyarsk, Russia.
[250] Naumenko O, Polovtseva ER. Database of the hydrogen sulfide absorption in the 4400–11400 cm^{-1} region. Atmos Oceanic Opt 2003;16:900–6.
[251] Polovtseva ER, Lavrentiev NA, Voronina SS, Naumenko OV, Fazliev AZ. Information system for molecular spectroscopy. 5. Rovibrational transitions and energy levels of the hydrogen sulfide molecule. Atmos Oceanic Opt 2012;25:157–65.
[252] Ulenikov ON, Liu AW, Bekhtereva ES, Gromova OV, Hao LY, Hu SM. High-resolution Fourier transform spectrum of H_2S in the region of the second hexade. J Mol Spectrosc 2005;234:270–8.
[253] Ulenikov ON, Liu AW, Bekhtereva ES, Gromova OV, Hao LY, Hu SM. On the study of high resolution rovibrational spectrum of H_2S in the region of 7300–7900 cm^{-1}. J Mol Spectrosc 2004;226:57–70.
[254] Ding Y, Naumenko O, Hu S-M, Zhu Q, Bertseva E, Campargue A. The absorption spectrum of H_2S between 9540 and 10000 cm^{-1} by intracavity laser absorption spectroscopy with a vertical external cavity surface emitting laser. J Mol Spectrosc 2003;217:222–38.
[255] Naumenko O, Campargue A. Local mode effects in the absorption spectrum of H_2S between 10780 and 11330 cm^{-1}. J Mol Spectrosc 2001;209:242–53.
[256] Bykov AD, Naumenko OV, Smirnov MA, Sinitsa LN, Brown LR, Crisp J, et al. The infrared spectrum of H_2S from 1 to 5 μm. Can J Phys 1994;72:989–1000.
[257] Cherchneff I, Glassgold AE. The formation of carbon chain molecules in IRC+10216. Astrophys J Lett 1993;419:L41.
[258] de Graauw T, Feuchtgruber H, Bézard B, Drossart P, Encrenaz T, Beintema DA, et al. First results of ISO-SWS observations of Saturn: detection of CO_2, CH_3C_2H, C_4H_2 and tropospheric H_2O. Astron Astrophys 1997;321:L13–6.
[259] Fouchet T, Bézard B, Encrenaz T. The planets and Titan observed by ISO. Space Sci Rev 2005;119:123–39.
[260] Waite JH, Young DT, Cravens TE, Coates AJ, Crary FJ, Magee B, et al. The process of tholin formation in Titan's upper atmosphere. Science 2007;316:870–5.
[261] Cernicharo J, Heras AM, Tielens AGGM, Pardo JR, Herpin F, Guélin M, et al. Infrared space observatory's discovery of C_4H_2, C_6H_2, and benzene in CRL 618. Astrophys J Lett 2001;546:L123–6.
[262] Bernard-Salas J, Peeters E, Sloan GC, Cami J, Guiles S, Houck JR. The Spitzer IRS spectrum of SMP LMC 11. Astrophys J Lett 2006;652:L29–32.
[263] Kunde VG, Aikin AC, Hanel RA, Jennings DE, Maguire WC, Samuelson RE. C_4H_2, HC_3N and C_2N_2 in Titan's atmosphere. Nature 1981;292:686–8.
[264] Kunde VG, Flasar FM, Jennings DE, Bézard B, Strobel DF, Conrath BJ, et al. Jupiter's atmospheric composition from the Cassini thermal infrared spectroscopy experiment. Science 2004;305:1582–7.
[265] Burgdorf M, Orton G, van Cleve J, Meadows V, Houck J. Detection of new hydrocarbons in Uranus' atmosphere by infrared spectroscopy. Icarus 2006;184:634–7.
[266] Meadows VS, Orton G, Line M, Liang M-C, Yung YL, van Cleve J, et al. First Spitzer observations of Neptune: detection of new hydrocarbons. Icarus 2008;197:585–9.
[267] Dang-Nhu M, Guelachvili G, Ramsay DA. Absolute line intensities of the 5-μm ν_5-fundamental band of diacetylene. J Mol Spectrosc 1991;146:513–5.
[268] McNaughton D, Bruget DN. The high-resolution infrared spectrum of diacetylene and structures of diacetylene, triacetylene and dicyanoacetylene. J Mol Struct 1992;273:11–25.
[269] Arié E, Johns JWC. The bending energy levels of C_4H_2. J Mol Spectrosc 1992;155:195–204.
[270] Jolly A, Fayt A, Benilan Y, Jacquemart D, Nixon CA, Jennings DE. The ν_8 bending mode of diacetylene: from laboratory spectroscopy to the detection of ^{13}C isotopologues in Titan's atmosphere. Astrophys J 2010;714:852–9.
[271] Bizzocchi L, Degli Esposti C, Dore L. Submillimetre-wave spectrum of diacetylene and diacetylene-d2. Mol Phys 2010;108:2315–23.
[272] Bizzocchi L, Tamassia F, Esposti CD, Fusina L, Canè E, Dore L. High-resolution infrared spectroscopy of diacetylene below 1000 cm^{-1}. Mol Phys 2011;109:2181–90.
[273] Matsumura K, Kawaguchi K, Hirota E, Tanaka T. Stark modulation infrared diode laser spectroscopy of the $\nu_6+\nu_8$ band of diacetylene. J Mol Spectrosc 1986;118:530–9.
[274] Ho PTP, Moran JM, Lo KY. The submillimeter array. Astrophys J Lett 2004;616:L1–6.
[275] Pilbratt GL, Riedinger JR, Passvogel T, Crone G, Doyle D, Gageur U, et al. Herschel Space Observatory. An ESA facility for far-infrared and submillimetre astronomy. Astron Astrophys 2010;518:L1.
[276] Snell RL, Schloerb FP, Young JS, Hjalmarson A, Friberg P. Observations of HC_3N, HC_5N, and HC_7N in molecular clouds. Astrophys J 1981;244:45–53.
[277] Jolly A, Benilan Y, Fayt A. New infrared integrated band intensities for HC_3N and extensive line list for the ν_5 and ν_6 bending modes. J Mol Spectrosc 2007;242:46–54.
[278] Komasa J, Piszczatowski K, Lach G, Przybytek M, Jeziorski B, Pachucki K. Quantum electrodynamics effects in rovibrational spectra of molecular hydrogen. J Chem Theory Comput 2011;7:3105–15.
[279] Pachucki K, Komasa J. Rovibrational levels of HD. Phys Chem Chem Phys 2010;12:9188–96.
[280] Schwartz C, Le Roy RJ. Nonadiabatic eigenvalues and adiabatic matrix-elements for all isotopes of diatomic hydrogen. J Mol Spectrosc 1987;121:420–39.
[281] Wolniewicz L, Simbotin I, Dalgarno A. Quadrupole transition probabilities for the excited rovibrational states of H_2. Astrophys J Suppl Ser 1998;115:293–313.
[282] Pachucki K, Komasa J. Electric dipole rovibrational transitions in the HD molecule. Phys Rev A 2008;78:52503.
[283] Kassi S, Campargue A. Electric quadrupole and dipole transitions of the first overtone band of HD by CRDS between 1.45 and 1.33 μm. J Mol Spectrosc 2011;267:36–42.
[284] Campargue A, Kassi S, Pachucki K, Komasa J. The absorption spectrum of H_2: CRDS measurements of the (2–0) band, review of the literature data and accurate ab initio line list up to 35000 cm^{-1}. Phys Chem Chem Phys 2012;14:802.
[285] Cheng C-F, Sun YR, Pan H, Wang J, Liu A-W, Campargue A, et al. Electric-quadrupole transitions of H_2 determined to 10^{-9} precision. Phys Rev A 2012;85:24501.
[286] Hu S-M, Pan H, Cheng C-F, Sun YR, Li X-F, Wang J, et al. The $\nu=3\leftarrow S$(0)–S(3) electric quadrupole transitions of H_2 near 0.8 μm. Astrophys J 2012;749:76.
[287] Gupta M, Owano T, Baer DS, O'Keefe A. Quantitative determination of the Q(1) quadrupole hydrogen absorption in the near infrared via off-axis ICOS. Chem Phys Lett 2006;418:11–4.
[288] Tran H, Hartmann JM, Chaussard F, Gupta M. An isolated line-shape model based on the Keilson–Storer function for velocity changes. II. Molecular dynamics simulations and the Q(1) lines for pure H_2. J Chem Phys 2009;131:154303.
[289] Canaves MV, de Almeida AA, Boice DC, Sanzovo GC. On the chemistry of CS and NS in cometary comae. Adv Space Res 2007;39:451–7.
[290] Moreno R, Marten A, Matthews HE, Biraud Y. Long-term evolution of CO, CS and HCN in Jupiter after the impacts of comet Shoemaker–Levy 9. Planet Space Sci 2003;51:591–611.
[291] Bogey M, Demuynck C, Destombes JL. Millimeter and submillimeter wave spectrum of CS $^1\Sigma$ in high vibrational states: isotopic dependence of Dunham coefficients. J Mol Spectrosc 1982;95:35–42.

[292] Bogey M, Demuynck C, Destombes JL. Millimeter spectrum of carbon monosulfide rare isotopes. Chem Phys Lett 1981;81:256–60.
[293] Ram RS, Bernath PF, Davis SP. Fourier transform infrared emission spectroscopy of CS. J Mol Spectrosc 1995;173:146–57.
[294] Chandra S, Kegel WH, Le Roy RJ, Hertenstein T. Einstein A-coefficients for vib-rotational transitions in CS. Astron Astrophys Suppl Ser 1995;114:175.
[295] Blanquet G, Walrand J, Bouanich J-P. N_2 broadening of carbon disulfide $^{12}C^{32}S_2$ in the ν_3 and $3\nu_3-\nu_1$ bands. J Mol Spectrosc 1999;198:408–15.
[296] Misago F, Lepère M, Bouanich J-P, Blanquet G. Self-broadening coefficients in the $\nu_3-\nu_1$ band of CS_2. J Mol Spectrosc 2009;254:16–9.
[297] Rawlins WT, Hensley JM, Sonnenfroh DM, Oakes DB, Allen MG. Quantum cascade laser sensor for SO_2 and SO_3 for application to combustor exhaust streams. Appl Opt 2005;44:6635–43.
[298] Zhang X, Liang M-C, Montmessin F, Bertaux J-L, Parkinson C, Yung YL. Photolysis of sulphuric acid as the source of sulphur oxides in the mesosphere of Venus. Nat Geosci 2010;3:834–7.
[299] Meyer V, Sutter DH, Dreizler H. The centrifugally-induced pure rotational spectrum and the structure of sulfur-trioxide: a microwave Fourier-transform study of a nonpolar molecule. Z Naturforsch A 1991;46:710–4.
[300] Underwood DS, Tennyson J, Yurchenko SN. An ab initio variationally computed room-temperature line list for SO_3. Phys Chem Chem Phys 2013;15:10118–25.
[301] Kaldor A, Maki AG, Dorney AJ, Mills IM. Assignment of ν_2 and ν_4 of SO_3. J Mol Spectrosc 1973;45:247–52.
[302] Ortigoso J, Escribano R, Maki AG. The ν_2 and ν_4 IR bands of SO_3. J Mol Spectrosc 1989;138:602–13.
[303] Maki A, Blake TA, Sams RL, Vulpanovici N, Barber J, Chrysostom ETH, et al. High-resolution infrared spectra of the ν_2, ν_3, ν_4 and $2\nu_3$ bands of $^{32}S^{16}O_3$. J Mol Spectrosc 2001;210:240–9.
[304] Sharpe SW, Blake TA, Sams RL, Maki A, Masiello T, Barber J, et al. The ν_3 and $2\nu_3$ bands of $^{32}S^{16}O_3$, $^{32}S^{18}O_3$, $^{34}S^{16}O_3$ and $^{34}S^{18}O_3$. J Mol Spectrosc 2003;222:142–52.
[305] Maki A, Blake TA, Sams RL, Frieh J, Barber J, Masiello T, et al. Analysis of some combination-overtone infrared bands of $^{32}S^{16}O_3$. J Mol Spectrosc 2004;225:109–22.
[306] Harrison JJ, Allen NDC, Bernath PF. Infrared absorption cross sections for ethane (C_2H_6) in the 3 μm region. J Quant Spectrosc Radiat Transfer 2010;111:357–63.
[307] Harrison JJ, Bernath PF. Infrared absorption cross sections for propane (C_3H_8) in the 3 μm region. J Quant Spectrosc Radiat Transfer 2010;111:1282–8.
[308] Harrison JJ, Allen NDC, Bernath PF. Infrared absorption cross sections for acetone (propanone) in the 3 μm region. J Quant Spectrosc Radiat Transfer 2011;112:53–8.
[309] Harrison JJ, Humpage N, Allen NDC, Waterfall AM, Bernath PF, Remedios JJ. Mid-infrared absorption cross sections for acetone (propanone). J Quant Spectrosc Radiat Transfer 2011;112:457–64.
[310] Allen NDC, Harrison JJ, Bernath PF. Acetonitrile (CH_3CN) infrared absorption cross sections in the 3 μm region. J Quant Spectrosc Radiat Transfer 2011;112:1961–6.
[311] Harrison JJ, Bernath PF. Mid- and long-wave infrared absorption cross sections for acetonitrile. J Quant Spectrosc Radiat Transfer 2012;113:221–5.
[312] Harrison JJ, Allen NDC, Bernath PF. Infrared absorption cross sections for methanol. J Quant Spectrosc Radiat Transfer 2012;113:2189–96.
[313] Harrison JJ, Bernath PF. ACE-FTS observations of acetonitrile in the lower stratosphere. Atmos Chem Phys 2013;13:7405–13.
[314] Waterfall A.M. Measurement of organic compounds in the upper troposphere using infrared remote sensing [DPhil thesis]. University of Oxford, 2004.
[315] Moore DP, Remedios JJ, Waterfall AM. Global distributions of acetone in the upper troposphere from MIPAS spectra. Atmos Chem Phys 2012;12:757–68.
[316] Boone CD. Private communication; 2012.
[317] Allen G, Remedios JJ, Smith KM. Low temperature mid-infrared cross-sections for peroxyacetyl nitrate (PAN) vapour. Atmos Chem Phys 2005;5:3153–8.
[318] Allen G, Remedios JJ, Newnham DA, Smith KM, Monks PS. Improved mid-infrared cross-sections for peroxyacetyl nitrate (PAN) vapour. Atmos Chem Phys 2005;5:47–56.
[319] Tereszchuk KA, Moore DP, Harrison JJ, Boone CD, Park M, Remedios JJ, et al. Observations of peroxyacetyl nitrate (PAN) in the upper troposphere by the Atmospheric Chemistry Experiment Fourier Transform Spectrometer (ACE-FTS). Atmos Chem Phys 2013;13:5601–13.
[320] Tereszchuk KA, Bernath PF. Infrared absorption cross-sections for acetaldehyde (CH_3CHO) in the 3 μm region. J Quant Spectrosc Radiat Transfer 2011;112:990–3.
[321] Clerbaux C, Colin R, Simon PC, Granier C. Infrared cross sections and global warming potentials of 10 alternative hydrohalocarbons. J Geophys Res 1993;98:10491.
[322] Le Bris K, Strong K. Temperature-dependent absorption cross-sections of HCFC-142b. J Quant Spectrosc Radiat Transfer 2010;111:364–71.
[323] Höpfner M, Orphal J, von Clarmann T, Stiller G, Fischer H. Stratospheric $BrONO_2$ observed by MIPAS. Atmos Chem Phys 2009;9:1735–46.
[324] Brasseur G, Solomon S. Aeronomy of the middle atmosphere (third edition). Atmos. Oceanograph. Sci. Lib. Dordrecht, The Netherlands: Springer; 2005 (369 ff.).
[325] Birk M, Friedl RR, Cohen EA, Pickett HM, Sander SP. The rotational spectrum and structure of chlorine peroxide. J Chem Phys 1989;91:6588–97.
[326] Wetzel G, Oelhaf H, Kirner O, Ruhnke R, Friedl-Vallon F, Kleinert A, et al. First remote sensing measurements of ClOOCl along with ClO and $ClONO_2$ in activated and deactivated Arctic vortex conditions using new ClOOCl IR absorption cross sections. Atmos Chem Phys 2010;10:931–45.
[327] Chance K, Orphal J. Revised ultraviolet absorption cross sections of H_2CO for the HITRAN database. J Quant Spectrosc Radiat Transfer 2011;112:1509–10.
[328] Thomas GE, Stamnes K. Radiative transfer in the atmosphere and ocean. Cambridge: Cambridge University Press; 1999.
[329] Downing HD, Williams D. Optical constants of water in the infrared. J Geophys Res 1975;80:1656–61.
[330] Kou L, Labrie D, Chylek P. Refractive indices of water and ice in the 0.65- to 2.5-μm spectral range. Appl Opt 1993;32:3531–40.
[331] Warren SG, Brandt RE. Optical constants of ice from the ultraviolet to the microwave: a revised compilation. J Geophys Res [Atmos] 2008;113:D14220.
[332] Fenn RW, Clough SA, Gallery WO, Good RE, Kneizys FX, Mill JD, et al. Optical and infrared properties of the atmosphere. In: Jursa AS, editor. Handbook of geophysics and the space environment. Springfield: National Technical Information Service; 1985 [Chapter 18].
[333] Palmer KF, Williams D. Optical constants of sulfuric acid: application to the clouds of Venus? Appl Opt 1975;14:208–19.
[334] Remsberg EE, Lavery D, Crawford B. Optical constants for sulfuric and nitric acids. J Chem Eng Data 1974;19:263–5.
[335] Tisdale RT, Glandorf DL, Tolbert MA, Toon OB. Infrared optical constants of low-temperature H_2SO_4 solutions representative of stratospheric sulfate aerosols. J Geophys Res [Atmos] 1998;103:25353–70.
[336] Niedziela RF, Norman ML, DeForest CL, Miller RE, Worsnop DR. A temperature- and composition-dependent study of H_2SO_4 aerosol optical constants using Fourier transform and tunable diode laser infrared spectroscopy. J Phys Chem A 1999;103:8030–40.
[337] Biermann UM, Luo BP, Peter T. Absorption spectra and optical constants of binary and ternary solutions of H_2SO_4, HNO_3, and H_2O in the mid infrared at atmospheric temperatures. J Phys Chem A 2000;104:783–93.
[338] Querry MR, Tyler IL. Reflectance and complex refractive indices in the infrared for aqueous solutions of nitric acid. J Chem Phys 1980;72:2495–9.
[339] Norman ML, Qian J, Miller RE, Worsnop DR. Infrared complex refractive indices of supercooled liquid HNO_3/H_2O aerosols. J Geophys Res [Atmos] 1999;104:30571–84.
[340] Toon OB, Tolbert MA, Koehler BG, Middlebrook AM, Jordan J. Infrared optical constants of H_2O ice, amorphous nitric acid solutions, and nitric acid hydrates. J Geophys Res [Atmos] 1994;99:25631–54.
[341] Niedziela RF, Miller RE, Worsnop DR. Temperature- and frequency-dependent optical constants for nitric acid dihydrate from aerosol spectroscopy. J Phys Chem A 1998;102:6477–84.
[342] Richwine LJ, Clapp ML, Miller RE, Worsnop DR. Complex refractive indices in the infrared of nitric acid trihydrate aerosols. Geophys Res Lett 1995;22:2625–8.
[343] Sutherland RA, Khanna RK. Optical properties of organic-based aerosols produced by burning vegetation. Aerosol Sci Technol 1991;14:331–42.

[344] Magi BI, Fu Q, Redemann J. A methodology to retrieve self-consistent aerosol optical properties using common aircraft measurements. J Geophys Res [Atmos] 2007;112:D24S12.
[345] Stagg BJ, Charalampopoulos TT. Refractive indices of pyrolytic graphite, amorphous carbon, and flame soot in the temperature range 25° to 600 °C. Combust Flame 1993;94:381–96.
[346] Chang H, Charalampopoulos TT. Determination of the wavelength dependence of refractive indices of flame soot. Proc: Math Phys Sci 1990;430:577–91.
[347] Alexander DTL, Crozier PA, Anderson JR. Brown carbon spheres in East Asian outflow and their optical properties. Science 2008;321:833–6.
[348] Lund Myhre CE, Nielsen CJ. Optical properties in the UV and visible spectral region of organic acids relevant to tropospheric aerosols. Atmos Chem Phys 2004;4:1759–69.
[349] Hasenkopf CA, Beaver MR, Trainer MG, Langley Dewitt H, Freedman MA, Toon OB, et al. Optical properties of Titan and early earth haze laboratory analogs in the mid-visible. Icarus 2010;207:903–13.
[350] Zarzana KJ, De Haan DO, Freedman MA, Hasenkopf CA, Tolbert MA. Optical properties of the products of α-dicarbonyl and amine reactions in simulated cloud droplets. Environ Sci Technol 2012;46:4845–51.
[351] Querry MR. Optical constants of minerals and other materials from the millimeter to the ultraviolet. Aberdeen: Chemical Research, Development Engineering Center; 1987.
[352] Toon OB, Pollack JB, Sagan C. Physical properties of the particles composing the Martian dust storm of 1971–1972. Icarus 1977;30:663–96.
[353] Wagner R, Ajtai T, Kandler K, Lieke K, Linke C, Muller T, et al. Complex refractive indices of Saharan dust samples at visible and near UV wavelengths: a laboratory study. Atmos Chem Phys 2012;12:2491–512.
[354] Sinyuk A, Torres O, Dubovik O. Combined use of satellite and surface observations to infer the imaginary part of refractive index of Saharan dust. Geophys Res Lett 2003;30:1081.
[355] Grainger RG, et al. Measuring volcanic plume and ash properties from space. In: Pyle D, Mather T, editors. Remote sensing of volcanoes and volcanic processes: integrating observation and modeling. London: Special Publ Geo Soc; 2013.
[356] Ramanathan V, Carmichael G. Global and regional climate changes due to black carbon. Nat Geosci 2008;1:221–7.
[357] Massie S, Hervig M. HITRAN 2012 refractive indices. J Quant Spectrosc Radiat Transfer 2013 [this issue], http://dx.doi.org/10.1016/j.jqsrt.2013.06.022.
[358] Dubernet ML, Boudon V, Culhane JL, Dimitrijevic MS, Fazliev AZ, Joblin C, et al. Virtual atomic and molecular data centre. J Quant Spectrosc Radiat Transfer 2010;111:2151–9.
[359] Hill C, Gordon IE, Rothman LS, Tennyson J A new relational database structure and online interface for the HITRAN database. J Quant Spectrosc Radiat Transfer 2013 [this issue]; http://dx.doi.org/10.1016/j.jqsrt.2013.04.027.
[360] Laraia AL, Gamache RR, Lamouroux J, Gordon IE, Rothman LS. Total internal partition sums to support planetary remote sensing. Icarus 2011;215:391–400.
[361] Fischer J, Gamache RR, Goldman A, Rothman LS, Perrin A. Total internal partition sums for molecular species in the 2000 edition of the HITRAN database. J Quant Spectrosc Radiat Transfer 2003;82:401–12.